FLUID PHYSICS BRANCH

RESEARCH DIVISION

OFFICE OF ADVANCED RESEARCH AND TECHNOLOGY

FIFTH INTERCENTER AND CONTRACTORS CONFERENCE ON PLASMA PHYSICS

Part II NASA Langley Research Center

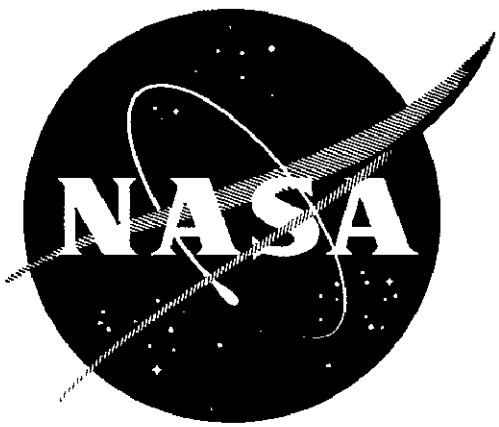

WASHINGTON, D. C.

MAY 24 – 26, 1966

FIFTH NASA INTERCENTER AND CONTRACTORS CONFERENCE ON PLASMA PHYSICS.

Part II: Plasma Physics Research at NASA Langley Research Center

Washington, D. C.
May 24-26, 1966

Table of Contents

RESULTS OF DIAGNOSTICS OF THE FLOW FROM THE LANGLEY 1-INCH PLASMA ACCELERATOR

W. R. Weaver, A. F. Carter, D. R. McFarland and G. P. Wood

NASA, Langley Research Center
Hampton, Virginia

Research on linear crossed-field d.c. plasma accelerators at Langley has continued with one phase of recent research being concentrated on diagnostics of the flow from the Langley 1-Inch-Square Accelerator. This accelerator has 24 electrode pairs in a length of 12 inches, is fed with about 275 volts and 55 amperes per electrode pair, and accelerates the nitrogen-plus-0.3-percent-cesium plasma from an entrance velocity of about 2000 meters per second to an exit velocity of about 6000 meters per second with an exit density corresponding to an altitude of about 45 km.

A velocity-measuring technique has been developed for use with the accelerator and it has provided the capability of determining the velocity profile both vertically and horizontally over the main portion of the flow. The technique is a time-of-flight measurement utilizing a spark and an image-converter camera. A spark is discharged across the flow and the resulting luminosity is tracked photographically. The spark electrodes are motorized so that they move vertically. During a test, one spark is discharged horizontally across the flow at each of five vertical positions as the electrodes move vertically from the anode toward the cathode side of the flow. In figure 1 is shown the velocity profile at each of the five positions. It is seen that the velocity variation over the central portion of the flow is reasonably small. There is a velocity asymmetry present in the vertical direction with the maximum value of velocity occurring near the bottom of the flow which is the cathode side of the accelerator. These nearly uniform velocity profiles have significance in that they indicate a nearly uniform spreading of current over essentially the entire cross section.

Pitot pressure surveys were made across the channel from the top to the bottom of the flow. They show that there is a large central portion of the flow over which the pitot pressure is reasonably uniform. The pitot pressure is, however, higher on the cathode side of the channel centerline than on the anode side, as was the case with the velocity.

A series of tests was made to determine the effects of shifting the cathodes with respect to the anodes in the axial direction. Due to the nonzero value of $\omega_e \tau_e$, the current across the channel is from the downstream edge of the anode into the upstream edge of the cathode; therefore, it might be expected that displacing the electrodes axially would change the angle of current flow with respect to the channel axis and affect the performance of the accelerator. In particular, it might be expected that the shifted position that gives the shortest current path and presumably the smallest component of current in the axial direction; i.e., the downstream edge of the anode

slightly upstream of the upstream edge of the cathode, would result in maximum current, Hall potential difference, and acceleration. The results of this series of tests are shown in figure 2, where the 0 position corresponds to the electrodes directly opposed and the +1 and -1 positions correspond to the cathodes displaced 1 electrode and 1 insulator thickness downstream or upstream, respectively. It can be seen that the pitot pressure, the average current per electrode, and the Hall potential difference all have maxima when the cathodes are shifted one position downstream, albeit the maxima tend to be rather broad.

A limited study was made of ablation in the accelerator flow. The stagnation enthalpy is 4.8×10^7 J/kg. This high value results in a high heat-transfer rate to a nonablating body, calculated by the method of Fay and Kemp to be 700 $R^{-\frac{1}{2}}$ Btu-ft^{-2}-sec^{-1} at the stagnation region of a hemisphere, which rate seems to be somewhat higher than in any other NASA steady-flow facility. The experiments were conducted with 1/4-inch-diameter hemisphere-cylinder models made of teflon. If the effect of the ablated gas on the calculated heat-transfer rate is taken into account by the method of Voyvodich and Pope, the experimentally observed rate of ablation turns out to be 83 percent of the theoretical rate. What is seriously lacking in the experiments is a measurement of heat-transfer rate to a nonablating body. Both steady-state and transient calorimeters for measuring this rate are under construction.

In addition to the above-mentioned experimental work, several theoretical studies have been completed. An analysis of the flow through the arc-heater nozzle has shown that the flow is in a frozen state. Diagnostics on the exit flow indirectly verify this result. When the equations describing the flow through the accelerator are integrated numerically to obtain the expected exit flow velocity, good agreement between measured and calculated velocity is obtained when the friction factor calculated by the theory of Fay, rather than that of Hartmann and Lazarus, is used. Also, the accelerator flow equations have been simplified so that all real-gas effects are contained in one quantity, which is described in the abstract of S. K. Park.

References:

Wood, G. P., Carter, A. F., Sabol, A. P., McFarland, D. R., and Weaver, W. R.: Research on Linear Crossed-Field Steady-Flow D-C Plasma Accelerators at Langley Research Center, NASA. AGARDograph 84, 1-45, September 1964.

Carter, A. F., Wood, G. P., McFarland, D. R., and Weaver, W. R.: Research on a Linear Direct-Current Plasma Accelerator. AIAA J., 3, 1040-1045, (1965).

Carter, A. F., McFarland, D. R., Weaver, W. R., Park, S. K., and Wood, G. P.: Operating Characteristics, Velocity and Pitot Distribution, and Material Evaluation Tests in the Langley One-Inch-Square Plasma Accelerator. AIAA Paper No. 66-180, March 1966.

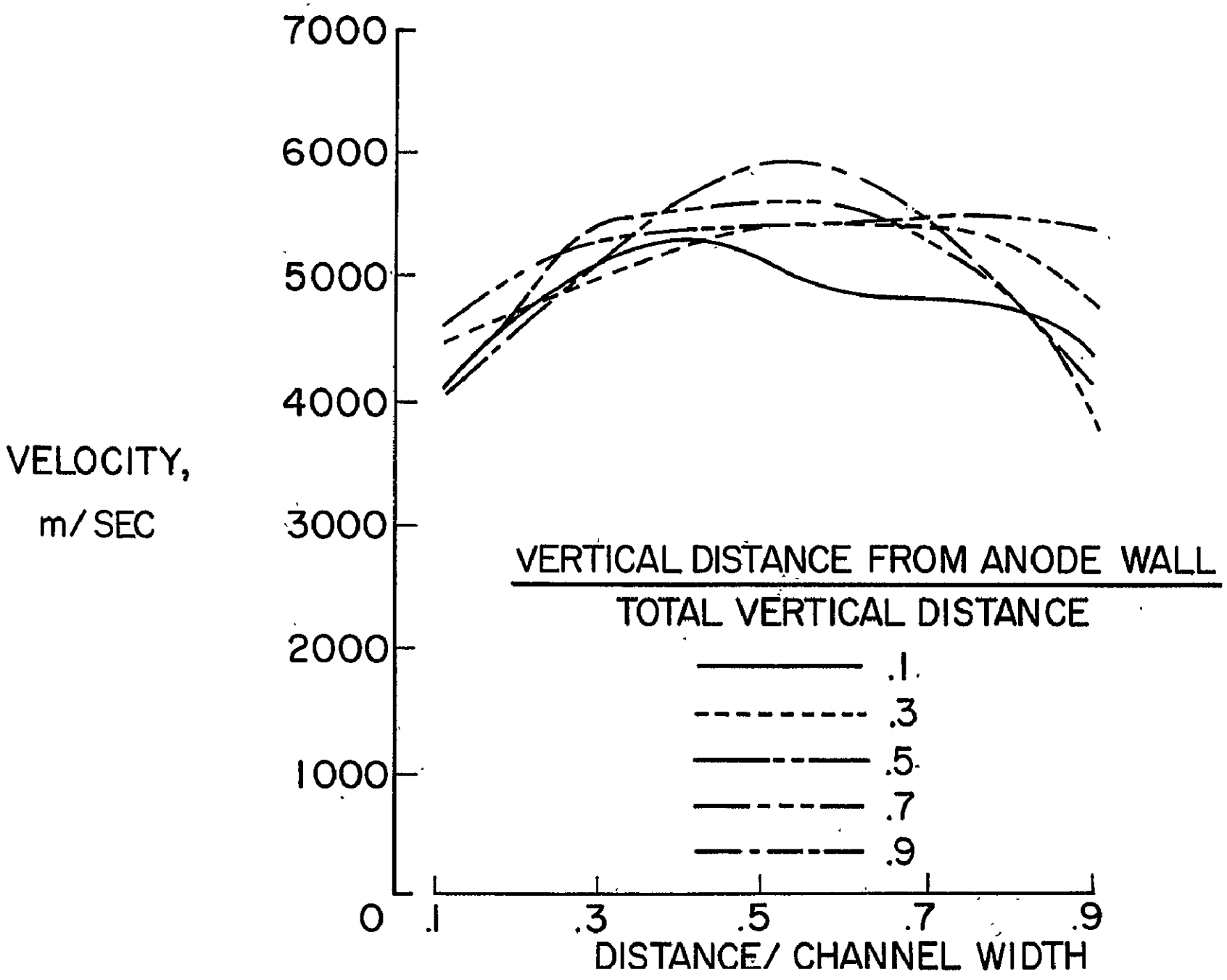
7000
6000
5000
4000
3000
2000
1000
0
VELOCITY,
m/SEC
VERTICAL DISTANCE FROM ANODE WALL
TOTAL VERTICAL DISTANCE
.1
.3
.5
.7
.9
.1
.3
.5
.7
.9
DISTANCE/ CHANNEL WIDTH

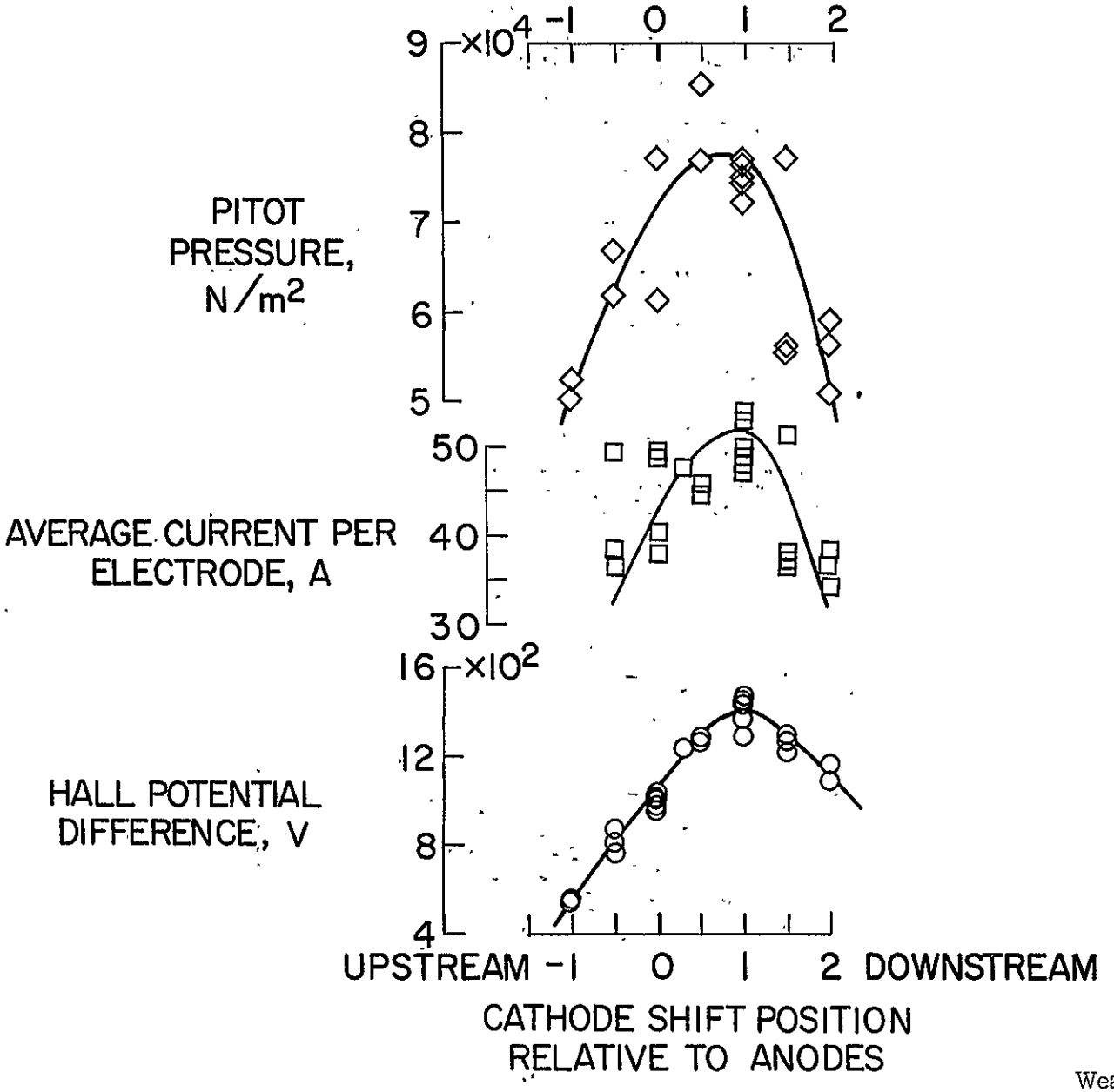

Weaver et al-2

STATUS REPORT ON 20-MW LINEAR PLASMA ACCELERATOR FACILITY

A. F. Carter, G. P. Wood, W. R. Weaver, D. R. McFarland, and S. K. Park

NASA, Langley Research Center
Hampton, Virginia

The Langley Research Center has designed and is constructing a 20-megawatt linear plasma accelerator facility as the next step in a program to develop a high-speed steady-flow facility for aerodynamic testing at reentry velocities. This accelerator is designed to provide a velocity of 13,000 m/sec at a density corresponding to an altitude of 53 km.

The basic accelerator design philosophy that was used includes the following points: (1) the effect on the velocity of the Lorentz force should be much greater than the effect of Joule heating; (2) the Lorentz force should derive from a reasonably small current density j and a reasonably large magnetic flux density B; (3) the product $j \times B$ should be reasonably large in order to achieve a specified velocity with a short channel length; (4) the quantity j should be approximately constant and within the limit set by an allowable erosion rate of the insulators between the anodes; (5) the axial or Hall potential gradient E_x should have a constant value over the channel cross section at any given axial location. If there is no current j_x in the axial direction, then $j_y B_z = n_e e E_x$ and, if n_e is constant across the channel, a constant gradient across the channel then should give uniform acceleration of the plasma over the channel cross section. Constant E_x can be obtained only with the same voltage difference applied across the plasma at all locations along the channel; (6) the axial potential gradient should not exceed approximately 50 volts/cm, which is an approximate limit above which breakdown along the walls may occur

One of the first steps in the design of the accelerator is selection of a satisfactory channel geometry. This task was complicated somewhat by the fact that it was necessary to utilize an already existing 10-megawatt power supply to power the accelerator. This power supply consists of eight separate modules, each rated at 500 volts and 2500 amperes. An accelerator designed with more than eight electrode pairs would be unable to have a separate power supply for each pair. The present 1-inch accelerator has a separate supply for each of 24 electrode pairs and operates equally well if the plasma generates the proper value of E_x or if it is applied. Since the former method is much simpler, it would be preferable to let the plasma supply its own E_x. With the larger accelerator, however, a resistor bank is required not only to supply the proper voltage gradient across the channel at each electrode but also the proper axial gradient. The available power-supply voltage thus limits the channel height as well as the Hall potential difference that can be applied.

A divergent geometry for the accelerator channel was considered, but difficulty in achieving a constant E_x over the channel cross section as

well as the limitations imposed by the power supply made this geometry unacceptable. A constant-area channel appeared to be the best compromise, and a detailed design of such a channel was made. We believe that the final design is a good compromise among the several conflicting criteria. The resulting accelerator is shown in figure 1. The channel is 2.5 inches square, the length is 18 inches, and the number of electrode pairs is 36. The accelerator has water-cooled copper electrodes. The sidewalls are boron-nitride plates, backed by water-cooled copper coated with beryllium oxide to prevent electrical breakdown. The expected variation along the channel of velocity, current density, and magnetic flux density is shown in figure 2.

When this accelerator performs as we hope it will, it should provide a means of investigating such things as heat transfer ($\dot{q}R^{1/2}$ in a stagnation region will be 3 or 4 times as large as in any other NASA steady-flow facility), aerodynamic forces, lifting bodies, and wakes, at a velocity corresponding approximately to Venus entry or to minimum-velocity Earth reentry from Mars.

A schematic of the 20-megawatt plasma accelerator facility is shown in figure 3. The arc heater that generates the plasma for the accelerator has been installed and is presently undergoing acceptance tests. The magnet has been designed and constructed. The resistor network to supply the proper voltages to the accelerator electrodes consists of inconel strips submerged in tanks of deionized water. This system has been designed and is presently being installed. The accelerator is to be cooled by a 1500 psi, 2000 gpm water system, which has been installed. The accelerator exhausts into a large duct 5 feet in diameter cooled by water sprayed over the outside surface. The duct pressure can be maintained at any value from atmospheric to 0.5 mm Hg, with mass flows as high as 0.2 lb/sec, by a four-stage steam-ejector pump. The duct and pumping systems have been completed and are in use.

NASA
L-66-1913

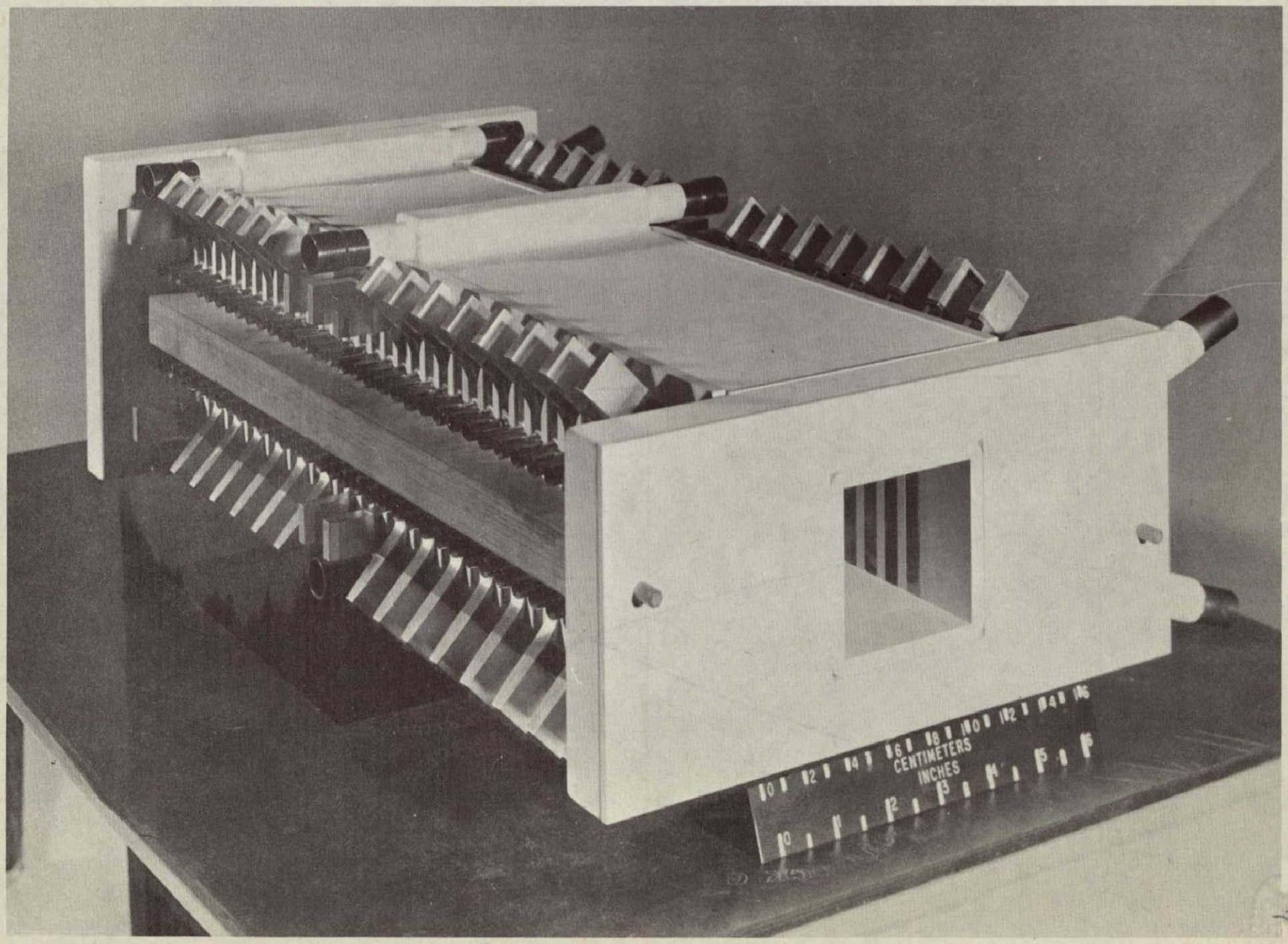

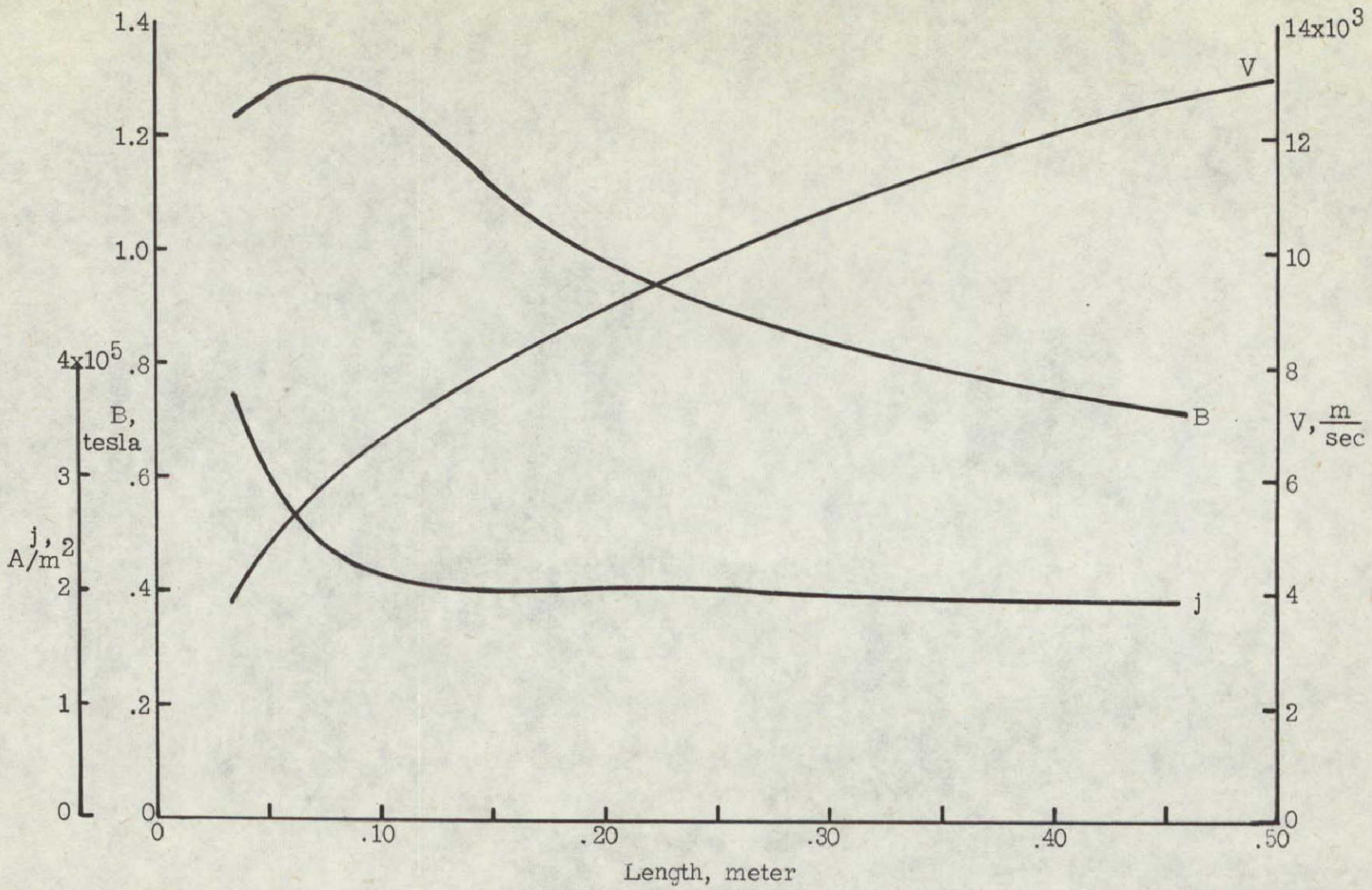

Carter et al-2

20 - MEGAWATT PLASMA ACCELERATOR FACILITY

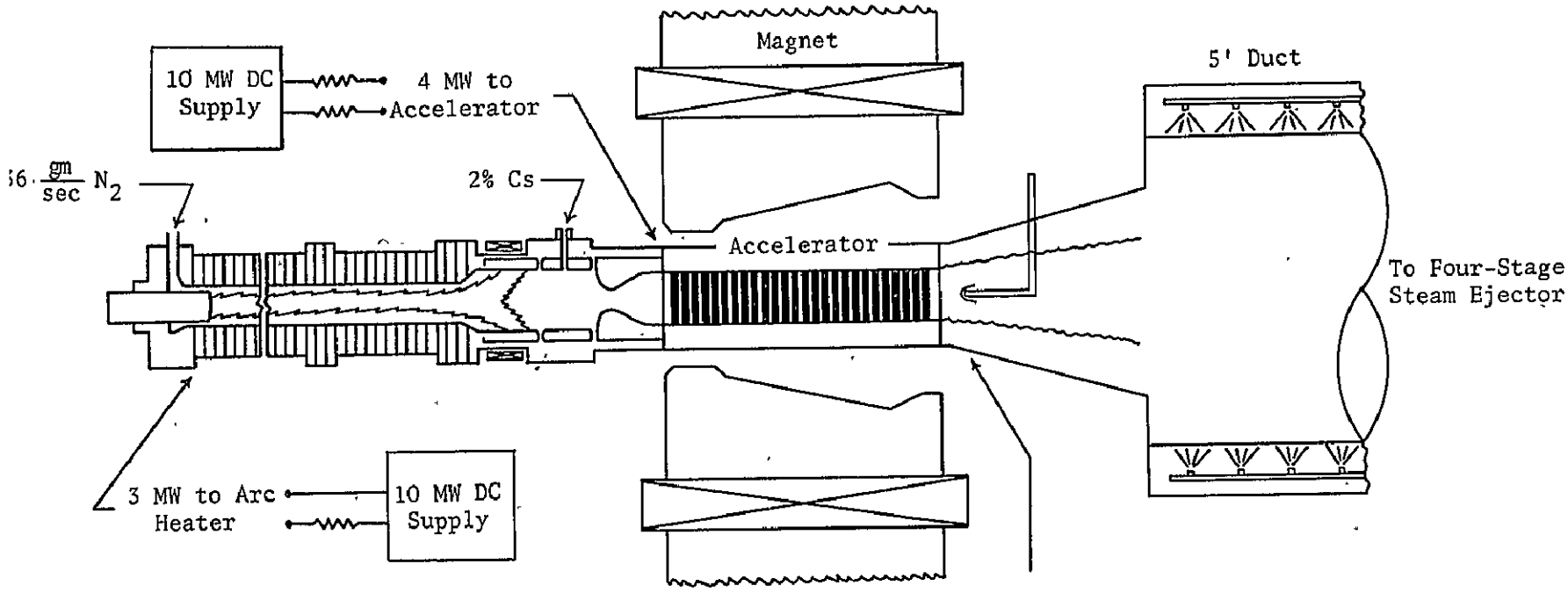

At Accelerator Exit

u = 13,000 m/sec	p = 0.03 atm
T = 8,000 ^{o}K	h_s = 12.5 × 10^7 J/kg
M = 5.0	A^s = 6.35 × 6.35 cm^2
ρ → 53 km Altitude	

Carter et al-3

THE THERMODYNAMIC PROPERTIES OF SEEDED NITROGEN

S. K. Park
NASA Langley Research Center
Hampton, Virginia

Certain high temperature plasma devices such as MHD generators and plasma accelerators use as a working fluid nitrogen seeded with an alkali metal vapor. It is usually assumed that since the degree of seeding is small the thermodynamic properties of this mixture are essentially those of nitrogen. To determine the validity of this assumption a study has been made of the equilibrium thermodynamic properties of high temperature (1000 to 20,000 $^{\circ}$K), moderate pressure (.003 to 3 atm.), seeded (0 to 5%) nitrogen. Calculations were based on a partition function analysis similar to those used in several studies of unseeded nitrogen, oxygen, and argon (ref. 1 and 2).

It was found that, because of the low ionization potentials and small partial pressures of the seed materials, their ionization could represent a significant energy sink in regions where nitrogen is essentially chemically inactive. In addition the increased number density of electrons resulting from ionization of the seed material causes a delay, until a higher temperature, in the ionization of nitrogen. These two effects tend to produce for a given seed material, rather well defined temperature - pressure regions in which even small degrees of seeding (1 to 2%, based on number density) produce large variation in a thermodynamic property, 10 to 40% in c_p/R, for example (fig. 1). In other regions the effect of seeding is found to be quite small even for as much as 5% seeding. It should be emphasized that the preceding statement is true only if proper allowances are made for the change in the average atomic weight of the mixture (and consequently a change in the mixture gas constant) caused by the mass fraction of seed material.

In general it was found that the effect of seeding on the thermodynamic properties of the mixture tends to become more pronounced at lower pressures. Also as might be expected the effect usually, but not always, becomes more pronounced as the seeding percentage is increased. In addition certain properties (the specific heats and, to a lesser degree, enthalpy and internal energy) are significantly more sensitive to seeding than others (entropy, speed-of-sound, departure coefficient Z, etc.). It is pointed out in reference 3 that essentially all the real gas effects inherent in the generator and accelerator equilibrium flow equations can be incorporated in the term

$$\beta = \gamma RZ \frac{\left[1 + \frac{T}{Z}\left(\frac{\partial Z}{\partial T}\right)_p\right]}{c_p} .$$

It is found that β is a strongly varying function of temperature, pressure (fig. 2), and degree of seeding.

1. Drellishak, K. S., "Partition Functions and Thermodynamic Properties of High Temperature Gases," Arnold Engineering Development Center, AEDC-TDR-64-22 (1964).

2. Ahyte, W. F., and Peng, Tzy-Cheng, "Approximations for the Thermodynamic and Transport Properties of High Temperature Nitrogen with Shock Tube Applications," NASA TND-1303 (1962).

3. Carter, A. F., McFarland, D. R., Weaver, W. R., Park, S. K., and Wood, G. P., "Operating Characteristics, Velocity and Pitot Distribution, and Material Evaluation Tests in the Langley One-Inch-Square Plasma Accelerator," presented at AIAA Plasmadynamics Conference, Monterey, California, March 2-4, 1966, paper no. 66-180.

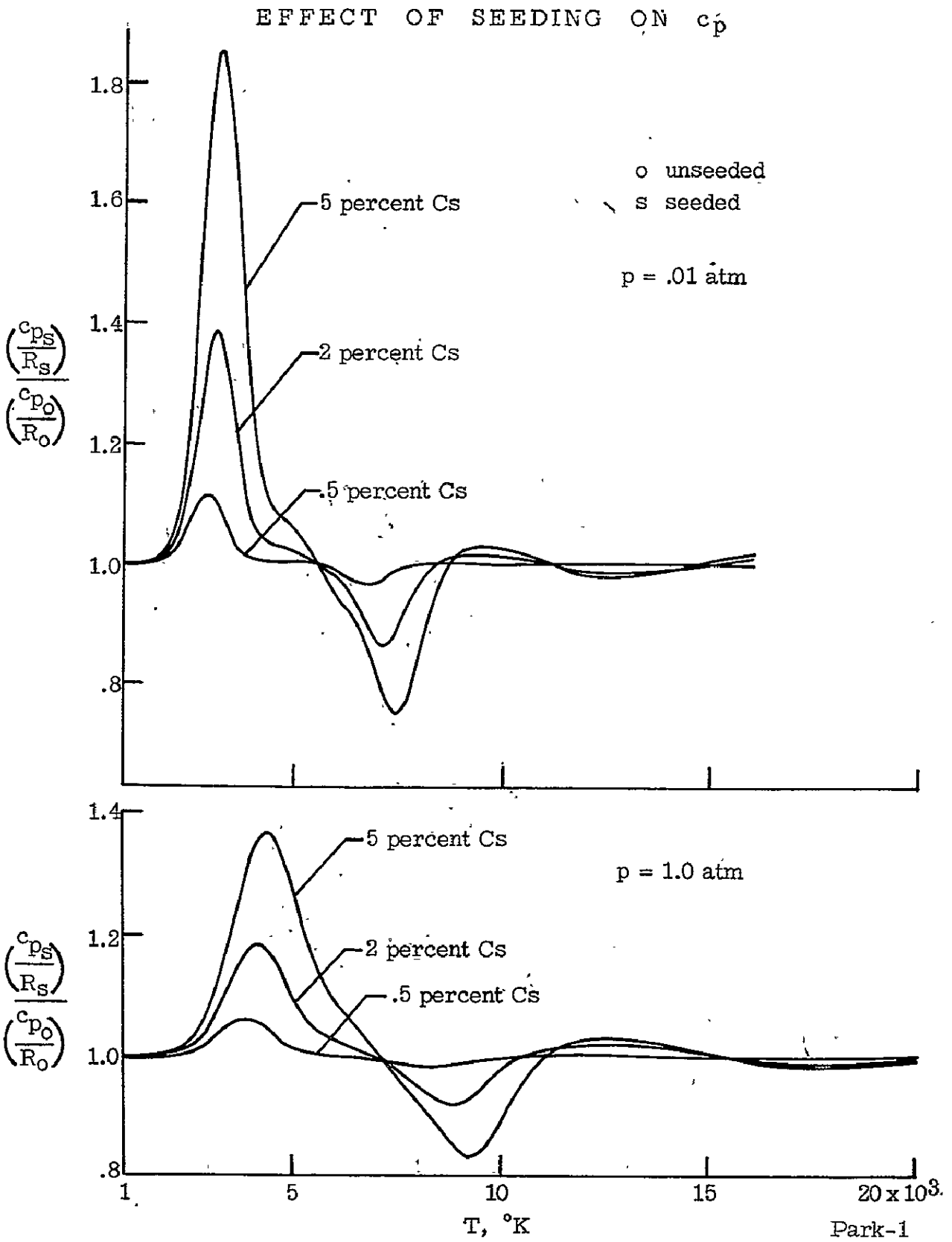
EFFECT OF SEEDING ON c_p
o unseeded
s seeded
p = .01 atm
5 percent Cs
2 percent Cs
.5 percent Cs
p = 1.0 atm
5 percent Cs
2 percent Cs
.5 percent Cs
$\left(\frac{c_{p_s}}{R_s}\right) / \left(\frac{c_{p_o}}{R_o}\right)$
1.8
1.6
1.4
1.2
1.0
.8
1
5
10
15
20 x 10³
T, °K
Park-1

VARIATION OF β WITH TEMPERATURE AND PRESSURE

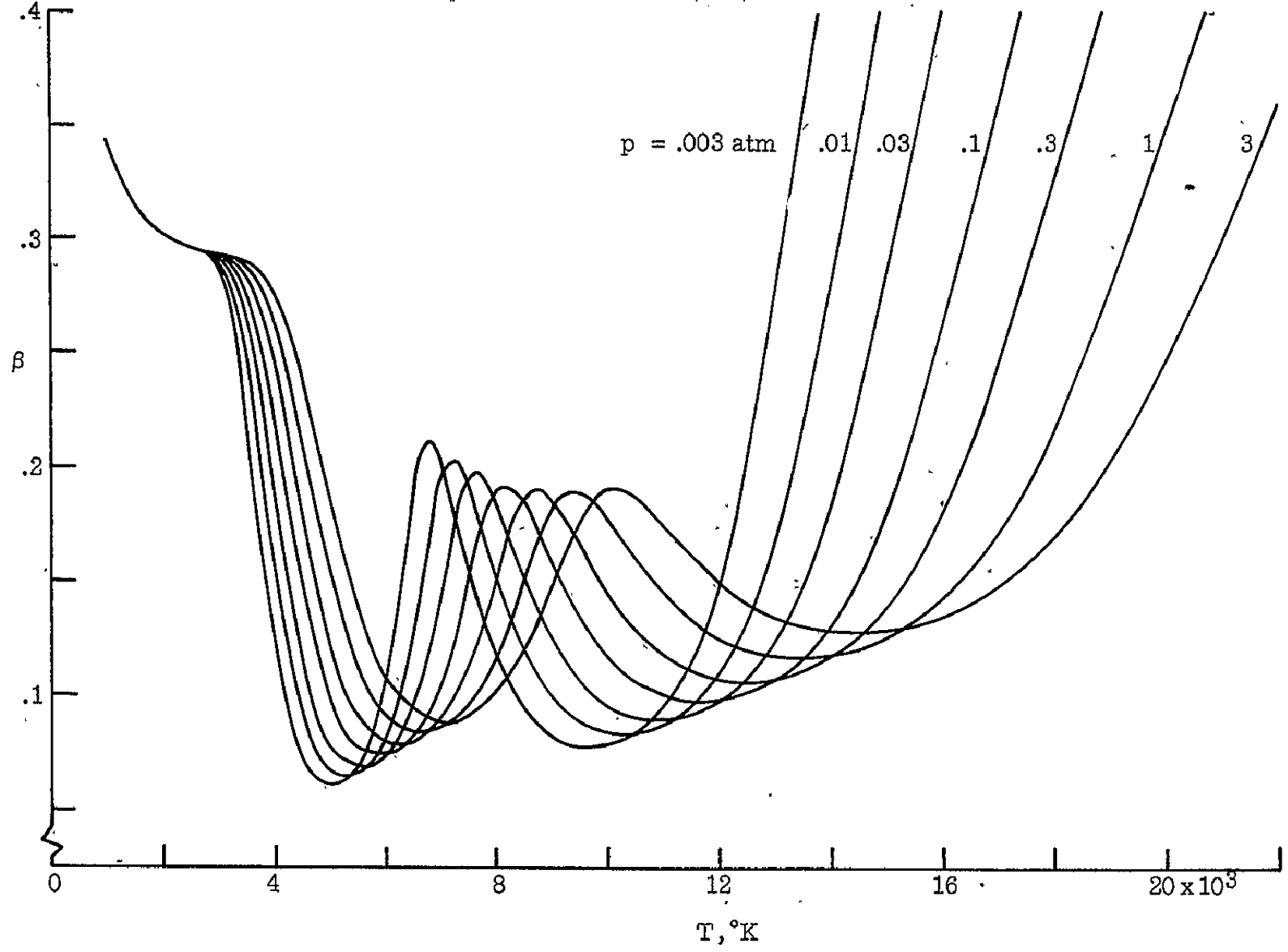

Park-2

ELECTRIC DRAGS AND TORQUES ON SATELLITES

F. Hohl and G. P. Wood

NASA, Langley Research Center
Hampton, Virginia

Conducting bodies moving through the rarefied and partially ionized upper atmosphere and magnetic field of the earth aquire charges, potentials, and sheaths. The charge distribution on and the potential distribution on and in the sheath of Explorer IX, a 4-meter-diameter sphere, and Echo II, a 41-meter sphere, have been calculated.

Inasmuch as Explorer IX is used to determine upper atmospheric density from the effect of aerodynamic drag on its orbital elements, the various electromagnetic drags were investigated to determine whether they might have a large effect on the derived density. The drag due to the increased effective cross section for ion impact, the drag due to ion scattering, and the induction drag due to the Lorentz force were calculated and shown to total only about 3 percent of the aerodynamic drag of the (uncharged) sphere.

With regard to Echo II, the Goddard Research Center had observed that it had a very nearly constant rate of spin for 280 days after launch. In order to attempt to explain how the spin rate could remain nearly constant for a long period, we calculated the various torques that might act on the satellite. These include the aerodynamic torque, the surface-charge torque due to relative rotation between the satellite and the portion of the surface charge that is due to induction, the Coulomb torque due to asymmetric impingement of ions on the polarized satellite, the eddy-current torque due to rotation of the conductive satellite in a magnetic field, and the induction torque due to asymmetry of the $j \times B$ force, where the j is due to non-uniform acquisition of ions and electrons over the surface. The results are summarized in the following table, which shows the average for a complete orbit of the calculated value of each torque about the axis of spin, in newton-meters:

Surface-charge	-6×10^{-21}
Aerodynamic	-1×10^{-7}
Coulomb	7×10^{-7}
Eddy-current	-8×10^{-5}
Induction	4×10^{-5}

It is seen that three of the torques that might affect the rate of spin of Echo II are small in comparison with the eddy-current (decelerating) torque and the induction (accelerating) torque. A balance (to better than an order of magnitude) between these two opposing torques has been obtained and is therefore the likely cause of the constancy of the rate of spin of the satellite.

References:

Hohl, F., and Wood, G. P.: The Electrostatic and Electromagnetic Drag Forces on a Spherical Satellite in a Rarefied Partially Ionized Atmosphere, in Rarefied Gas Dynamics II, ed. J. A. Laurmann (New York): Academic Press, 1963, 45-64.

Wood, George P., and Hohl, Frank: Electric Potentials, Forces and Torques on Bodies Moving Through Rarefied Plasmas. Paper No. 65-628, Am. Inst. Aeron. Astronaut., Aug. 1965.

Hohl, Frank: The Electromagnetic Torques on Spherical Earth Satellites in a Rarefied Partially Ionized Atmosphere. NASA TR R-231, Feby. 1966.

MAGNETIC COMPRESSION EXPERIMENT

By G. K. Oertel, J. Norwood and M. D. Williams
NASA Langley Research Center
Hampton, Virginia

A large theta pinch magnetic compression experiment has been built at Langley for the simulation of ultraviolet and soft x-ray spectra as observed by rockets and satellites from the solar corona. It is the primary goal of the experiment to generate the coronal ultraviolet spectra and record them with high spectral resolution in order to obtain the information for a detailed analysis of the spectra of highly ionized elements of solar interest. Since the excitation and ionization equations for this laboratory plasma are still of the coronal type, although the density is much higher than in the corona, and since the ionization equation is density independent, the spectrum should look characteristically much like the coronal spectrum, even as far as intensities of different lines are concerned, as long as the temperature is reproduced. Typical pinch experiments, including the present one, can easily achieve this end. Barring possible effects of nonuniformities in the temperature distribution, it may therefore be possible to draw certain conclusions regarding ionization and recombination rate coefficients and transition probabilities.

The need for extensive spectroscopic work of this type was emphasized by the 1965 Woods Hole Summer Study by the Space Science Board of the NAS-NRC: "The XUV spectrum of the sun has shown the existence of a great gap in our knowledge of the spectra of highly ionized atoms. For example, the observed solar lines from 171 to 500 Angstroms have defied identification. . . . It is important to assure the vigorous continuation of this work, persuading more spectroscopists to enter the field, and using computer methods of analysis, until the energy level systems of the common solar elements are completely known in all stages of ionization encountered in the corona."

Table I lists the parameters of the three capacitor banks which are connected in parallel to a common collector plate and coil. The present coil is 137 cm. long with 10 cm. inner diameter and constitutes approximately 65 percent of the total inductance of the main discharge system. An ultrahigh vacuum system (base pressure below 10^{-8} Torr) serves to insure clean operating conditions in the quartz shock tube. Observations may be made side-on down to the transmission cut-off of air, and end-on in the vacuum ultraviolet. The tube is filled with highly purified hydrogen (Palladium leak) and traces of the impurities the spectra of which are to be studied. The operation of the theta pinch need not be described here; it is quite analogous to that of Pharos at the NRL.

The spectra obtained from the magnetic compression experiment are being evaluated in association with the University of Florida under grant NGR 10-005-049, including the development of a computer program for the detailed analysis of energy level systems.

At the present time, the spectroscopic investigations in the XUV have been carried out with a normal incidence monochromator converted for film recording of spectra in a limited wavelength range. All spectra recorded so far are time integrated, i.e., over all half-cycles of the discharge. The spectrum from the hottest phase is masked by the more intense spectra emitted during cooler but more contaminated later phases. They are, nevertheless, being carefully evaluated at this time because they can serve as a convenient reference spectrum for later time-resolved spectra.

A unique shutter is under procurement which will permit the attainment of exposure times of the order of 1 microsecond at predetermined times, and possibly the recording of several spectra at different times from a single event on the same plate. A normal-incidence 2 meter Eagle spectrograph for high spectral resolution and wide spectral coverage is likewise under procurement. Its effective use with the shutter will require a collector plate extension which is being procured.

Supporting experiments in house include a spectroscopic preheater study with time and space resolution which is described in a separate abstract. A mock-up experiment on half-scale for precision magnetic field measurements is now being completed. It will serve to investigate the effects of flux concentrators and other techniques on the uniformity of the magnetic field in the coil. Experiments with preliminary field shapers on the magnetic compression experiment have demonstrated an improvement in the containment times under typical operating conditions. More work is, however, needed before definite conclusions can be drawn. A special coil with a non-zero minimum magnetic field (magnetic well) has been constructed and is being tested. Both of these efforts towards greater plasma stability and longer containment times are described in more detail in separate abstracts. They are important for this effort, because relaxation times for the establishment of ionization equilibrium tend to be of the order of 10 microseconds (or the quarter period of the discharge) for the highest stages of ionization.

In a proposed out-of-house experiment, the Zeeman splitting of some spectrum lines could be observed in a much smaller device with the aid of a unique technique for the observation of extremely weak spectrum lines developed by R. T. Schneider under contract NASw-922. This would greatly aid in the identification of the spectra, providing direct checks on the level assignment made on the basis of the spectra obtained from the magnetic compression experiment.

TABLE 1. CAPACITOR BANK PARAMETERS

	PREHEATER	BIAS FIELD	MAIN	UNITS
Capacitance	9	10^3	5×10^3	MicroFarads
Energy Storage	2	70	1000	KJoules
Operating Voltage	20	12	20	KVolts
Coil Voltage	6	3	16	KVolts
Frequency	300	10	20	Kcycles/sec
Peak Current	350	700	1.2×10^4	KAmps
Coil Inductance: 10^{-8} Henries				

A PRELIMINARY STUDY OF FIELD NONUNIFORMITY IN A LONG THETA-PINCH COIL

Joseph Norwood, Jr.
NASA Langley Research Center
Hampton, Virginia

As a device for producing and containing a high temperature plasma, the theta-pinch has enjoyed considerable success. It has the advantages that the plasma is not contaminated by contact with metal electrodes and high densities and temperatures can be attained. The instabilities, while numerous and varied, are not felt to be incurable.

The most "dangerous" of these instabilities are the drift of the plasma column into the tube wall and the break-up of the column into Rayleigh - Taylor flutes due to plasma rotation. For experimental geometries common to most of the large theta pinches, these instabilities limit the confinement time to typically ten microseconds, often less than the half period of coil current oscillation.

The drift instability is caused by a gradient in the magnetic field of the coil in the plane of the current feed slot. The plasma column possesses a certain magnetic moment per unit length due to its azimuthal current, hence a force is exerted antiparallel to the field gradient, i.e. toward the feed slot. For a hydrogen plasma with a kinetic temperature of one keV in an average axial field of 10^5 gauss the drift time to the wall is 5 microseconds if the gradient across the coil diameter of 10 centimeters is 100 gauss.

The cause of the rotation of the plasma column is being debated, however, the mechanism proposed by Haines and analyzed by Thronemann and Kolb seems best to fit the situation in long theta-pinches. In this model an axial Hall current is assumed to be generated by the interaction of the azimuthal current with the radial component of magnetic field. The Hall current and the radial component of field then produce a Lorentz force on the plasma column in the azimuthal direction. For stability, the finite cyclotron radius theory requires that transverse fields be held to less than a few per mil of the axial field.

The requirement for a collector plate in a large theta-pinch experiment dictates the geometry to a large extent. A large number of coaxial cables must be connected to the plate which must transfer the current with low inductance to a coil one or two meters in length. This requirement suggests a long narrow set of plates with close spacing. The

cables are connected to one of the long sides and the coil is symmetrically attached to the other. The current must then funnel into the coil giving rise to a field curvature in the coil. It is this field curvature and the consequent gradient of the field in the coil which contributes most to drift instability in large theta-pinches.

Due to the finite length of the coil the field lines diverge producing an azimuthally symmetric radial gradient which increases as one approaches the end of the coil from the center plane. The field approaches uniformity within one per mil at a distance of two radii from the end, hence stabilization against drift due to the "minimum B" well is confined to the very ends and cannot be expected to stabilize the drift in large experiments where the ratio of length to radius is near 20.

Plasma shape may also influence the magnetic field shape. In the event the plasma contracts axially such as to concentrate itself near the median plane of the coil, that portion of the coil will have lower inductance and the driving currents will concentrate more heavily there.

For the case where the skin depth is much less than the thickness of the plates, the partition of the current in a parallel plate transmission line between the inside and outside surfaces of the conductor plates is a function of the gap spacing, h, and the plate width, b. If h/b varies along the transmission line the current must spill around the end to get from the inside to the outside or vice versa. From the feed slot to the center of the coil h/b changes from 10^{-3} to 10^{-1}. The effect on the field gradient in the coil is opposite to that induced by the current geometry, i.e., the gradient points toward the slot.

The axial distribution of current in a high frequency coil is not uniform as in the D.C. case. The limiting value of field at the end of the coil is 5.4×10^5 gauss for the beryllium - copper alloy in the Langley Magnetic Compression Experiment. Typically, 75 percent of the current is concentrated within one radial length of the coil ends. The effect on the current is that upon entering the coil, axial current components are set up both on the inside and outside surfaces of the coil. The effect on the field is a gradient pointing toward the feed slot.

A half-scale model of the coil and collector plate of the Langley Magnetic Compression Experiment has been built in order to measure the non-uniformity of the field and to serve as a test facility for different coil configurations designed to improve the uniformity of the field. The model is powered by a 13.5 KJ capacitor bank. The discharge is tuned by variable inductors such that the skin depth scales also as 1:2. A system of probe coils is being constructed which will measure $B_z(r,\theta,z)$ and $B_r(0,0,z)$ with an anticipated accuracy of a few per mil.

Solutions to the problem of field gradients which have been employed by other theta-pinch groups have involved modifications to the current collector plates. The solution which is being pursued at Langley involves the use of flux concentrators. Any good conductor

which is introduced into a high frequency magnetic field develops skin currents which exclude the field from its interior. The axial current components in the coil above and below the feed slot are antiparallel. Thus closed current loops will be formed on the outer surface of the flux concentrator and the axial component of current will be shielded from the coil interior. The contribution of axial current components to the field gradient in the coil can thus be eliminated except for non-symmetric axial currents which cross the median plane. These are expected to be small.

FLUX CONCENTRATOR FOR THE SUPPRESSION OF FIELD GRADIENTS

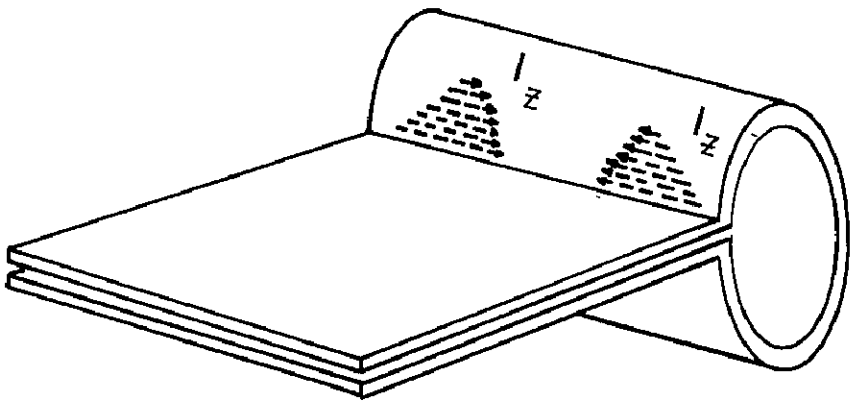

COIL

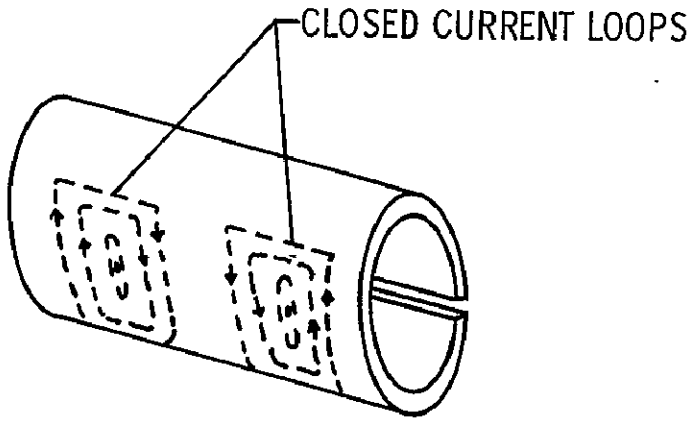

FLUX CONCENTRATOR

A MINIMUM-B TYPE COIL

By W. A. Cilliers[+]
NASA Langley Research Center
Hampton, Virginia

In the search for ways of stable confinement of θ-pinch plasmas, many configurations have been tried out. So far all of these suffer from instabilities that turned out to be intolerable. Ways have, however, been found to eliminate the more serious of these instabilities in some cases - or to reduce their growth rates.

Theory gives some criteria that have to be satisfied for achieving hydromagnetic stability. One such criterion is that the magnetic field lines must be convex towards the plasma. This is achieved in the cusp geometries. Here, however, the loss rate is high since it is impossible to satisfy the condition everywhere over a closed surface.

In the theta-pinch,end losses can be reduced by means of mirror fields. Particles having kinetic energy parallel to the coil axis will be reflected provided that the angle between the velocity vector of the particle and the coil axis at the end plane is greater than a certain angle determined by the mirror ratio. Furthermore, a condition that a charged particle be reflected is that its magnetic moment, μ, be an adiabatic invariant. This implies that the magnetic field varies little (as seen by the particle) during one gyration. The drift energy of the particle is slowly changed into gyration energy.

In the mirror machine the magnetic field in the central portion of the pinch is decreasing in the radial direction. Hence, instabilities that tend to carry plasma in the radial direction, at the midplane, e.g., can extract energy from the plasma to support their own growth since

$$\mu = \left(\frac{\frac{1}{2} m v_{\perp}^{2}}{B} \right)$$

is constant.

The obvious remedy for this is to make the field increase in all directions from the center of the container. This has led to the idea of the so-called minimum $|B|$ field configuration or magnetic well. It has been shown by various people (e.g. Taylor (2) and Schmidt (1)) that min $|B|$ fields offer hydromagnetic stability for low density plasmas.

In practice the so-called Joffe experiment has shown that a min $|B|$ field results in some improvement of containment for a low density plasma in the mirror machine.

[+]NAS-NRC Senior Post-Doctoral Resident Research Associate.

We are investigating a coil that gives such a magnetic well at its center. This type of coil was first proposed by Andreoletti and could be described as a tetrahedral spire (see fig. 1). Calculations of the magnetic field everywhere inside the coil for uniform (DC) current distribution in the coil were carried out with the slopes of the sides and the aspect ratio as parameters. It was found that slopes of 0.75 and -0.375 respectively for the two sides and an aspect ratio of 0.5 give the best well. Even so the region over which the contours of constant $|B|$ are completely closed is quite small in the x-z plane as shown in figure 2. In figure 3, the contours are shown in a plane at 45° to the x-z plane. It seems that most particles moving away from the center of the coil will encounter an increasing magnetic field.

Preliminary measurements of the field when a current of frequency 25 kc/s is sent through the coil indicates that the well region is bigger than at DC. Measurements at 400 kc/s are at present under way.

It is realized that when a plasma is introduced into the coil, the contours of $|B|$ could be changed considerably for anything but a very low β plasma. Theoretically, the depth of the well is not important. There should, however, not exist high field gradients that can destroy the "adiabatic" movement of the particles.

If the present field measurements should give promising results, an attempt will be made to study the behavior of a plasma inside the coil.

---

[1] Schmidt, G., Phys. Fluids 8, 754.

[2] Taylor, J. B., Phys. Fluids 7, 767.

NASA
L-66-2788

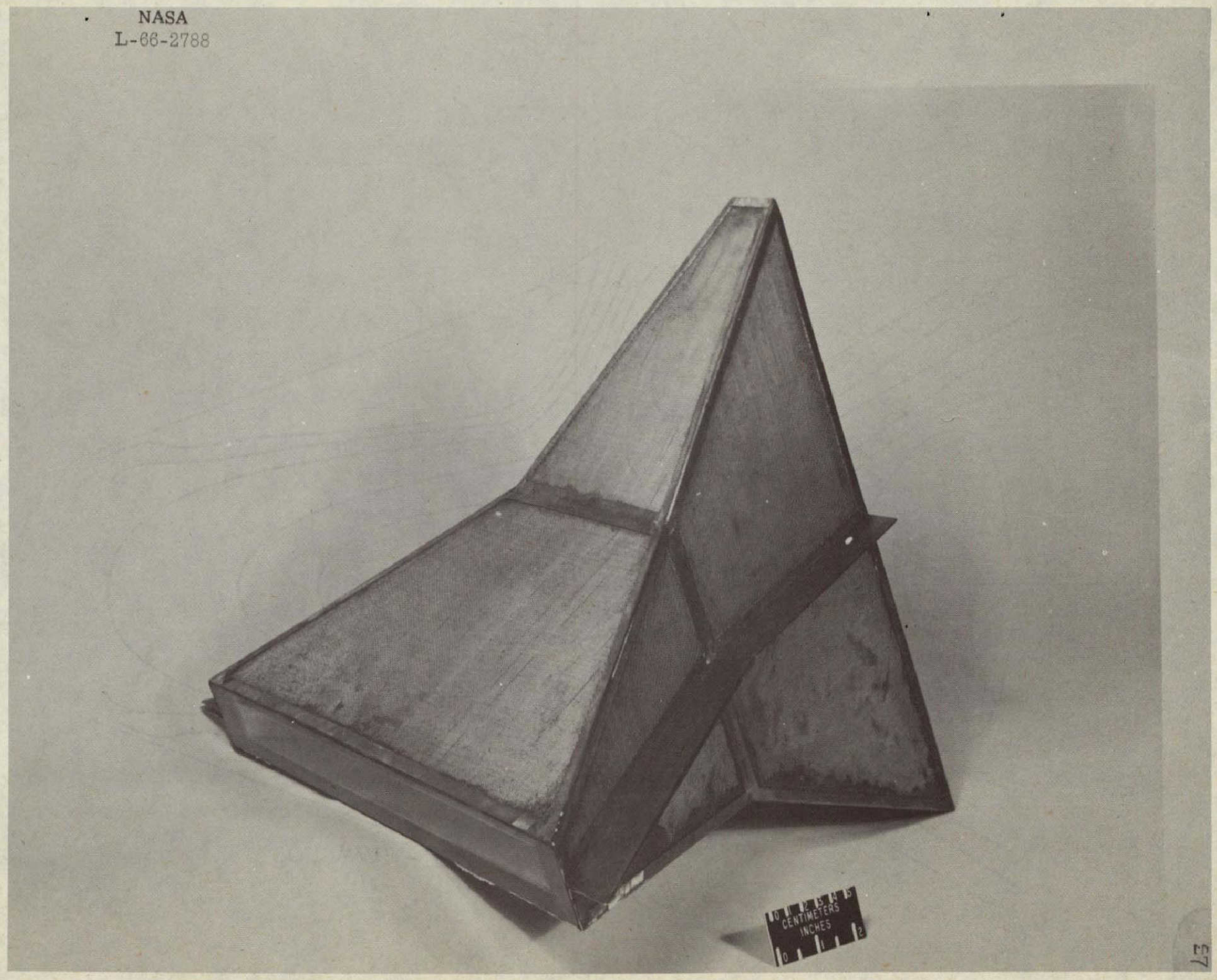

CONTOURS OF |B| IN x - z PLANE

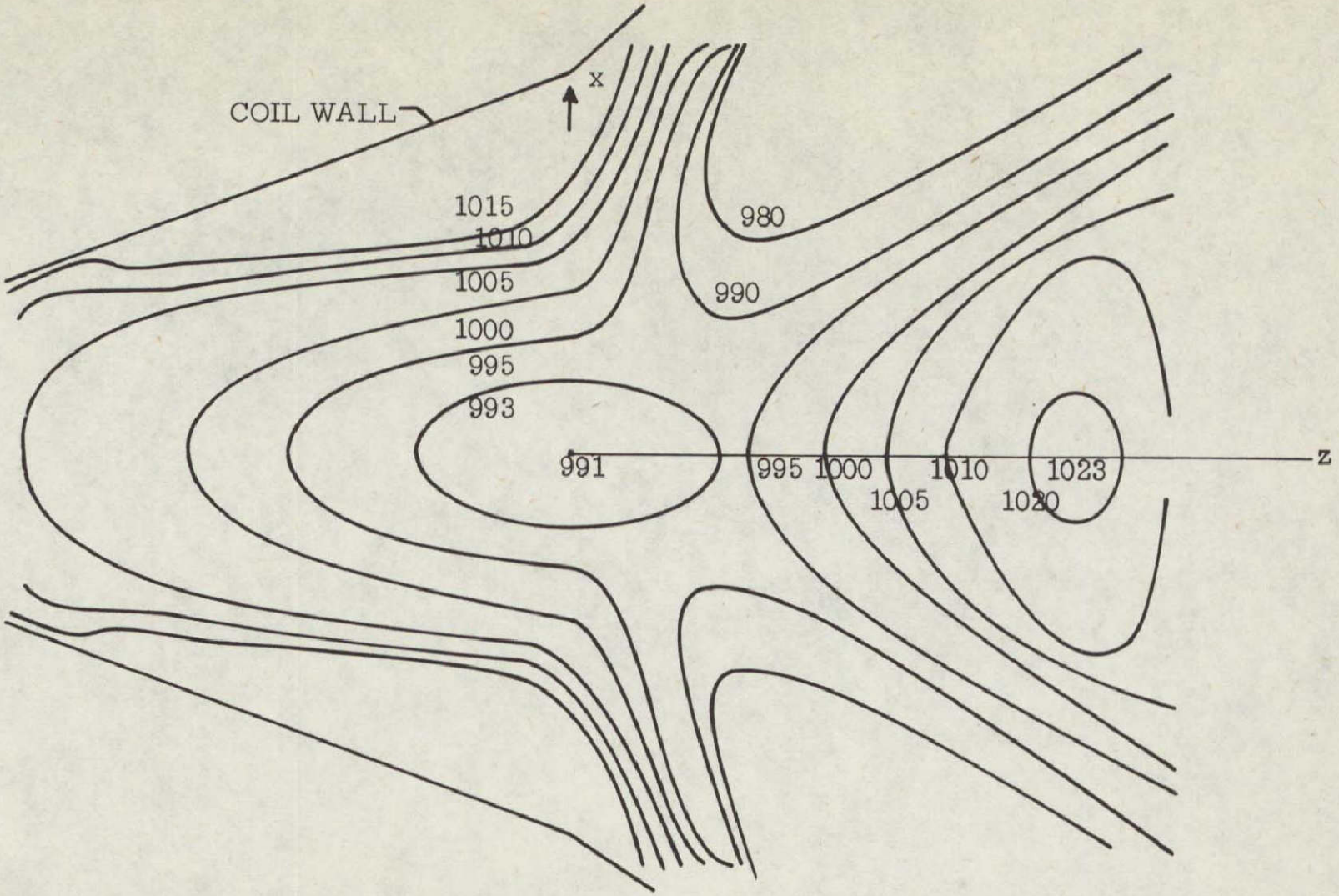

CONTOURS OF |B| IN PLANE AT 45° TO x - z PLANE

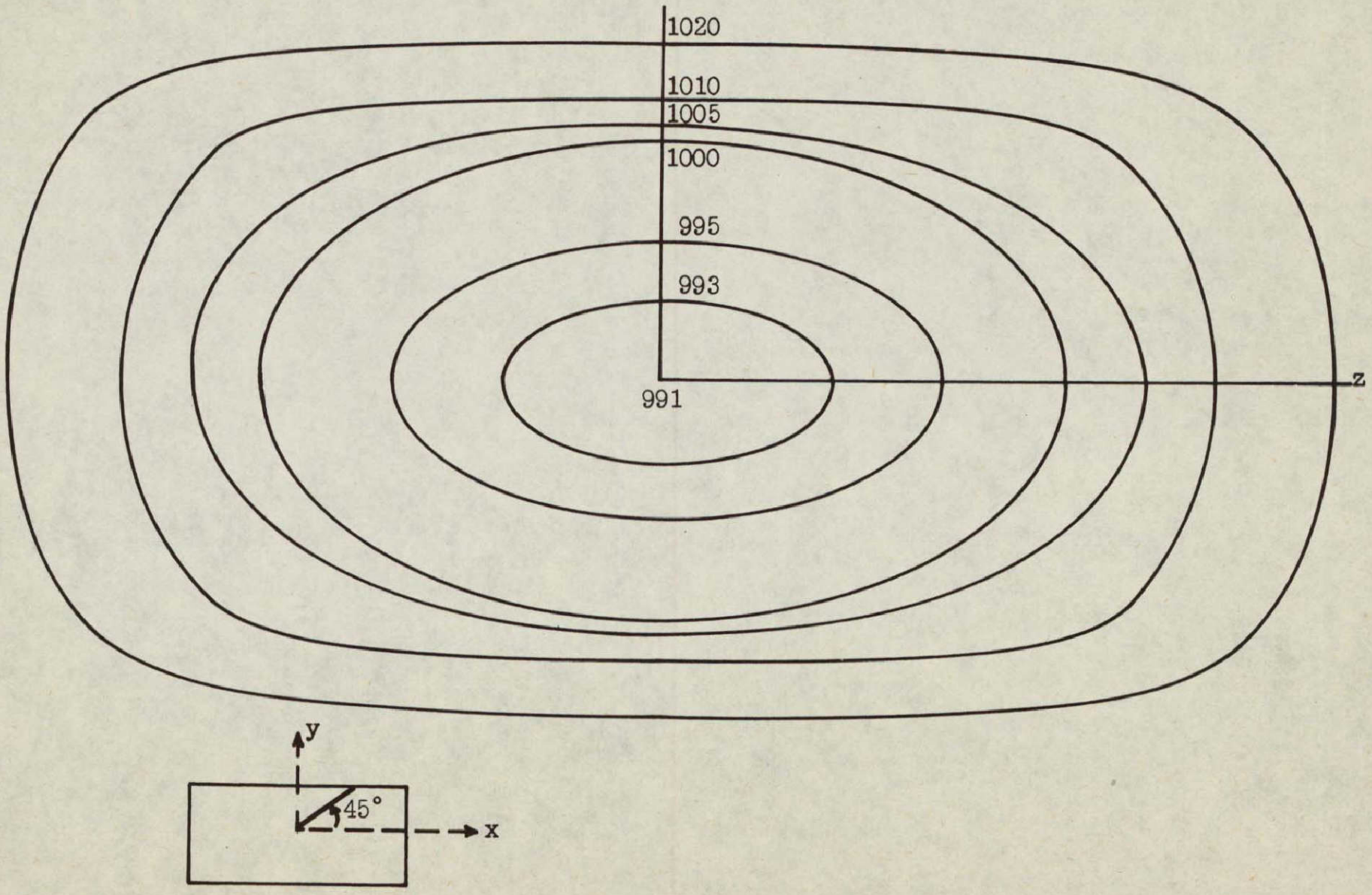

NEW JITTER MEASURING TECHNIQUE AND APPLICATION TO SPARK GAP STUDIES

M. D. Williams
NASA Langley Research Center
Hampton, Virginia

The capacitor bank is a popular source of energy for plasma experiments and its switches play an important role in determining how well it performs. A better understanding of the factors that govern the performance of switches is therefore desirable.

The perfect switch will switch unlimited energy in zero time. The practical switch is limited in both respects. In today's typical bank the energy limitation is met by using more and/or larger switches. This approach puts greater demands on switch synchronization, however, and provides a stimulus to improve switch synchronization.

It is well known that spark gap switches, although triggered simultaneously, nevertheless conduct at different times. This phenomenon gives rise to the term "switch jitter." Switch jitter affects system performance several ways: (1) it determines the magnitude of circulating currents; (2) it determines the voltage rate of rise at the load; (3) it determines the magnitude of voltages reflected from the load; and (4) low switch jitter is desirable any time synchronization of other associated systems is involved. The purpose of this project is to determine what factors affect switch jitter and how they affect it in order to be able to minimize switch jitter, or, perhaps, to reveal compelling reasons for an improved switch. Because of its wide-spread use, the trigatron switch (two hemispherical electrodes with a trigger pin inserted in one of them) will be used in the project.

During tests of the apparatus for the Magnetic Compression Experiment at NASA Langley, it was necessary to measure jitter of the switches. A system using a novel optical technique was devised (ref. 1). A number of light pipes were positioned near and pointed at a sample number of the 205 switches of the system. The other ends of these light pipes were positioned to form a horizontal slit in the field of an image converter camera. By triggering the camera streak shortly before ignition of the switches, a time history of switching was obtained on photographs. A typical result is shown in figure 1. This same general method will be used in the investigation of the parameters that affect switch jitter. With the arrangement used in reference 1, the intensity of the light transmitted to the camera was limited by the solid angle of acceptance of the light pipes, the different attenuations of the light pipes, and the suspected movement of the switch discharge. These factors resulted in errors in the recorded initiation times of the discharges. For illustration, let figure 2 represent the light intensities at the camera

of switches A, B, C versus time (not to scale). It is evident that although A and B actually switched at the same time, their streak representations would begin at different times, t_1 and t_2. Also, any irregularities in later portions of the light pulse would produce similar effects, as illustrated by C.

The illustrated errors will be minimized by the present apparatus which is just becoming operational. In it six ellipsoidal cavity reflectors are mounted in a compact hexagonal configuration. A spark gap is located at one focus of each reflector so that practically all the light from it will converge to the other focus where it will be collected by a short light pipe and fed directly to the photocathode of the electronic streak camera. Light intensity is expected to be increased by several orders of magnitude. (The effect could be represented on figure 2 by increasing the respective slopes thereby yielding a truer streak representation of the actual firing times.) The system also includes other features that will facilitate investigation of the effect of such parameters as trigger voltage risetime, electric field, and pressure.

The switching times to be observed are expected to consist of two components, (1) a constant component due to the parameters, and (2) a random component due to the availability of a particle to start the discharge. Figure 3 shows results obtained from tests on the Magnetic Compression Experiment apparatus. The two components are evident from the plot of the number of switches fired, $\frac{n}{100}$. No switch fired earlier than 40 ns. Part of the 40 ns is the formative time of discharge required by each switch and determined by the various parameters. (The other part is due to the time difference of streak and switch triggers.) The various additional times are random components that can be predicted from a probability curve represented by $\frac{dn}{dt}$. (It is interesting to note that the curve is not Gaussian as is usually assumed.) Similar data will be taken with the new apparatus. It will be treated statistically by a computer technique to recover these components.

1. G. K. Oertel, M. D. Williams, Rev. Sci., Instr., vol. 36, no. 5, 672-673, May 1965.

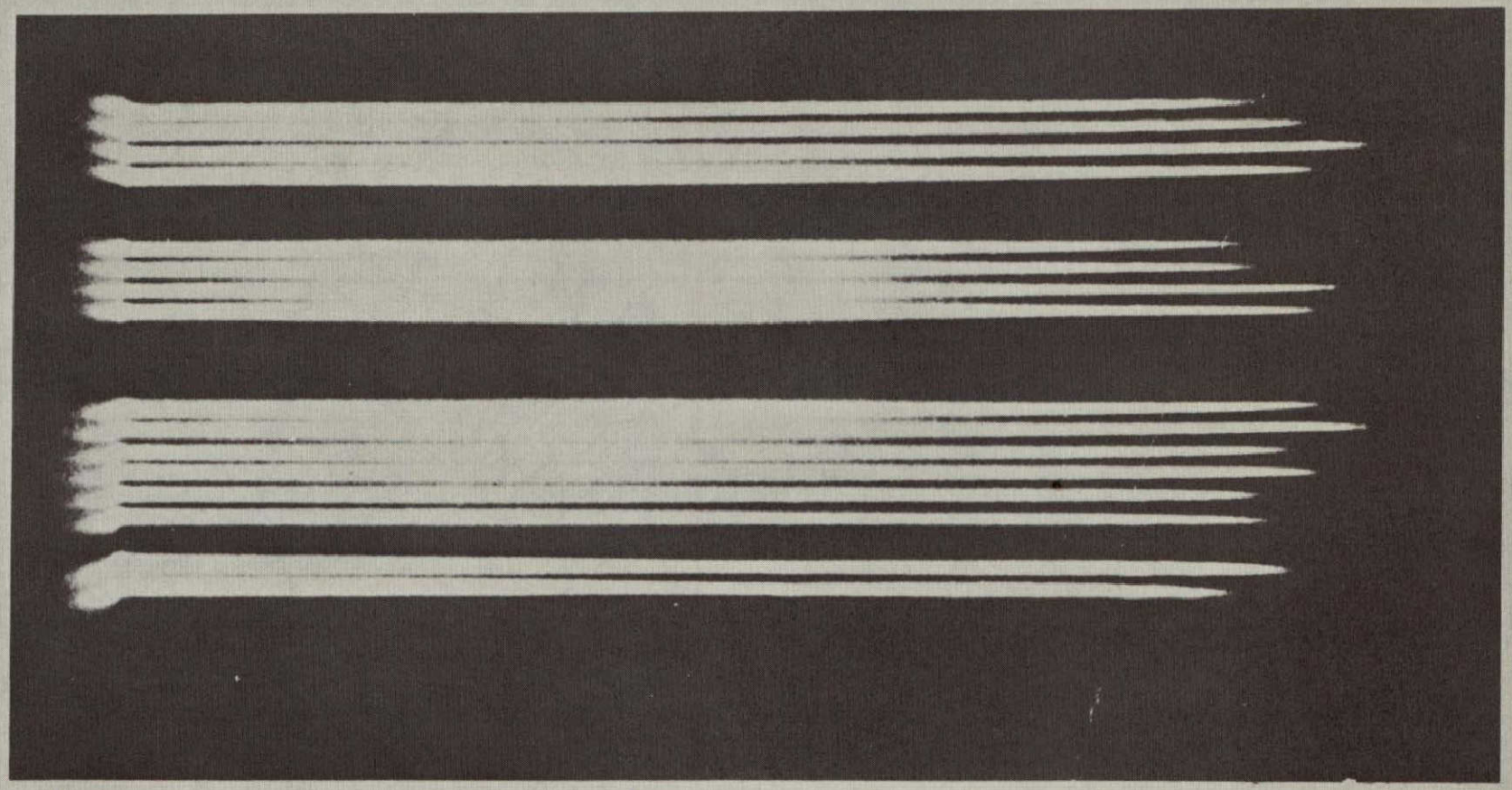

.2 μ sec

EFFECT OF LIGHT INTENSITY VARIATIONS

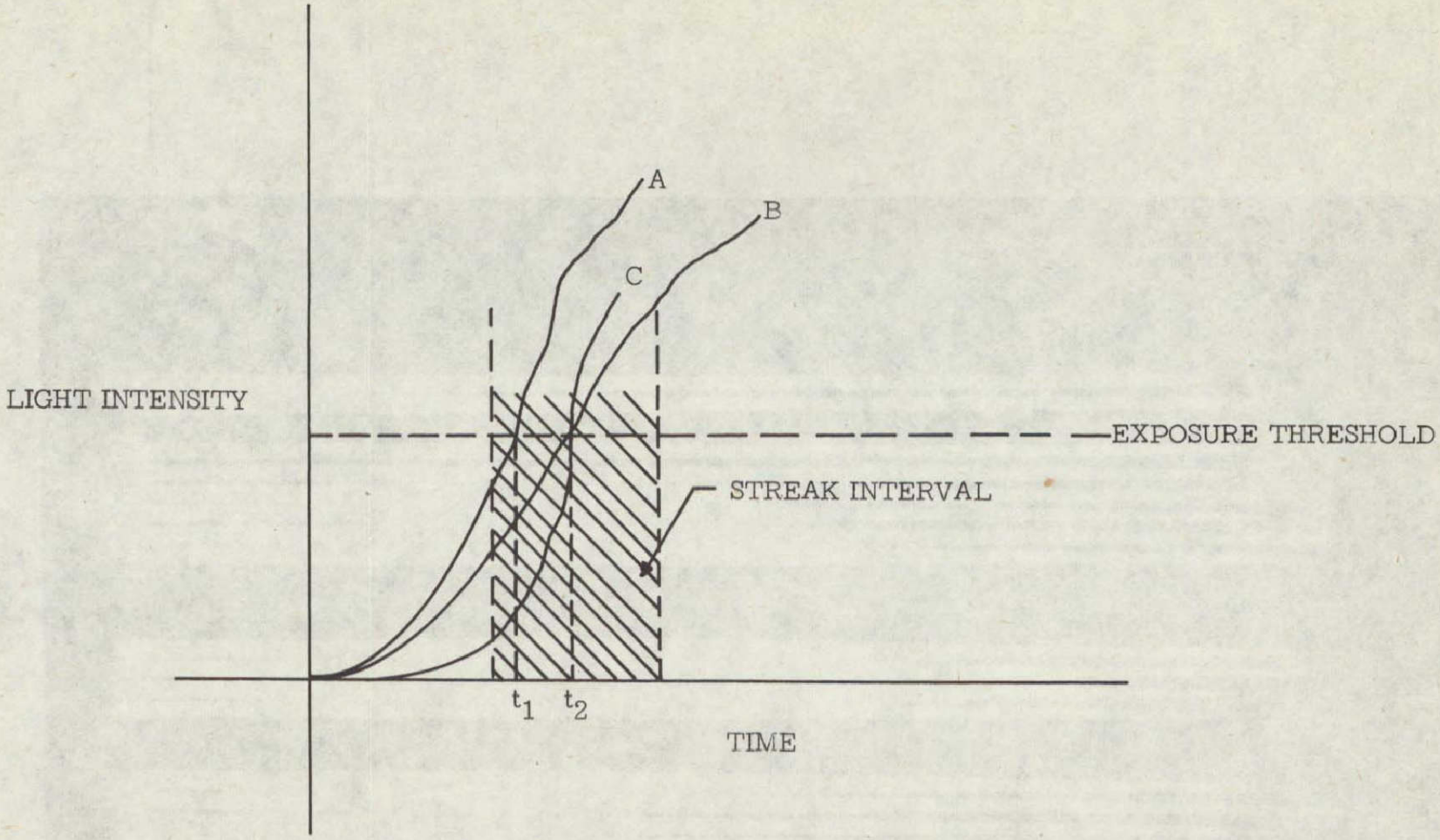

Williams-2

SWITCHING TIMES AND PROBABILITY OF SWITCHING

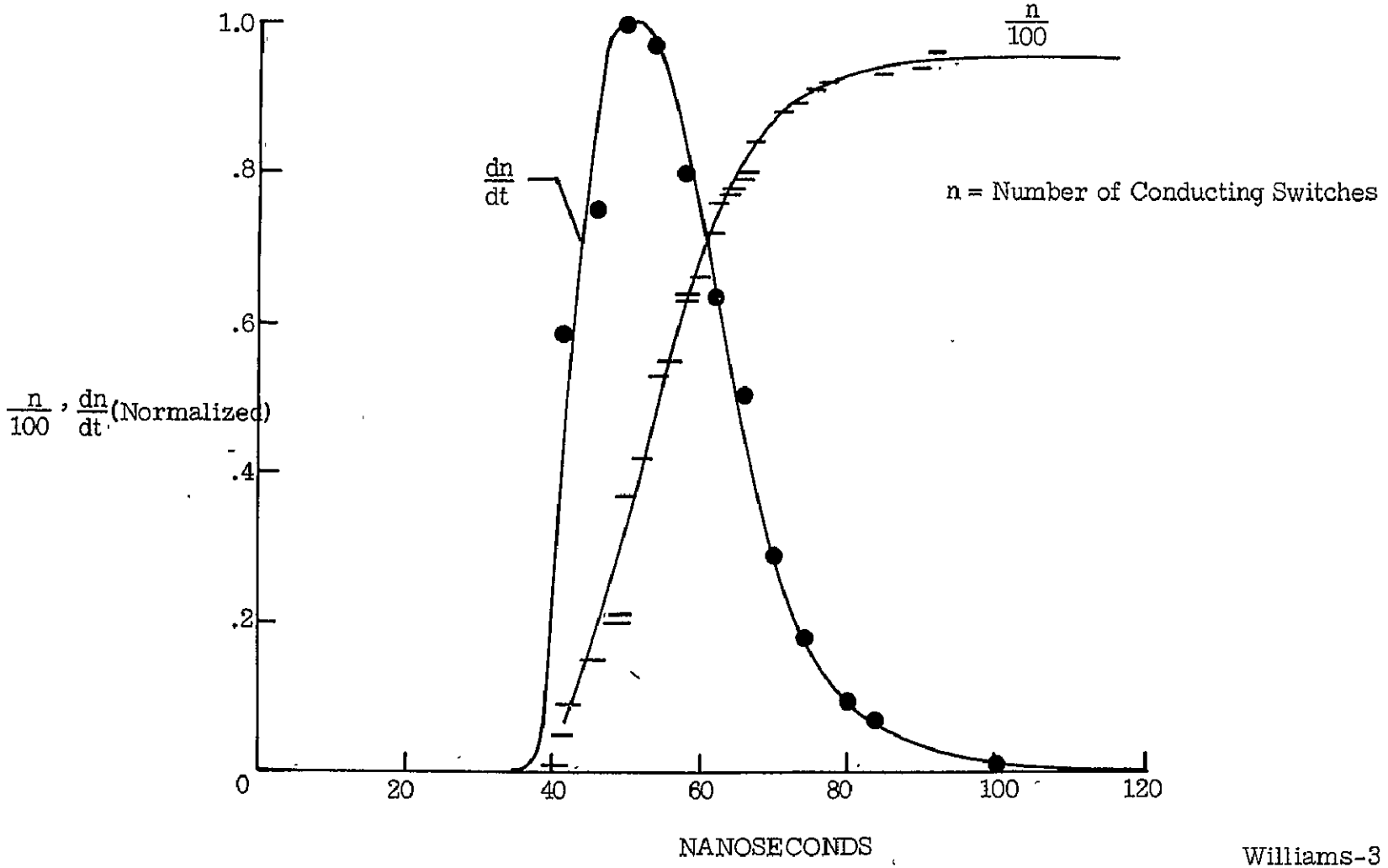

Williams-3

SEMI-CORONA IONIZATION EQUATIONS

G. K. Oertel
Langley Research Center
Hampton, Virginia

In local thermodynamic equilibrium (LTE) the ionization is described by the Saha equation

$$\frac{N_1^Z N_e}{N_1^{Z-1}} = 2\,\frac{g_1^{\,Z}}{g_1^{\,Z-1}} \cdot \frac{1}{a_0^3}\left(\frac{kT}{4\pi E_H}\right)^{\frac{3}{2}} e^{-\frac{E_\infty^{Z-1} - \Delta E_\infty^{Z-1}}{kT}} \qquad (1)$$

where N^Z and N_e are the number densities of atoms in the stage of ionization Z ($Z = 1$ for neutrals) and electrons, respectively, a_0 is the Bohr radius, E_H the ionization energy of hydrogen, kT the temperature in energy units, $E_\infty^{Z-1} - \Delta E_\infty^{Z-1}$ the corrected ionization energy of atoms in the stage of ionization Z, and the g_1's are statistical weights of the respective ground states. Among the many causes of deviations of the actual ionization equilibrium from the ideal LTE one of the most prominent occurs in optically thin low density plasmas. The assumption of small optical thickness implies that most of the emitted radiation leaves the plasma without reabsorption; therefore the principle of detailed balancing is violated and deviations from the Saha equation may be expected.[1,2,3] The extreme case occurs in the solar corona, where collisional excitation and ionization rates are balanced exclusively by radiative rates; it is referred to as corona equilibrium.[4,5] In the more general case of competing radiative and collisional rates one speaks of semi-corona equilibrium.

The more comprehensive approach to finding the ionization equation in this general case was taken by D. R. Bates et al[6] who solved the complete set of rate equations for all atomic states, neutral and ionized, in hydrogen, as well as in a pseudo-alkali atom consisting of a hydrogen atom with omission of the ground state $n = 1$. This had to be carried out numerically on an electronic computer; and the results are given in tabular form. Griem[1] has proposed a functional form which, in the case of hydrogen, agrees rather well with Bates' et al results, but which is so complicated as to make practical calculations extremely difficult, and which must itself be programmed for a computer if results of any extent are desired. A correction factor for the Saha equation was derived previously[3] on the basis of a simple model and has been compared here to correction factors computed from the tables of Bates' et al. It became apparent that with a minor empirical modification the simple correction factor agrees well within the precision of the

cross sections used by Bates et al with their results for all electron densities and temperatures. It should be used as a factor on the right side of the Saha equation (1) in the form

$$\tau = \begin{cases} \tau' = 18\ \xi N_e \left(\frac{a_o}{\alpha}\right)^3 \left(\frac{E_H}{E_\infty^Z - \varepsilon_o}\right)^3 \sqrt{\frac{E_H}{E_\infty^Z}};\ \left(\frac{\alpha}{a_o}\right)^3 = 2.9 \times 10^{18} \text{cm}^{-3} \\ 1 \quad \text{for} \quad \tau' \geq 1 \end{cases} \tag{2}$$

where the collision limit ε_o is given by

$$\varepsilon_o = E_H \left[\frac{3}{4} N_e \left(\frac{a_o}{\alpha}\right)^3 \left(\frac{E_H}{E_\infty^Z}\right)^2 Z^7\right]^{\frac{2}{9}} \tag{3}$$

and ξ is the number of equivalent electrons in the ground state. It can be shown that this factor scales with Z in the same way as the equivalent factor computed by Bates et al (except for the collision limit ε_o). A comparison between the present and Bates' correction factors is shown in tables 1 and 2 for hydrogen and pseudo-alkali atoms.

REFERENCES

1. H. R. Griem, Plasma Spectroscopy, McGraw-Hill, New York (1964).

2. R. Wilson, J. Quant. Spectr. and Rad. Transfer 2, 477 (1962).

3. G. K. Oertel, Dissertation University of Maryland, 1964, AFCRL-63-851, also Phys. Fluids 8, 186 (1965).

4. R. v. d. R. Woolley and C. W. Allen, M. N. 110, 358 (1950).

5. G. Elwert, Z. Narturforsch. 7a, 432 (1952).

6. D. R. Bates, A. E. Kingston and R. W. P. McWhirter, Proc. Roy. Soc. A 267, 297 (1962).

COMPARISON OF IONIZATION EQUATIONS

Neutral ground state populations hydrogen and pseudo-alkali atoms according to present estimates divided by those according to Bates et al.

Electron Density (cm^{-3})	Temperature (^{o}Kelvin)								
	Hydrogen					Pseudo-Alkali			
	64,000	32,000	16,000	8,000	4,000	8,000	4,000	2,000	1,000
→ 0	1.3	1.3	1.3	1.4	1.5	1.2	1.2	1.4	1.5
10^{8}	1.3	1.3	1.3	1.4	1.5	1.2	1.2	1.3	1.4
10^{9}	1.3	1.3	1.3	1.3	1.5	1.2	1.2	1.3	1.4
10^{10}	1.3	1.3	1.2	1.3	1.5	1.2	1.2	1.3	1.4
10^{11}	1.3	1.2	1.2	1.3	1.4	1.2	1.2	1.2	1.3
10^{12}	1.3	1.2	1.1	1.2	1.3	1.1	1.0	1.1	1.1
10^{13}	1.2	1.1	1.0	1.1	1.1	1.1	1.1	1.1	1.1
10^{14}	1.0	0.92	.85	.83	.83	2.7	2.7	2.7	2.7
10^{15}	.83	0.73	.68	.66	.68	1.2	1.2	1.2	1.2
10^{16}	1.2	1.1	1.0	.99	1.0	1	1	1	1
10^{17}	1.7	1.6	1.5	1.5	1.6	1	1	1	1
10^{18}	1.1	1.1	1.1	1.0	1.0	1	1	1	1
10^{19}	1.0	1.0	1.0	1.0	1.0	1	1	1	1
→ ∞	1	1	1	1	1	1	1	1	1

NEUTRAL DENSITY IN HYDROGEN AT 16,000° KELVIN AS FUNCTION OF ELECTRON DENSITY

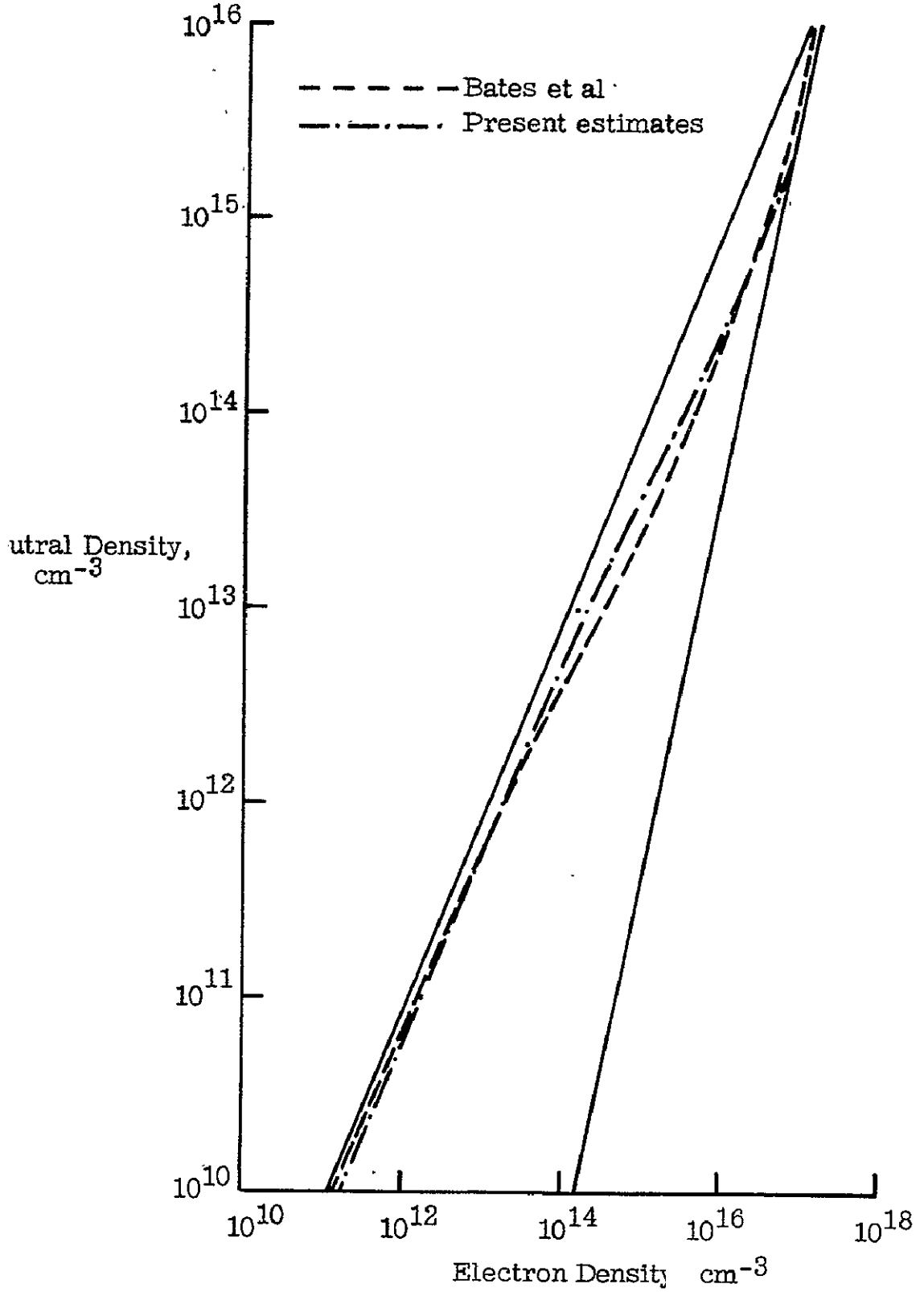

Oertel-1

NEUTRAL DENSITY IN PSEUDO-ALKALI (HYDROGEN WITH FORBIDDEN n = 1 STATE) AT 4,000° KELVIN AS FUNCTION OF ELECTRON DENSITY

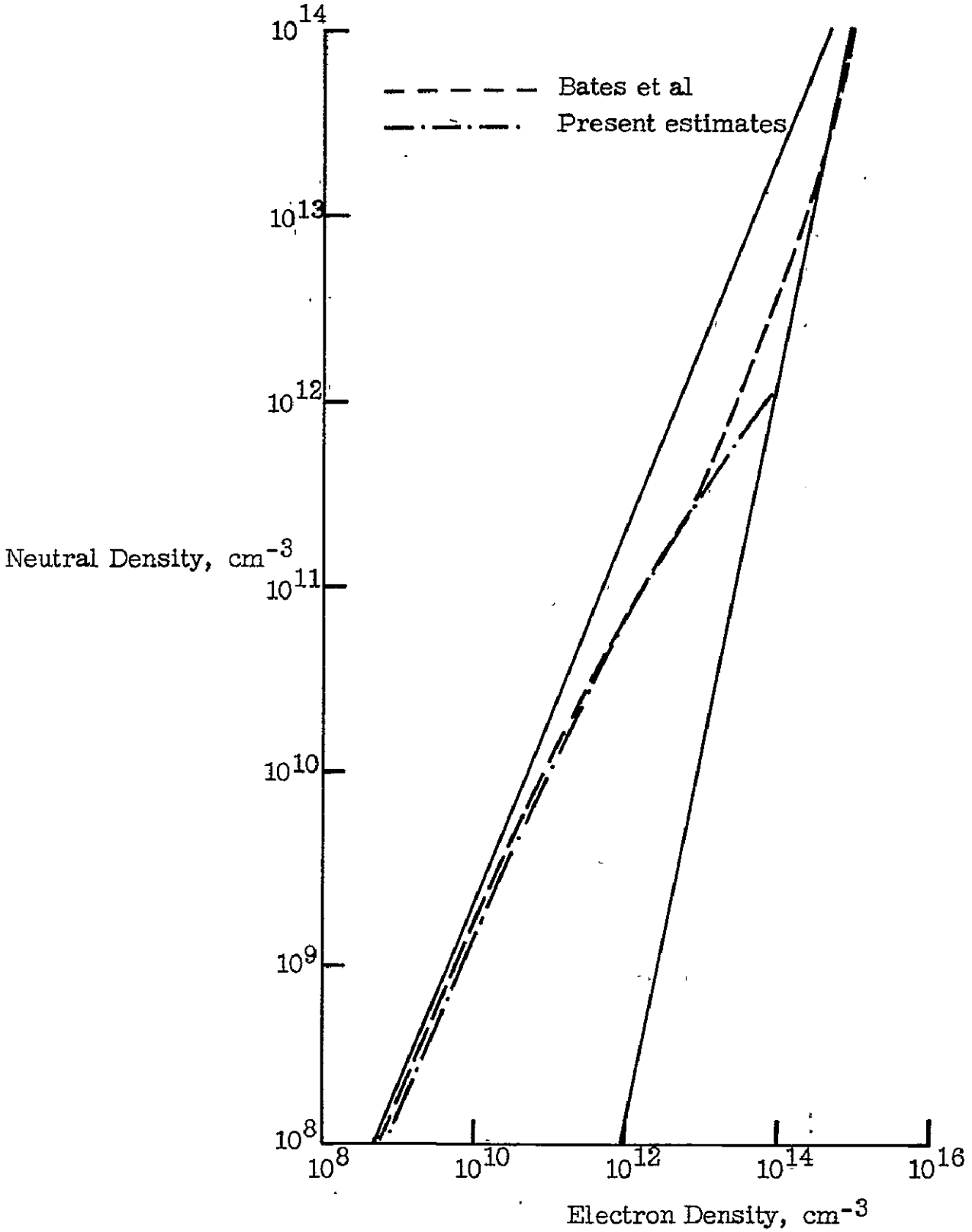

SPECTROSCOPIC INVESTIGATION OF A PREHEATER PLASMA

By L. P. Shomo and G. K. Oertel
NASA Langley Research Center
Hampton, Virginia

A spectroscopic determination of the electron density and temperature of the plasma generated by the preheater discharge in the Magnetic Compression Experiment (MCE) is in progress. The purpose is to establish space and time resolved information about the thermodynamic state of the preheater plasma at the time the main pinch event is initiated; it can be used to define initial conditions in MHD calculations. There is evidence that the initial conditions are extremely important for the theta-pinch process; i.e., during the first half-cycle there is no theta-pinch at all if preionization is absent.

The temperature is determined from the ratio of the intensities of the H beta line of hydrogen and the underlying continuum, while the electron density results both from absolute continuum intensity measurements and from the width of the H beta line of hydrogen. Time resolution is achieved by photomultiplier recording, while space resolution results from an Abel inversion assuming cylindrical symmetry.

With a gas filling of pure hydrogen of 100 microns of mercury, and using the preheater bank of the Magnetic Compression Experiment (for parameters see G. K. Oertel, J. Norwood and M. D. Williams, "Magnetic Compression Experiment," in this volume) typical electron densities and temperatures are several times $10^{15} cm^{-3}$ and 1 to 1.5 electron volts, respectively, with a typical decay time of 40 microseconds in the electron density near the coil axis. The plasma appears to be nearly uniform during the time from 10 to 25 microseconds after the initiation of the preheater discharge; it begins to peak more and more strongly near the axis at later times (see table 1). Similar results are obtained for the electron temperature; nonequilibrium effects become noticeable in the wall regions after about 30 microseconds.

There is some evidence that magnetic fields remain trapped in the plasma after the preheater discharge damps out (it does so after about 15 microseconds). In apparent agreement with computed decay times (assuming field diffusion by Ohmic losses) it seems to disappear after typically 20 to 25 microseconds.

The assumption of a uniform preheater plasma seems to be justified during the period from 10 to 25 microseconds after the initiation of the preheater discharge; and trapped magnetic fields have disappeared near the end of this period. A delay of 25 microseconds between the initiation of the preheater and theta-pinch (main) banks is judged to be the optimum operating condition in this experiment. More detailed measurements including the effect of the third (B_z bias field) discharge are in progress.

TABLE 1.- PREHEATER ELECTRON DENSITY, 10^{15} cm^{-3}.

R, cm \ t, μsec	15	20	25	30	35	40	45	50
0	2.68	2.03	2.09	1.87	1.59	1.48	1.35	1.17
0.5	2.67	2.21	2.07	1.88	1.63	1.36	1.30	1.09
1.0	2.48	2.11	2.11	1.85	1.62	1.31	1.26	1.11
1.5	2.53	2.22	2.01	1.82	1.57	1.31	1.29	1.12
2.0	2.51	2.13	1.96	1.71	1.54	1.29	1.37	1.08
2.5	2.42	2.09	1.90	1.56	1.38	1.32	1.15	0.95
3.0	2.52	2.21	1.85	1.62	1.33	1.31	1.04	.82
3.5	2.53	2.23	1.85	1.55	1.30	1.09	0.82	.61
4.0	2.52	2.23	1.78	1.35	1.15	0.73	.62	.45
4.5	2.38	2.21	1.62	1.35	0.96	.73	.48	.34

MEASUREMENTS OF STARK WIDTHS OF ARGON ION LINES IN A T-TUBE PLASMA

N. W. Jalufka and G. K. Oertel
NASA Langley Research Center
Hampton, Virginia

Stark broadened profiles of the singly ionized argon lines at 4806 Å($4s^4P - 4p^4P^o$), 4736 Å($4s^4P - 4p^4P^o$) and 4426 Å($4s^4P - 4p^4D^o$) have been measured in a dense ($N_e = 1.03 \times 10^{17}/cm^3$) plasma behind the reflected shock wave in an electromagnetic T-tube.

The energy storage capacitor used to power the discharge stores 600 Joules at 40 kV. The circuit rings at 300 kc and is critically damped to prevent the formation of multiple shock waves. The position of the reflector is adjustable and all measurements are made 1 mm in front of the reflector through 2 mm diameter holes. Measurements are made at the center of the tube and at the wall (i.e., in the boundary layer) in order to test the plasma uniformity in the line of sight.

The optical arrangement is shown in figure 1. A $\frac{1}{2}$ meter monochromator, with an apparatus function (full) half-width of 0.2 Å, is used to scan the line profile shot to shot. The other two monochromators monitor the total intensity of the 4806 Å argon II line and a 33 Å wide continuum band centered at 5100 Å. Monitoring of the 4806 Å line insured reproducibility of the temperature while monitoring of the continuum band insured the same for the electron density. All runs for which the intensities vary by more than 10 percent from a predetermined level are rejected.

The vacuum system is initially evacuated to 1×10^{-6} Torr and then filled with a mixture of 97% helium and 3% argon to a pressure of 1 Torr.

The half-width of the 5876 A HeI line indicates an electron density of $1.03 \times 10^{17}/cm^3$ ($\pm$ 10%) at both positions. The ratio of its integrated intensity to that of a 100 Å band of the underlying continuum indicates a temperature of 18,000° K ($\pm$ 20%) uniformly throughout the plasma.

The 4806 Å ArII line is also measured at both positions in the tube and the two profiles agree well within experimental error. The profiles are corrected for underlying continuum and Voigt profiles fitted to the (corrected) experimental profiles (fig. 2). As the apparatus profile of the measuring instrument is nearly Gaussian this procedure allows the experimental profiles to be unfolded and the spectral line profile to be obtained.[1] The resulting profile has a (full) half-width of 0.39 Å ($\pm$ 10%). It is wider than the value predicted by Griem[2] by a factor $r \approx 2.6$. The

4736 Å ArII line in the same multiplet (6)[1], measured under the same conditions, is in agreement with the 4806 Å line (i.e. too wide by a factor $r \approx 2.6$).

The 4426 Å ArII line in multiplet 7 as measured under these same conditions has a (full) half-width between 0.3 Å and 0.4 Å. Comparison with the theoretical half-widths gives $r \approx 2.5$ to 3.3. The limits on r are large for this line due to a weak ArII line close by which distorts the continuum measurement, and which is only listed in the comprehensive tables of Minnhagen.[3] The results of this experiment are summarized in table I. Preliminary measurements at higher electron density ($N_e \approx 6 \times 10^{17}/cm^3$) indicate that the 3729 Å ArII line in multiplet 10 is also wider than predicted by a factor $r \approx 2.5$.

The lines measured in this experiment all have the same lower level ($4s^4P$) and exhibit more broadening than predicted. These results are consistent with the suggestion that the broadening of the lower state cannot be neglected. This is supported by recent calculations of Roberts[4] which also indicate that more perturbing states must be taken into account and that the effects of "strong collisions" may be larger than expected.

1. J. T. Davis and J. M. Vaughan, Astrophys. J. 137, 1302 (1963).

2. H. R. Griem, Plasma Spectroscopy (McGraw-Hill Book Co., Inc., New York, 1964).

3. L. Minnhagen, Arkiv för Fysik, 25, 203 (Stockholm, 1963).

4. D. F. Roberts and D. D. Burgess, to be published.

OPTICAL ARRANGEMENT

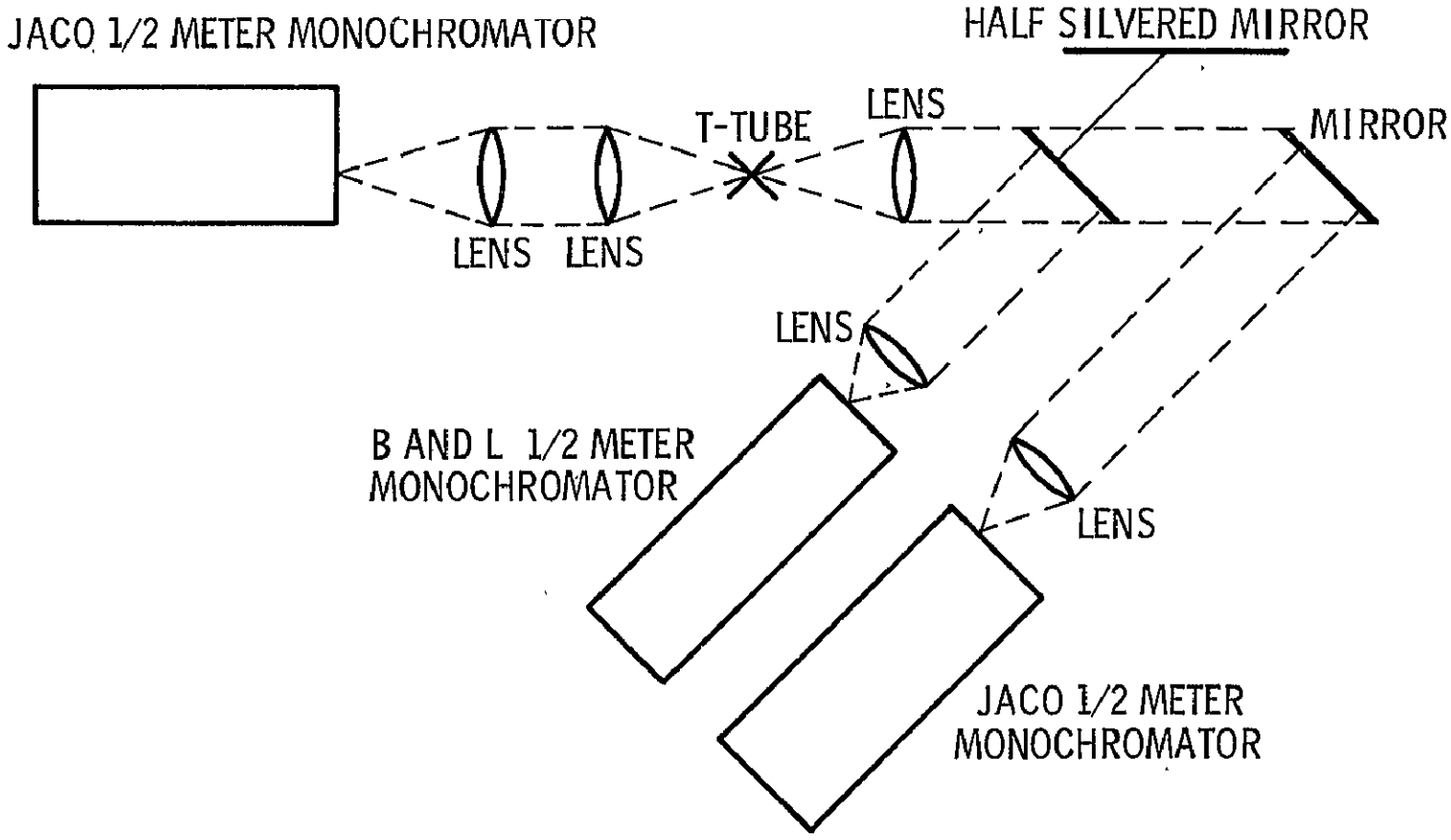

Jalufka et al-1

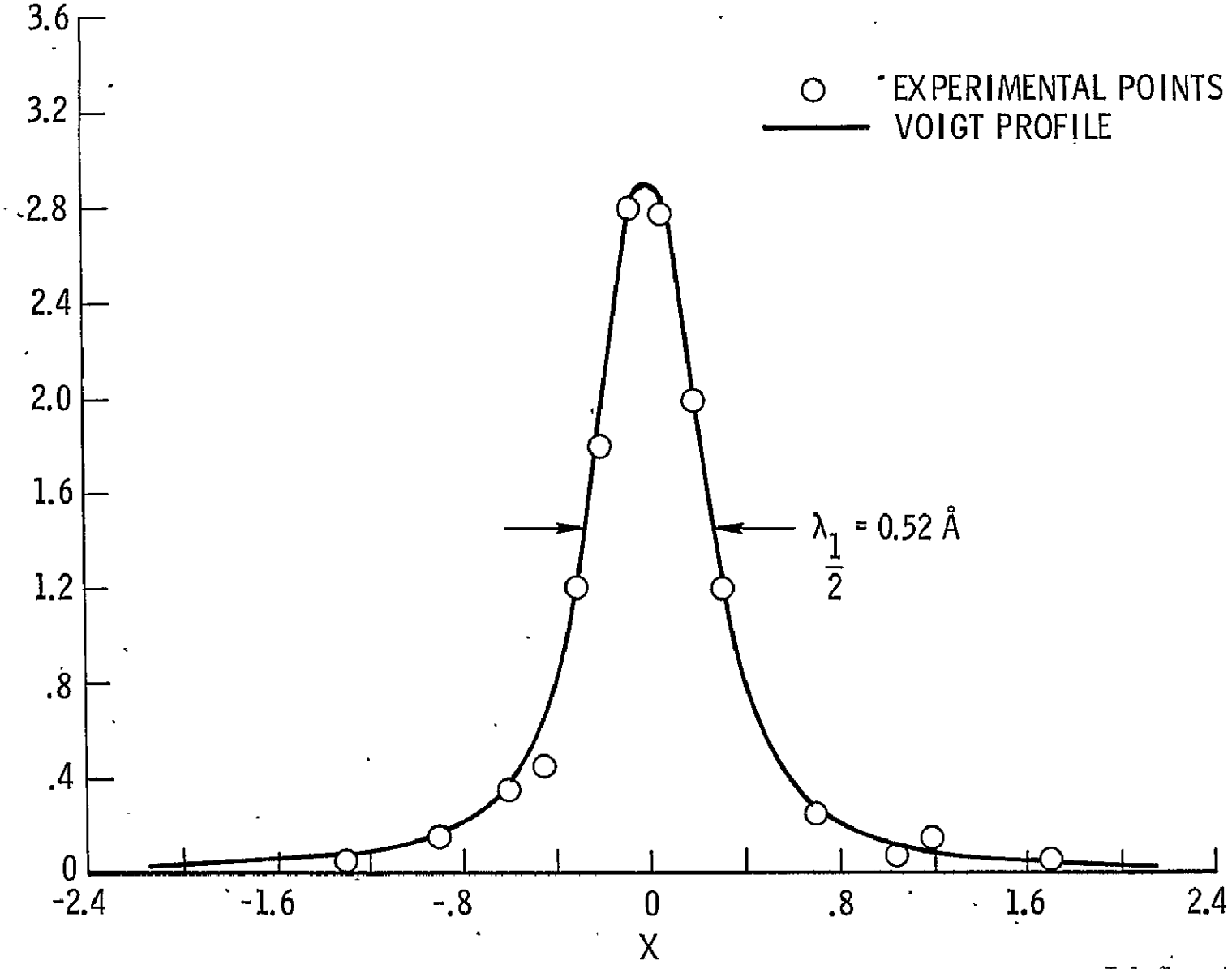

Jalufka et al-2

TABLE I

SUMMARY OF RESULTS

λ, Å	MULTIPLET	$\lambda_{1/2}$ (THEO.), Å	$\lambda_{1/2}$(MEAS.), Å	RATIO, r
4806	$4S^4P - 4P^4P^o$	0.15	0.39[a]	2.6
4736	$4S^4P - 4P^4P^o$	0.15	0.39[a]	2.6
4426	$4S^4P - 4P^4D^o$	0.12	0.30 - 0.40	2.5 - 3.3

[a]MOST PROBABLE ERROR ± 10 PERCENT.

Jalufka et al-3

THE EFFECT OF VISCOUS DRAG ON THE PERFORMANCE OF A COAXIAL PLASMA GUN

Joseph Norwood, Jr.
NASA Langley Research Center
Hampton, Virginia

This paper considers the effect of diffuse reflection of ions from the gun electrodes on the performance of a coaxial plasma gun. In order to isolate this effect for study the following simplifying assumptions are made: The plasma is assumed to be fully ionized. Only the slug mode of operation is considered. Electron emission is assumed to take place by ion impact, i.e., thermionic and field emission mechanisms are ignored. The Townsend secondary ionization coefficient, γ is assumed to be less than unity. The incoming ion will, for cathode work functions and plasma ionization potentials encountered in coaxial guns, be reflected as a neutral. The reflection angle will, most likely, be independent of the angle of incidence so that the kinetic energy corresponding to the axial component of velocity is lost to the cathode.

The viscous drag caused by ion impact on the cathode is just the x - component of ion momentum times the ion impact frequency which is just $\alpha|I|/e$ where I is the total current, e is the electronic charge (single ionization assumed) and α is the portion of the current carried by the ions. It can be shown that in a strongly radiating plasma ($T \geq 1$ eV), e.g., one composed of high z material, the photoelectric effect is sufficient to supply photoelectron emission to carry all the current. Hence for $\gamma << 1$ and a low radiation flux, α would approach unity, whereas either large radiation losses or a large value of γ would cause the current to consist mostly of electrons. For this case α would be quite small.

Another means by which particles may reach the electrodes and produce a drag force is by thermal diffusion. In this case the impact frequency will be given by the product of efflux velocity, $\sqrt{kT/2\pi m_i}$, the ion density, n_i, and the electrode area A. At the high ion densities encountered in coaxial guns ($n_i = 10^{16} - 10^{17}$ cm^{-3}) the mean free path for ions (or neutrals) is less than one millimeter, hence for temperature gradients which may be typical in coaxial guns, the impacting particles will have thermal energies corresponding to only a few tenths of an eV. Thus the large majority of the impacting particles may be neutrals for which the assumption of diffuse reflection at the electrode surface is not likely to hold. Taking $A = 30$ cm^2, $n_i = 10^{16}$/cm^3, and $T = 0.5$ eV one calculates an impact frequency for

hydrogen of 10^{23}/sec which must be reduced due to the fact that specular reflection of neutrals will yield no momentum transfer to the electrode. The impact frequency due to ion current, I/e for a current of 5×10^5 amps will be 3×10^{24}/sec, hence the effect of thermal diffusion is ignored.

The equations which are programed on a digital computer are shown in figure 1. The calculations have been made for $\alpha = 0$ and $\alpha = 1/2$. The gradient of gun inductance being logarithmic is relatively insensitive and so r_2/r_1 was chosen as 2.718 for convenience. The ohmic resistance was chosen as typical of such systems, 10^{-3} ohm.

A sample of the results is shown in figure 2 where gun efficiency defined as the plasma kinetic energy at $x = 40$ cm divided by the stored energy of the capacitor bank is plotted versus the plasma mass.

It is seen that the drag effect maximizes for low mass loading as one would expect since the velocities are large. Optimum mass loading from the point of view of maximum efficiency is from one to ten micrograms. This agrees within a factor of about 10 with the experimental results of a paper by Michels, Heighway, and Johansen which are replotted in figure 3.

A comparison of gun performance with and without viscous drag made at the point of maximum efficiency of the curves for $\alpha = 1/2$ shows that the effect can amount to as much as 27 percent for the range of parameters considered.

The effect of energy losses due to plasma heating and radiation have been ignored in this simplified treatment even though, as Oertel has pointed out, the radiation loss from a gun plasma may be quite severe. Thus the results do not pretend to accurately predict efficiencies to be expected in the operation of a laboratory device, but rather serve to point out that problems concerning the interaction of plasmas with electrodes are in need of further investigation.

EQUATIONS FOR THE COAXIAL PLASMA GUN

$$M\frac{d^2x}{dt^2} + \alpha\, l\, |I|\frac{m_i}{e}\frac{dx}{dt} = \frac{1}{2}\frac{\partial L}{\partial x}\, I^2$$

$$0 = \left\{L_o + \frac{\partial L}{\partial x}\, x\right\}\frac{d^2I}{dt^2} + 2\frac{\partial L}{\partial x}\frac{dx}{dt}\frac{dI}{dt} + \frac{\partial L}{\partial x}\, I\,\frac{d^2x}{dt^2} + R\frac{dI}{dt} + \frac{I}{C}$$

INITIAL CONDITIONS

$I(0) = 0$ $\qquad$ $x(0) = 0$

$\frac{dI}{dt}(0) = V_o/L_o$ $\qquad$ $\frac{dx}{dt}(0) = 0$

GUN EFFICIENCY AS A FUNCTION OF ACCELERATED MASS

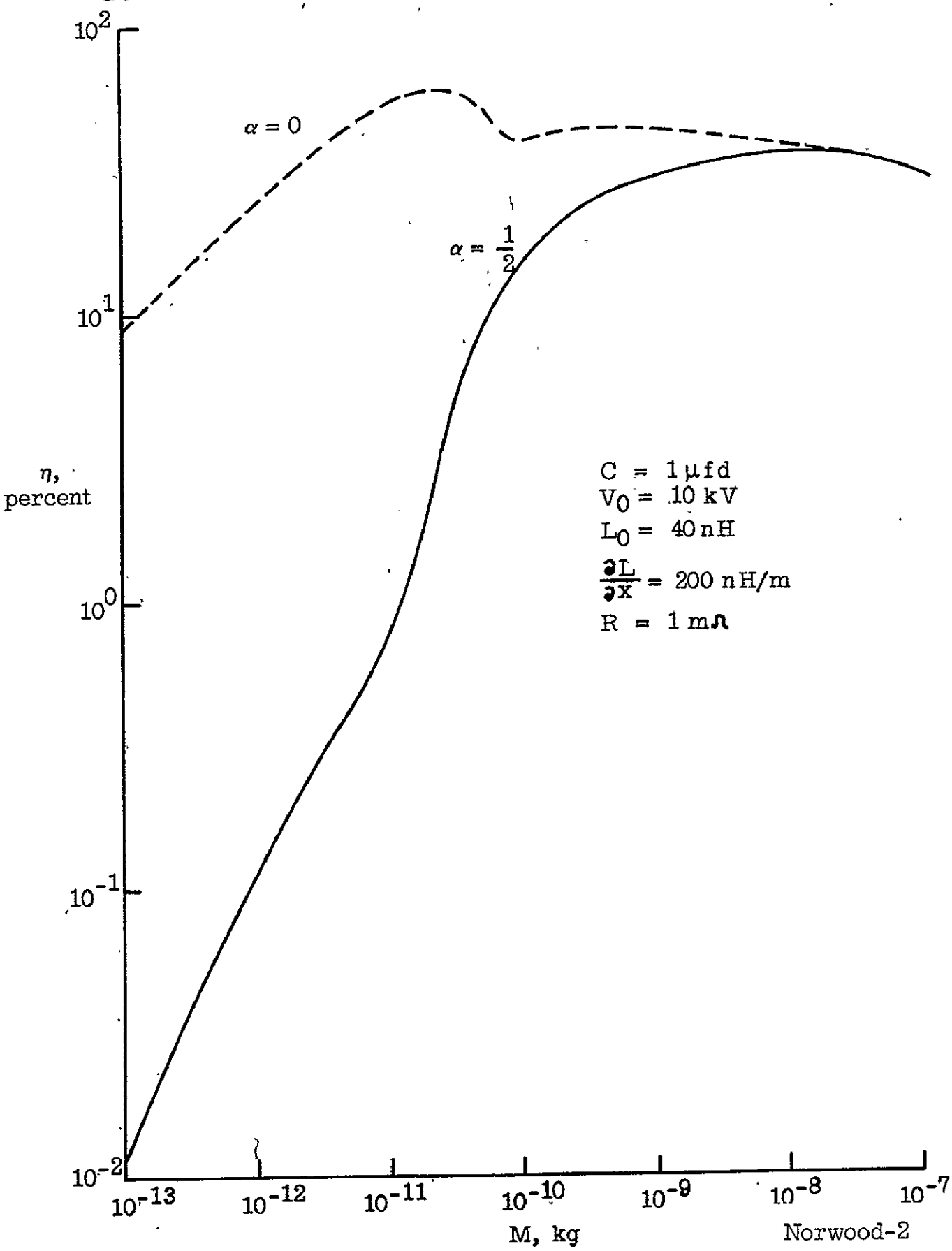

EXPERIMENTAL EFFICIENCIES AS A FUNCTION OF INJECTED PROPELLANT MASS

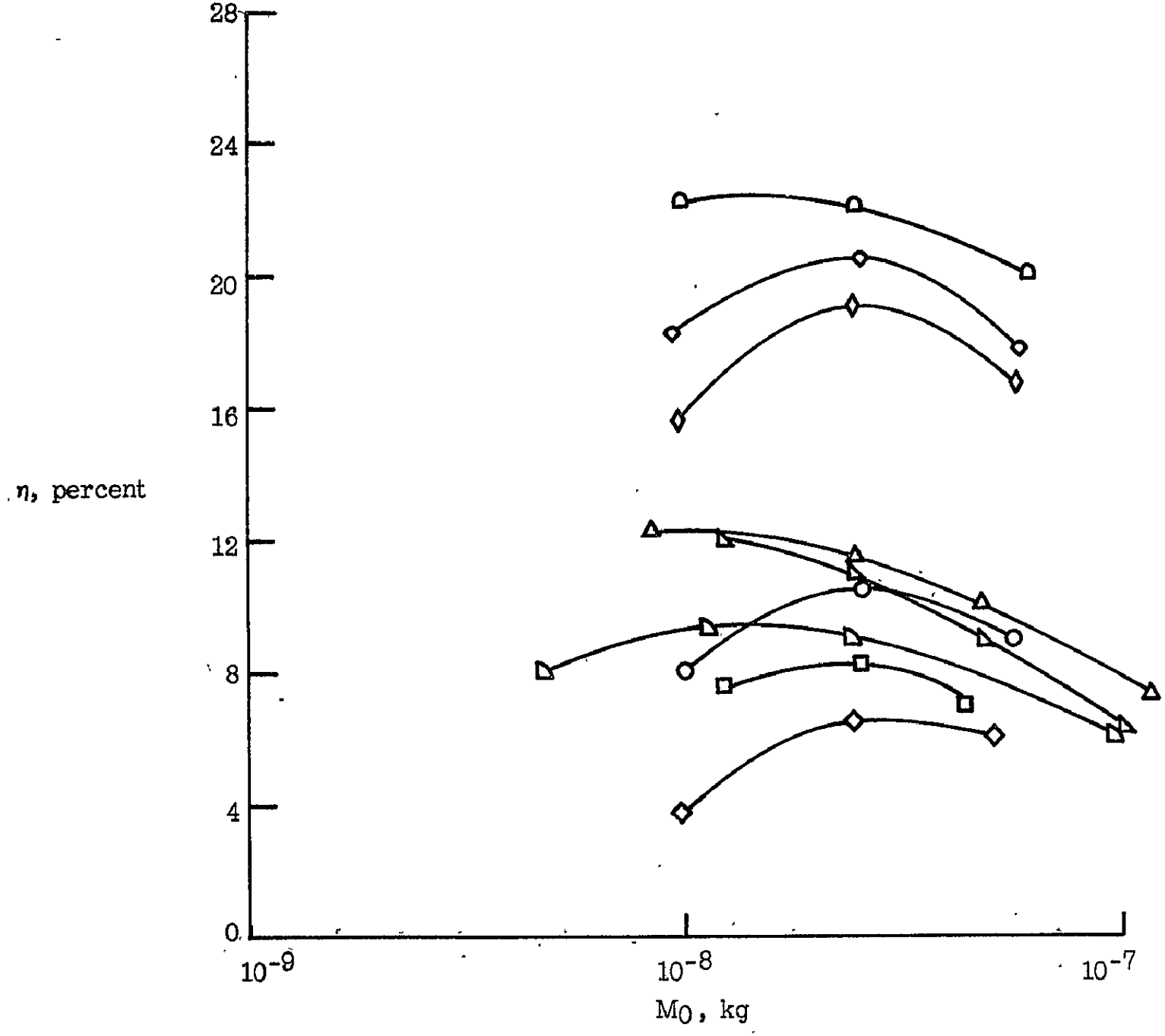

THE PRODUCTION AND PROPAGATION OF PLASMOIDS IN A NON-LINEAR ALFVEN WAVE

Daniel R. Wells
University of Miami
Coral Gables, Florida

and

Joseph Norwood, Jr.
NASA Langley Research Center
Hampton, Virginia

The most general solution of the linearized hydromagnetic equations is the hydromagnetic wave since any other solution can be expressed as a linear combination of these waves. In a compressible magneto-plasma the hydromagnetic waves consist of an Alfvén wave and an ordinary sound wave propagating along the magnetic field and a magneto-acoustic wave propagating across the field. This paper will confine itself to a discussion of the Alfvén waves, hence an incompressible fluid will be assumed for the most part.

In addition to being incompressible the fluid is assumed to be inviscid and of infinite electrical conductivity. The magnetic field is divided into a zero order uniform field and a first order perturbation field. The velocity is considered to be a first order quantity. All gradients of quantities perpendicular to the zero order field, $\vec{B}_o$, are ignored. With these assumptions one finds dispersionless, undamped wave equations for the perturbation field, $\vec{b}$, and velocity, $\vec{v}$, where the direction of propagation is along $\vec{B}_o$ and the velocity of propagation is the Alfvén velocity.

It can be shown by taking the curl of the linearized equations that the d'Alembertian commutes with the curl, hence the wave equations are also satisfied by the current density, $\vec{j}$, and the vorticity, $\vec{\phi}$. Thus, for vanishingly small perturbation velocities, $\vec{v}$, the current density and vorticity are propagated along the magnetic lines of force at Alfvén speed. From this point of view an Alfvén wave can be considered as a suitably arranged group of vortex filaments of vanishing strength aligned perpendicular to the magnetic field and moving parallel (or antiparallel) to the field.

The superposition of a vortex singularity on a parallel flow field gives rise to a lifting (Magnus) force $\rho(\vec{\phi} \times \vec{v})$. Thus the Helmholtz

theorem actually describes a force-free singularity. In hydromagnetics the most general force-free combination of $\vec{v}$ and $\vec{b}$ features $\vec{v}$ parallel to $\vec{b}$ with the vortex allowed to move parallel to $\vec{B}_o$. There are two possibilities according to whether magnetic and mass flow circulation are parallel or antiparallel. The two types of magneto-vortices do not interact destructively with others of their own kind, however, if a mixture of types were present in the Alfvén wave, then the wave would break up.

What now if $\vec{v}$ is not small and leads to a magnetic field which is comparable to or larger than the magnetic guide field $\vec{B}_o$? Special solutions can be obtained from the full non-linear equations. In a steady-state the left hand side of the equation of motion is zero. By taking the curl of this equation and assuming the magnetic and flow fields to be colinear ($\vec{v} = \beta\vec{B}$), where β is a scalar quantity, solutions are generated which describe a disturbance which moves with Alfvén speed and/or has its vorticity frozen into the plasma. The second solution corresponds, by virtue of the generalized Helmholtz theorem, to the condition for transport of fluid mass by the vortices. Either or both solutions may apply. The assumption of colinear flow is justified qualitatively by consideration of the dynamo action which seeks to align $\vec{v}$ and $\vec{B}$. A more powerful justification appears as a result of minimizing the total energy of the system subject to certain constraints. This analysis yields the result that the stable plasmoid propagated as a non-linear Alfvén wave has colinear fields (in support of our assumption) with flows having Alfvén velocity and is force-free.

Assuming that the fields are axisymmetric solutions are easily found in cylindrical coordinates. The boundary conditions exclude normal components of the fields at the boundary and require that the jump in $\vec{v}$ and $\vec{B}$ at the boundary be accompanied by a vorticity and current layer respectively. This layer must be of finite thickness since in a real fluid, finite viscosity precludes infinitely small vortices. The guide field and external flow (translation of the plasmoid) are assumed to be current- and vortex-free. In order that the Magnus and Lorentz forces balance at the boundary, the translation velocities must be Alfvénic. Contrarotating plasmoids can only propagate stably parallel to the guide field; corotating ones can only propagate stably antiparallel.

Plasmoid structures which appear stable have been observed not only in the laboratory but possibly also in ionospheric research. Recent work by Kvartskhava's group at Sukhumi has shown structures in theta pinchs and z-pinchs which are aligned parallel and perpendicular to the magnetic lines. The group at Stevens under Bostick have found both types of structures in a coaxial plasma gun. The senior author (DRW) has conducted experiments with a conical theta pinch wherein magneto-vortex rings are detected by image converter photography and electric and magnetic probes. Small at Grumman and Jones at General Electric have also detected these structures in similar devices.

The theory of plasmoid formation in the conical theta pinch predicts that contra- and corotational magneto-vortices will be produced on alternate half-cycles of the current oscillation in the conical coil. The structures will be expelled from the large end of the coil and projected into the mirror field. Measurements have shown that every other vortex structure is destabilized and destroyed upon entering the mirror field as one would expect since the contrarotating plasmoids can only move downstream and the corotating ones only upstream.

LINEARIZED ALFVÉN WAVE

$$\left(\frac{\partial^2}{\partial t^2} - V_A^2 \frac{\partial^2}{\partial z^2}\right)\vec{\Phi} = 0 \qquad \left(\frac{\partial^2}{\partial t^2} - V_A \frac{\partial^2}{\partial z^2}\right)\vec{j} = 0$$

COROTATING VORTEX LAYER

$$V = -\frac{B_0}{\sqrt{\mu_0 \rho}}$$

Norwood-1

THE NONLINEAR ALFVÉN WAVE

PARAMETRIC STUDY OF MPD ARC AT LOW EXHAUST PRESSURES (1μ to 1/10μHg)

P. Brockman, R. V. Hess, J. Burlock and D. Brooks

NASA, Langley Research Center
Hampton, Virginia

Thrust and velocity measurements have indicated that the coaxial plasma accelerator can produce velocities of the order of, or greater than, the velocity obtained by a singly ionized atom falling through the arc voltage. That is, $1/2\ mv^2 \geq eV$ where m is the mass of the atom, v the velocity, e the electronic charge and V the arc voltage (ref. 1, 2, 3, 4). Conservation of energy requires that the input power is greater than, or equal to, the directed kinetic energy, i.e., $JV \geq 1/2\ \dot{m}v^2$ where J is total arc current and $\dot{m}$ the mass flow. Combining the above inequalities,

$$\frac{JV}{\dot{m}} \geq \frac{1}{2} v^2 \geq \frac{eV}{m}$$

$$\frac{J/e}{\dot{m}/m} \geq \frac{\frac{1}{2} m v^2}{eV} \geq 1$$

The function $\frac{J}{e}\Big/\frac{\dot{m}}{m}$ is the ratio of the number of charges per second flowing in the arc current to the number of atoms per second flowing into the arc. If it is assumed that each atom can take part in the discharge once (no recirculation) and that each atom can be singly ionized, then

$$\frac{J/e}{\dot{m}/m} \leq \frac{Je+J_i}{J_{iz}} \leq \frac{Je+J_i}{J_i}$$

where Je and J_i are the radial electron and ion currents and J_{iz} is the axial ion current and is assumed greater than J_i. Then

$$Je \geq J_i \left[\frac{J/e}{\dot{m}/m} - 1\right]$$

and for $\frac{J}{e}\Big/\frac{\dot{m}}{m} > 1$ some electron current must flow, for $\frac{J}{e}\Big/\frac{\dot{m}}{m} > 2$, $Je > J_i$.

The measurements presented in this paper and also in references 1 and 2 were made for conditions where the velocities could exceed those obtained by the ions falling through the arc voltage, $J/e\Big/\dot{m}/m > 4$ for all measurements presented in this paper. However, for some of the operating conditions electron erosion or gas entrainment may increase the $\dot{m}$ seen by the arc and lower the ratio of $J/e\Big/\dot{m}/m$.

In reference 3 and 4, different theoretical approaches result in the introduction of effective mass flows. For both theories if the mass flow is above the effective mass flow the discharge will use only the effective mass

flow and the rest of the mass flow will not be accelerated. If the mass flow is below the effective mass flow and if entrainment or electrode erosion can be avoided the actual mass flow will be less than the effective mass flow, the arc voltage will be increased and higher specific impulse can be obtained. The condition for the mass flow to be less than the effective mass flow is in reference 3 for $J/e\dot{m}/m > 1$ and in reference 4 for $J/e\dot{m}/m > 2V_1/V$ where V_1 = ionization potential.

The above theories will be discussed further in reference 5, however, as mentioned above, the measurements in references 1 and 2 were made at $J/e\dot{m}/m > 4$ and that is at mass flows below the effective mass flow for both reference 3 and 4.

Schematics of 2 accelerators are shown in figure 1. Measurements reported in references 1 and 2 were performed with the configuration on the left which has an expanding anode. Results reported in reference 1 showed that performance depends on pressure in the electrode region and the configuration shown on the right was developed to increase pressure in the electrode region at low mass flow. The increased pressure at low mass flow will help to avoid electrode erosion and gas entrainment.

A study of various plasma parameters versus mass flow and tank pressure range was presented in reference 1 for the open anode configuration. Four conditions of arc current and magnetic field were used; 300 amps, 0.15 W/m^2; 300 amps, 0.3 W/m^2; 500 amps, 0.15 W/m^2 and 500 amps, 0.3 W/m^2. At each of these four constant JB conditions the vacuum system was operated at three different pumping speeds: 26,000, 1,200 and 340 liters per second, and at each pumping speed the mass flow was varied from 0.03-0 g/sec of argon. This yielded 3 pressure ranges of: 0.001-0.0001 torr, 0.01-0.006 torr, and 0.1-0.11 torr. At each condition voltage and thrust were measured and the velocity calculated from the measured thrust and mass flow. For each of the 12 operating conditions, 2 currents, 2 magnetic fields, and 3 pressure ranges the variation of thrust, arc voltage and 1/2 mv^2/eV with mass flow were plotted. As the maximum mass flow was 0.03 g/sec of argon, and the maximum current was 300 amperes, the ratio $J/e\dot{m}/m > 4$ for all operating conditions.

Figure 2 shows $\frac{1}{2}\frac{mv^2}{eV}$, thrust, arc voltage, and pressure, versus mass flow for one of the operating conditions, i.e., 300 amperes, 0.3 W/m^2 and the low-pressure range. The pressure variation is due only to the mass flow and pumping speed and is the same for all currents and magnetic fields. In this figure it can be seen that thrust decreases and voltage increases with decreasing mass flow, for J and B constant. Thus, the thrust cannot be purely electromagnetic and the voltage is not set solely by the gas used and the magnetic field. It should be pointed out that if the thrust was purely electromagnetic and remained constant with decreasing mass flow that the kinetic energy would increase as the reciprocal of the mass flow and that for constant current the voltage would have to increase with decreasing mass flow to keep the efficiency less than 100 percent.

The measurements in reference 1 showed that electrode erosion and gas entrainment could effect thrust measurements at certain operating conditions. It appears the discharge operation is controlled by pressure in the electrode region and that this pressure is set by gas entrainment at low mass flow and high tank pressure and by electrode erosion at very low mass flow and low to medium tank pressure. This is also a region at moderate mass flow about 0.008 g/sec argon and at low tank pressure where the thrust measurements may give accurate velocities. These regions were checked with Langmuir probe velocity measurements and the results were presented in reference 2. The ratio of directed to thermal ion saturation currents and the electron temperature were measured. The equation $v = 0.6\sqrt{\frac{kT_e}{m_i}}\frac{I_{11}}{I_\perp}$ where I_{11} and $I_\perp$ are the directed and thermal ion saturation currents T_e is the electron currents and 0.6 is an empirical factor that was used to calculate the velocity.

Typical results are shown in figure 3 where $\frac{I_{11}}{I_\perp}$ and $\frac{\frac{1}{2}mv^2}{eV}$ are plotted versus distance from axis. Although values above one for $\frac{1/2\ mv^2}{eV}$ are found, this may be due to errors in measurement of T_e and improved techniques of measuring T_e are currently in use and are being reported in reference 6.

Currently, measurements are being performed on the accelerator shown on the right in figure 1. The constricted anode helps keep the pressure high in the electrode region at low mass flow and thus entrainment and erosion can be reduced at low mass flow.

References:

1. Brockman, P., Hess, R., Bowen, F. and Jarrett, O.: Diagnostic Studies in a Hall Accelerator at Low Exhaust Pressure. Presented at AIAA Second Annual Meeting and Technical Display, San Francisco, Cal. July 26-29, 1965.
2. Burlock, J., Brockman, P., Hess, R. V. and Brooks, D. R.: Measurement of Velocities and Acceleration Mechanism for Coaxial Hall Accelerators. AIAA Fifth Elec. Propulsion Conf., San Diego, Cal. March 7-9, 1966.
3. Moore, R. A., Cann, G. L., Gallagher, L. R.: High Specific Impulse Thermal Arc Jet Thrustor Technology. Part I. Performance of Hall Arc Jets With Lithium Propellant. Tech. Report AFAPL-TR-65-48, Part I, June 1965.
4. Bennett, S., John, R. R., Enos, G. and Tuchman, A.: Experimental Investigation of the MPD Arcjet. Avco Corp. AIAA Paper No. 66-239, Fifth Elec. Propulsion Conf., San Diego, Cal. March 7-9, 1966.
5. Sidney, B., Hess, R. V. and Brockman, P.: Analysis of Acceleration Mechanisms and Ionization in MPD Arc. Fifth Intercenter and Contractor Conference on Plasma Physics, Washington, D. C., May 24-26, 1966.
6. Brooks, D. and Hoell, J.: Langmuir Probe Techniques for Measurement of Electron Temperature Distributions in High Energy Low Density Plasma Streams. Fifth Intercenter and Contractor Conference on Plasma Physics, Washington, D. C., May 24-26, 1966.

SCHEMATIC OF ACCELERATORS

THRUST , VOLTAGE , $\frac{1/2\ mv^2}{eV}$ AND PRESSURE VERSUS MASS FLOW

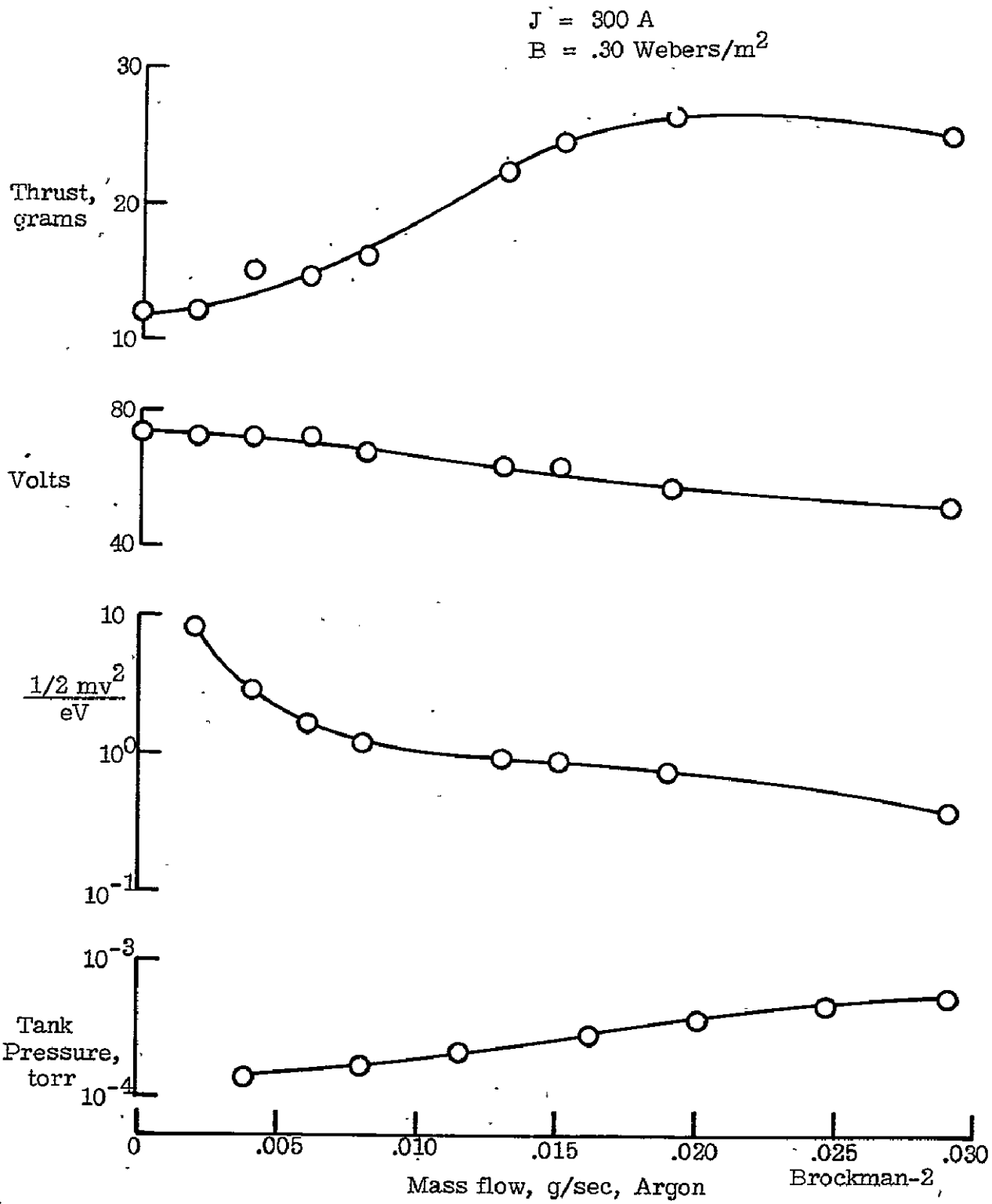

$\frac{1/2\,mv^2}{eV}$ AND ION CURRENT RATIO VERSUS DISTANCE FROM AXIS

$$v = .6\sqrt{\frac{kT_e}{m_i}}\,\frac{I_\parallel}{I_\perp}$$

	I	B	V	T_e
○	500 A	.15 Wb/m^2	40V	52,000 °K
□	300 A	.30 Wb/m^2	60V	24,000 °K

.008 g/sec Argon
4 Inches From Anode

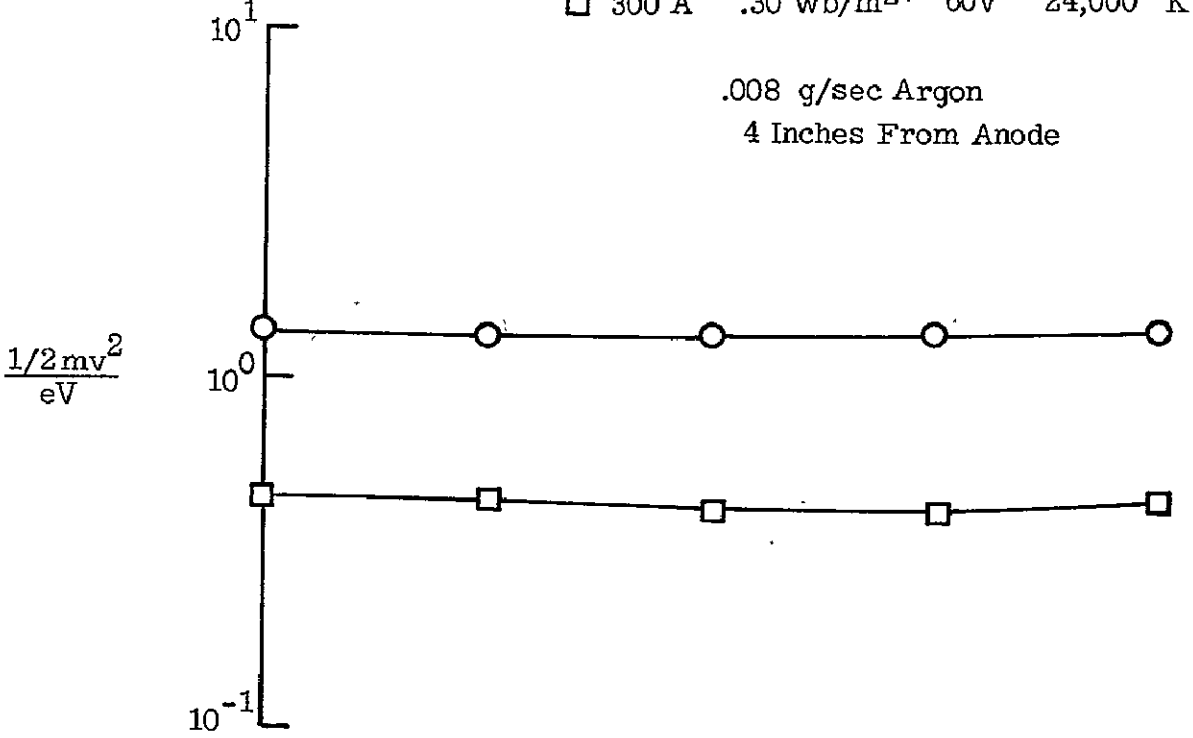

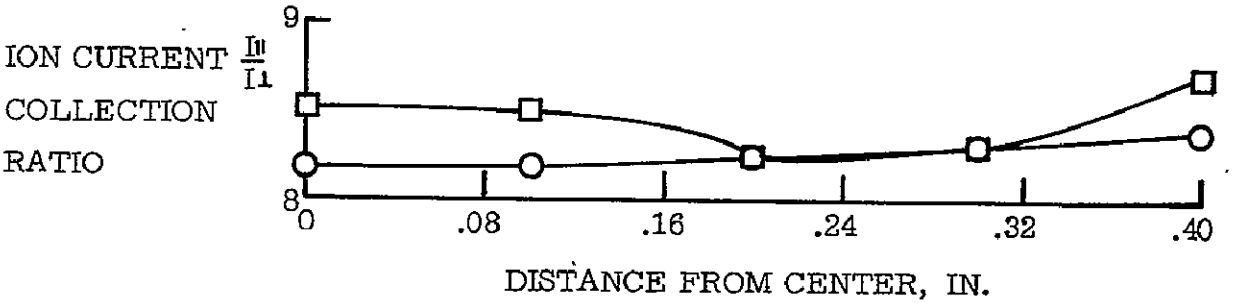

EFFECT OF MASS INJECTION ON VOLTAGE DISTRIBUTION IN HOLLOW CATHODE ACCELERATOR

By J. M. Hoell, Jr., D. R. Brooks, and R. H. Weinstein
NASA Langley Research Center
Hampton, Virginia

Detailed surveys are being conducted in a hollow cathode Hall current accelerator to determine radial and axial potential distributions in the exhaust plasma at various operating conditions. A knowledge of the potential distribution is necessary for analyzing the accelerating mechanism. The hollow cathode accelerator, shown in figure 1, utilizes a hollow tungsten cathode and a concentric carbon ring anode to produce an argon arc discharge in a diverging magnetic field. Separate controls allow argon to be injected through each electrode to assess the affect of the mode of gas injection on the potential distribution. Operating conditions of the present accelerator are: (1) total mass flows from .0157 g/sec to .0018 g/sec.; (2) arc currents ranging from 50 amps up to 300 amps; (3) magnetic fields ranging from 700 gauss to 3000 gauss; (4) tank pressures from 9×10^{-4} to 5×10^{-5} Torr.

Radial and axial surveys are being made using cylindrical Langmuir probes with parallel and perpendicular alignment to plasma flow. The probes are mounted on a probe driving mechanism which allows accurate position correlated data to be obtained. Langmuir probe characteristics are recorded and analyzed utilizing the data acquisition system described in reference 1. The local floating potential with respect to the reference electrode and the electron temperature can be obtained from the probe characteristics. (Maxwellian distributions have been found for all operating conditions studied so far.) The local plasma potential can be determined by calculating the difference between floating and plasma potential (this will in general be different from the measured floating potential which is with respect to the reference electrode) and algebraically adding this difference to the measured floating potential. The floating potential, found by equating the ion current and electron current, is given by

$$V_f = \frac{kT_e}{2e} \exp\left[\alpha_p^2 \, m_e/m_i\right]$$

(where k is Boltzmann's constant, e is the electronic charge, T_e is electron temperature, m_e/m_i is the ratio of electron to ion mass, and α_p is a normalized non-dimensional ion-current). Laframboise[2] has calculated the value of α_p for cylindrical probes as a function of potential, ratio of probe radius to Debye length, and of ratio of ion and electron temperature. In general the correct value of α_p for given plasma parameters must be obtained through an iterative process.

At this writing preliminary surveys have been made only for equal mass flows through each electrode. Figure 2 shows only floating potential distribution with respect to cathode potential for two equal mass flow conditions corresponding to total mass flows of .0157 grams/sec and .0018 grams/sec. The correction of the floating potential to plasma potential (discussed above) has not been obtained for all data points. Conversion of floating potential to plasma potential for several data points on the low total mass flow curves indicate that a radial gradient of approximately 8 volts/cm exists at an axial distance of 4 cm from the accelerator exit, while at an axial distance of 12 cm from the exit no radial gradient exists. The correction to plasma potential for the high total mass flow curves have not been obtained. It should be pointed out that while the high mass flow curves do not show a radial gradient in floating potential, this does not mean that one does not exist in the plasma potential, since variation in T_e across the jet would produce a radial gradient in the computed plasma potential.

At present, work on the potential surveys is continuing. Experiments are being conducted in a hollow cathode arc jet which has a slightly different configuration than the one shown in figure 1. In the new configuration, the cathode tip has been extended to a position midway of the anode and 1.6 cm in front of the forward edge of the magnetic coil. The anode has also been extended so that the forward edge is now flush with the accelerator exit. In the new configuration the arc attaches itself consistently inside the hollow cathode.

Plasma potential distributions will be obtained for various modes of propellant injection (i.e. equal mass flow through each electrode, anode mass flow > cathode mass flow, and anode mass flow < cathode mass flow) with arc current and magnetic field as parameters. Emitting probes will also be used to measure the plasma potential. The results of these measurements will be presented at the Fifth Intracenter and Contractor Conference on Plasma Physics if available, or in a future publication.

---

[1]Brooks, D. R., Hoell, J. M., Jr.: "Langmuir Probe Techniques for the Measurement of Electron Temperature Distributions in High Energy Low Density Plasma Streams;" to be presented at the Fifth Intracenter and Contractor Conference on Plasma Physics, Washington, D. C., May 24-26, 1966.

[2]Laframboise, J.: University of Toronto Institute for Aerospace Studies Report 100.

HOLLOW CATHODE ARC JET

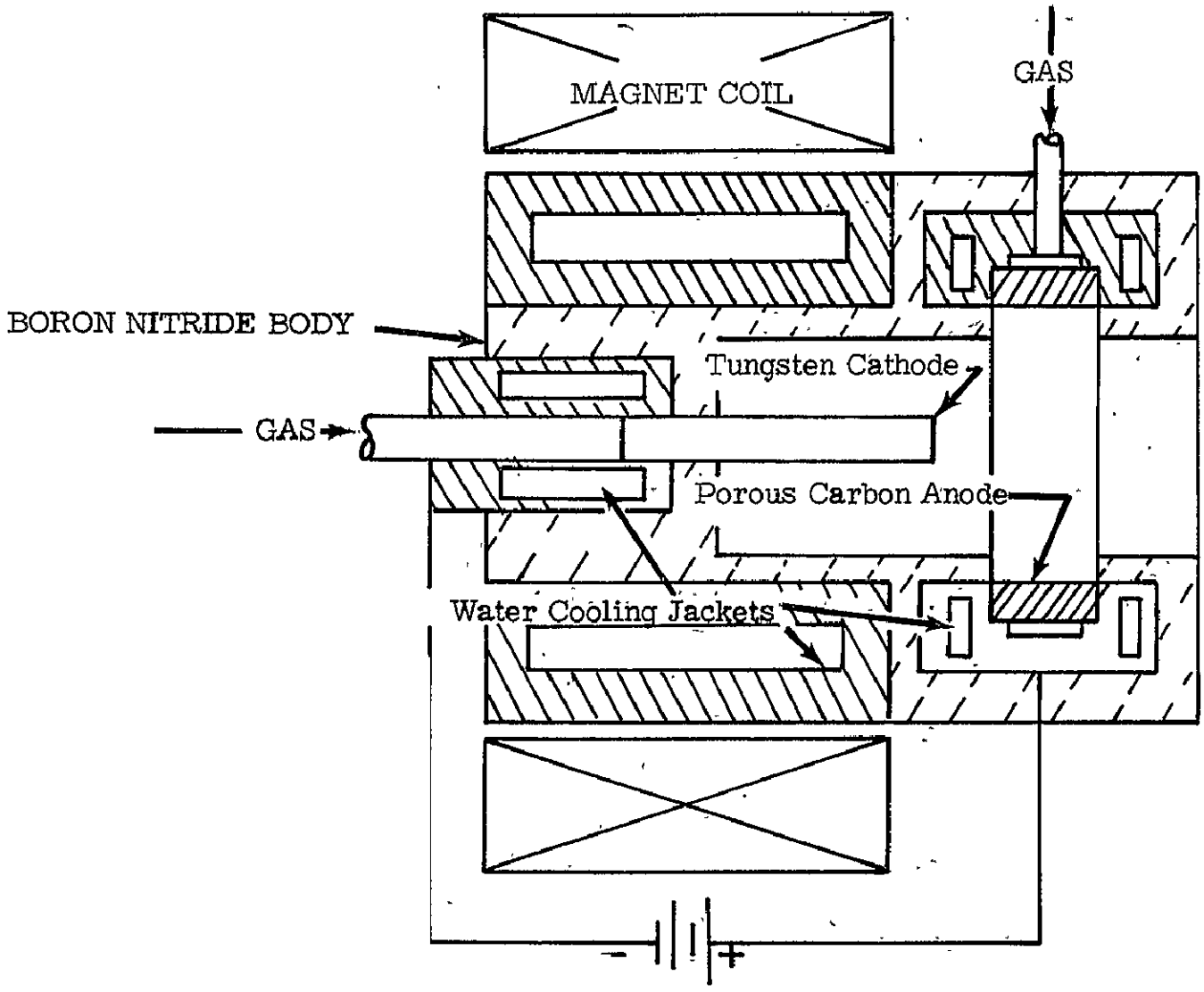

Hoell-1

FLOATING POTENTIAL DISTRIBUTION. FOR EQUAL MASS FLOW THROUGH EACH ELECTRODE

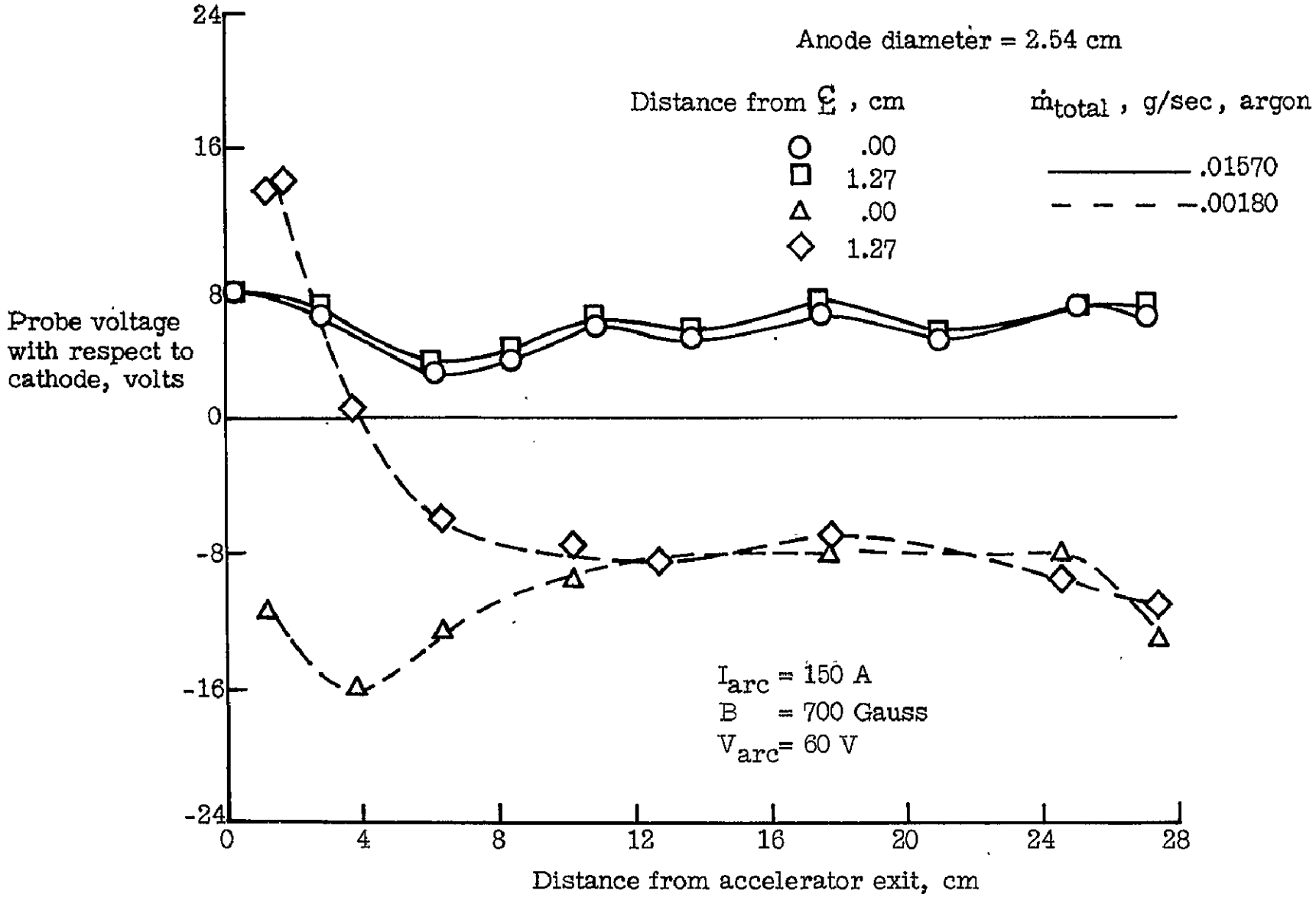

Hoell-2

ANALYSIS OF IONIZATION AND ACCELERATION IN MPD ARC

B. Sidney, R. V. Hess and P. Brockman

NASA, Langley Research Center
Hampton, Virginia

The purpose of the analysis is to obtain a better understanding of the experimental results given in reference 1 and to evaluate possible mechanisms for achieving efficiencies in excess of 50 percent. The experiments have been designed to check the possible existence of kinetic energies in excess of the applied or available voltage. The plasma stream produced by the MPD arc in argon at low mass flow is fully ionized when operating at high powers (ref. 2). The experiments further show some variation of thrust and voltage with mass flow for constant values of J and B indicating that the thrust is not purely electromagnetic. The experiments and the analysis thus pertain to an operating regime where some of the key problems of the MPD arc make their appearance. A possibility of reaching efficiencies in excess of 50 percent is also related to that regime as discussed in references 3 and 4.

The approach taken for analysis of the experiments is to start with careful evaluation of each term of the total energy equation in its complete form (ref. 5) for monatomic gases

$$JV = \dot{m}\left[\frac{Z\alpha eV_i}{m} + \frac{5}{2}\frac{k}{m}\left(Z\alpha T_e + T_i\right) + \frac{v_\theta^2 + v_r^2 + v_z^2}{2}\right] + Q \qquad (1)$$

where $\alpha = 1$ for full ionization and $Z = 1$ for the singly ionized atoms.

In order to understand the meaning of the individual kinetic energy terms the case is discussed first of a special MPD arc configuration where the plasma would be put into rotation which can subsequently be converted into directed motion. It has not been realized in some papers where this mechanism is postulated that for E/B drift motion $1/2\ m(E/B)^2$ would be stored for large ion slip in rotational Larmor motion in addition to the same amount in average drift motion. Thus the upper limit of the total stored energy would be $m(E/B)^2$. The random energy stored in the Larmor motion can be alternately accounted for as ion thermal motion. The inclusion of the energy stored in random ion Larmor motion and also in electron random energy could result in efficiencies in excess of 50 percent if these energies can be converted into axial kinetic energy. The heat losses, ionization energy and unrecovered random energy must, of course, be included in the considerations. In order to prove the existence of such mechanism ion temperature would have to be measured. Electron temperatures of the order of 5eV have been found two inches outside of the electrode region for the configuration used in the experiments of reference 1.

If it is assumed that the energies in the θ and r directions are small because they have been recovered or were initially small, the term $v_z^2/2$ can be conveniently expressed through the thrust $T = \dot{m}v_z$, which after regrouping of equation (1) is of the form

$$T = \dot{m}\left[\frac{2(JV-Q)}{\dot{m}} - \frac{2\alpha ZeV_i}{m} - \frac{5k}{m}\left(\alpha ZT_e+T_i\right)\right]^{1/2} \qquad (2)$$

The possible contributions of the individual terms under the square root to the deviation from purely electromagnetic thrust will be discussed. The influence of large electron currents will be evaluated for the experiments of reference 1 by expressing equation (2) in terms of the ratio $(J)/(\dot{m}e/m)$ which is equal to $(J_{ir}+J_{er})/J_{iz}$ for fully ionized plasmas. The specific conditions of the experiment where $(J_{ir}+J_{er})/J_{iz} > 4$ will be discussed.

The influence of electron currents on attainment of kinetic energies in excess of the applied or available voltage has also been analyzed by solving the differential equations for motion of ions and electrons in crossed E and B including the collision terms. This problem has been also approached in reference 6, however, the radial component of ion motion was neglected and thus the important effects of the relative magnitudes of ion Larmor radius and electrode gap were not evaluated.

Finally, the influence of ionization and transport properties (charge exchange cross-sections, etc.) on ion slip and the acceleration process has been analyzed in some detail. This is especially important in view of the frequently used assumption that when the MPD arc operates with partially ionized plasmas, ions and neutrals will not interact and the thrust is purely due to the ions. The validity of this assumption is being investigated for various mass flows and acceleration mechanisms using various gases and pressures in the acceleration region.

---

[1]Brockman, P., Hess, R. V., Burlock, J., and Brooks, D.: Parametric Study of MPD Arc at Low Exhaust Pressures (1μ to 1/10μHg). To be presented at the Fifth Intercenter and Contractor Conference on Plasma Physics, Washington, D. C., May 24-26, 1966.

[2]Bowen, F., Oertel, G., Hess, R. V., Jalufka, N., and Burlock, J.: Optical Measurements of Temperature and Velocity in Low Density Plasma Streams. To be presented at the Fifth Intercenter and Contractor Conference on Plasma Physics, Washington, D. C., May 24-26, 1966.

[3]Cann, G., Harder, R. L., Moore, R. A., Lenn, P. D.: Hall Current Accelerator, EOS Report 5470 - Final.

[4]Bennett, S., John, R. R., Enos, G., and Tuchman, A.: Experimental Investigation of the MPD Arcjet. AIAA Fifth Electric Propulsion Conf., San Diego, Calif., AIAA Paper No. 66-239, March 7-9, 1966.

[5]Hassan, H. A., Hess, R. V., and Grossmann, W.: Experiments and Analysis for Coaxial Hall Current Accelerators and the Role of Ionization Effects. Sixth Symposium on Engineering Aspects of Magnetohydrodynamics, April 21-22, 1965, pp. 83-84. Details given in prospective NASA TN by same authors.

[6]Penfold, A. S.: Recent Advances in the Development of Electromagnetic Thrustors for Space Propulsion. 4th Symposium on Advanced Propulsion Concepts, Palo Alto, Calif., April 26-28, 1965.

DEVELOPMENT OF MASS FLOW METER AND INJECTION THROUGH ELECTRODES FOR THE MPD LITHIUM ARC

By Olin Jarrett, Jr.
NASA Langley Research Center
Hampton, Virginia

The MPD arc has been operated continuously with lithium injection through the anode for one-half hour at 200 to 400 amps and magnetic field from 2000 to 5000 gauss at the cathode tip. Lithium injection was achieved by varporizing lithium in a resistance heated feed tube and by feeding the vapor to a distribution manifold in the tungsten anode (fig. 1). Visual inspection of the lithium flow simulated with smoke or water showed that good distribution through the eight feed holes was obtained (fig. 2). Stable operation was achieved and electrode and insulator erosion was negligible. Lithium flow was selected in the range of .02 to .03 gram per second for preliminary operation of the system.

Refinement of the lithium mass flow measurement system to obtain accurate metering in range of .01 grams per second is progressing. Liquid lithium is metered into the vaporizing tube from a reservoir by a manually controlled valve (fig. 3). The lithium is displaced in the reservoir by argon at several atmospheres pressure. The volume flow of lithium can be computed from the argon flow into the lithium reservoir as measured by the 0 to 5 cc/min Hastings flow meter.

MPD ACCELERATOR WITH ANODE LITHIUM INJECTION

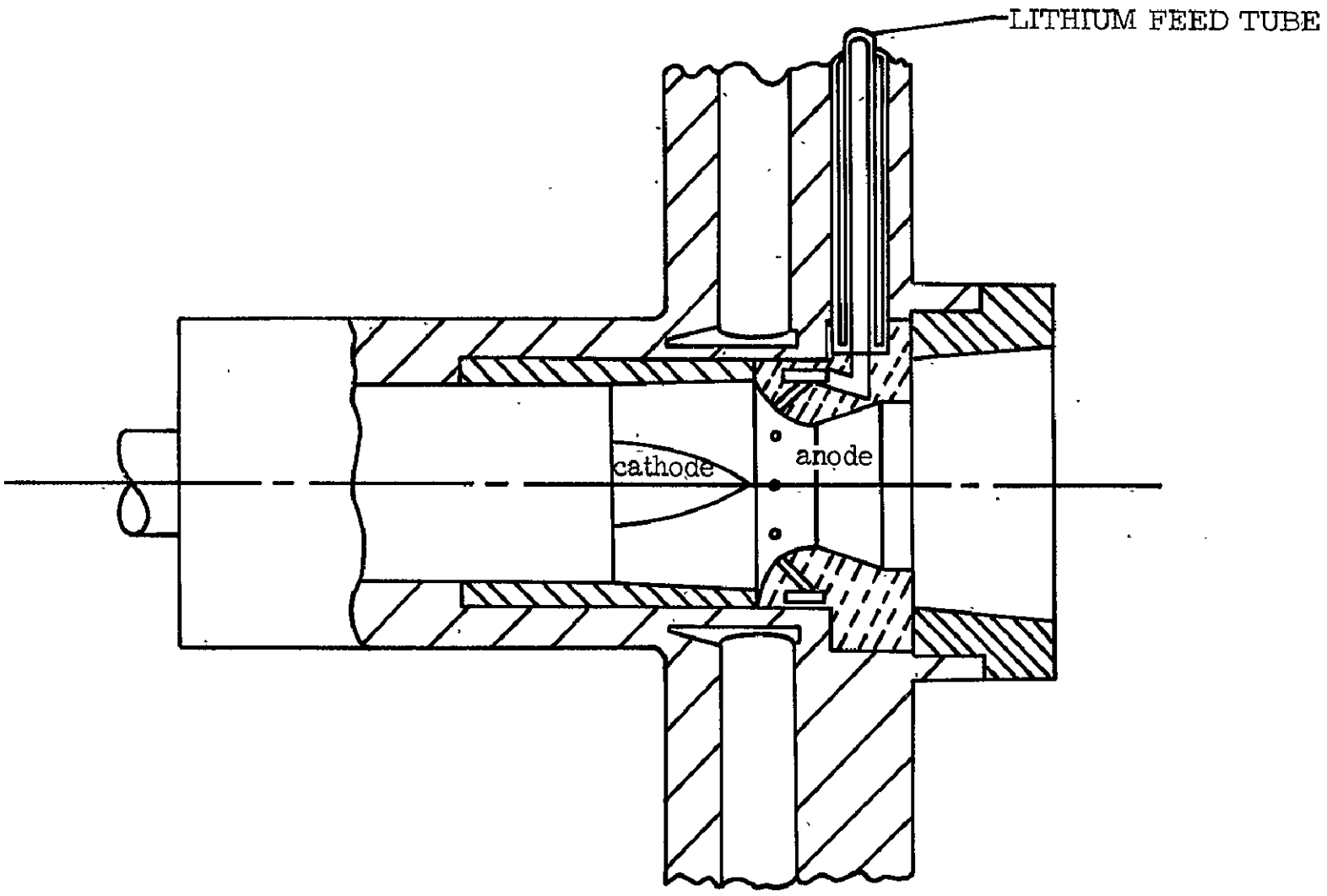

Jarrett-1

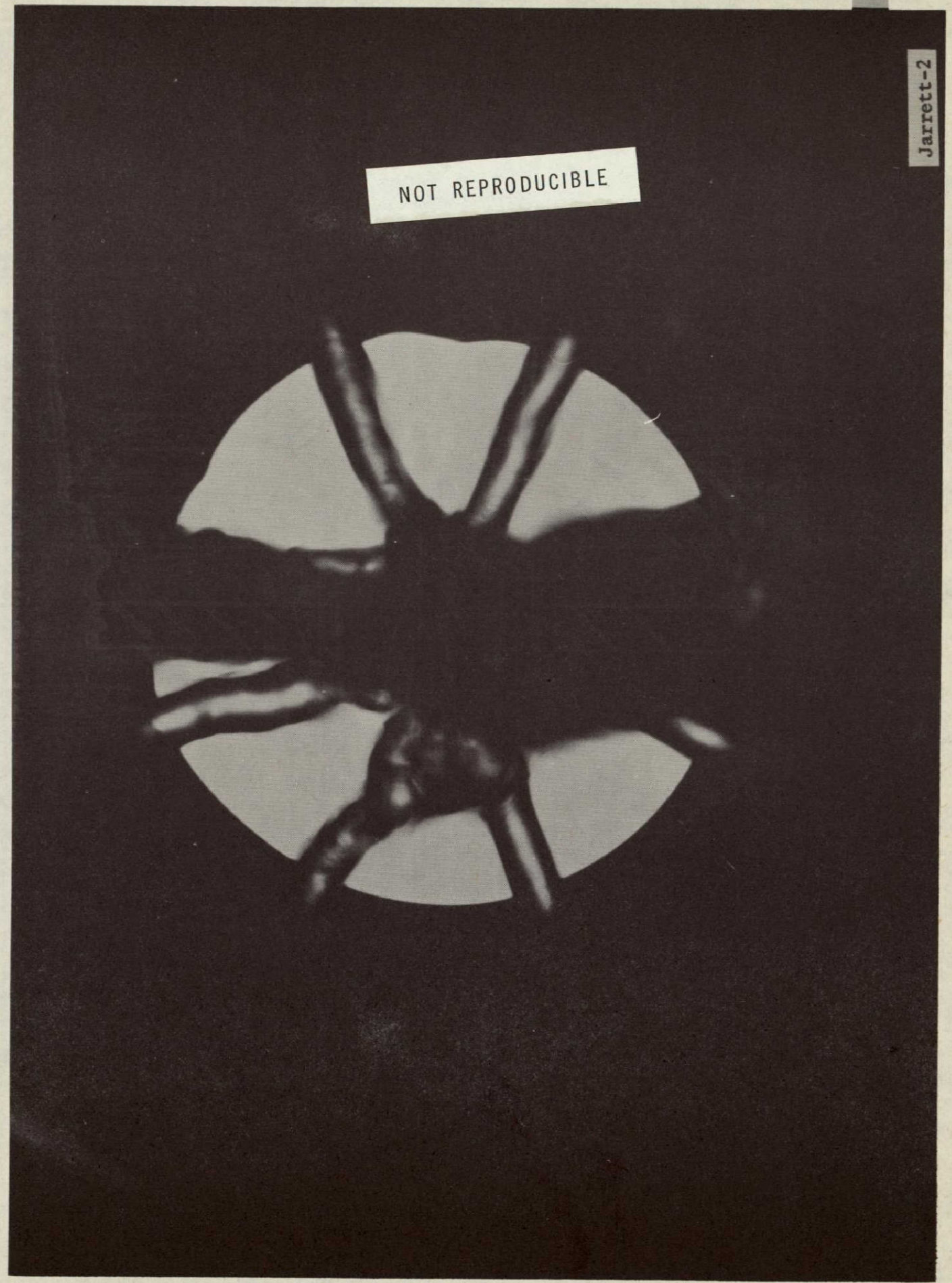

LITHIUM MASS FLOW METERING SYSTEM

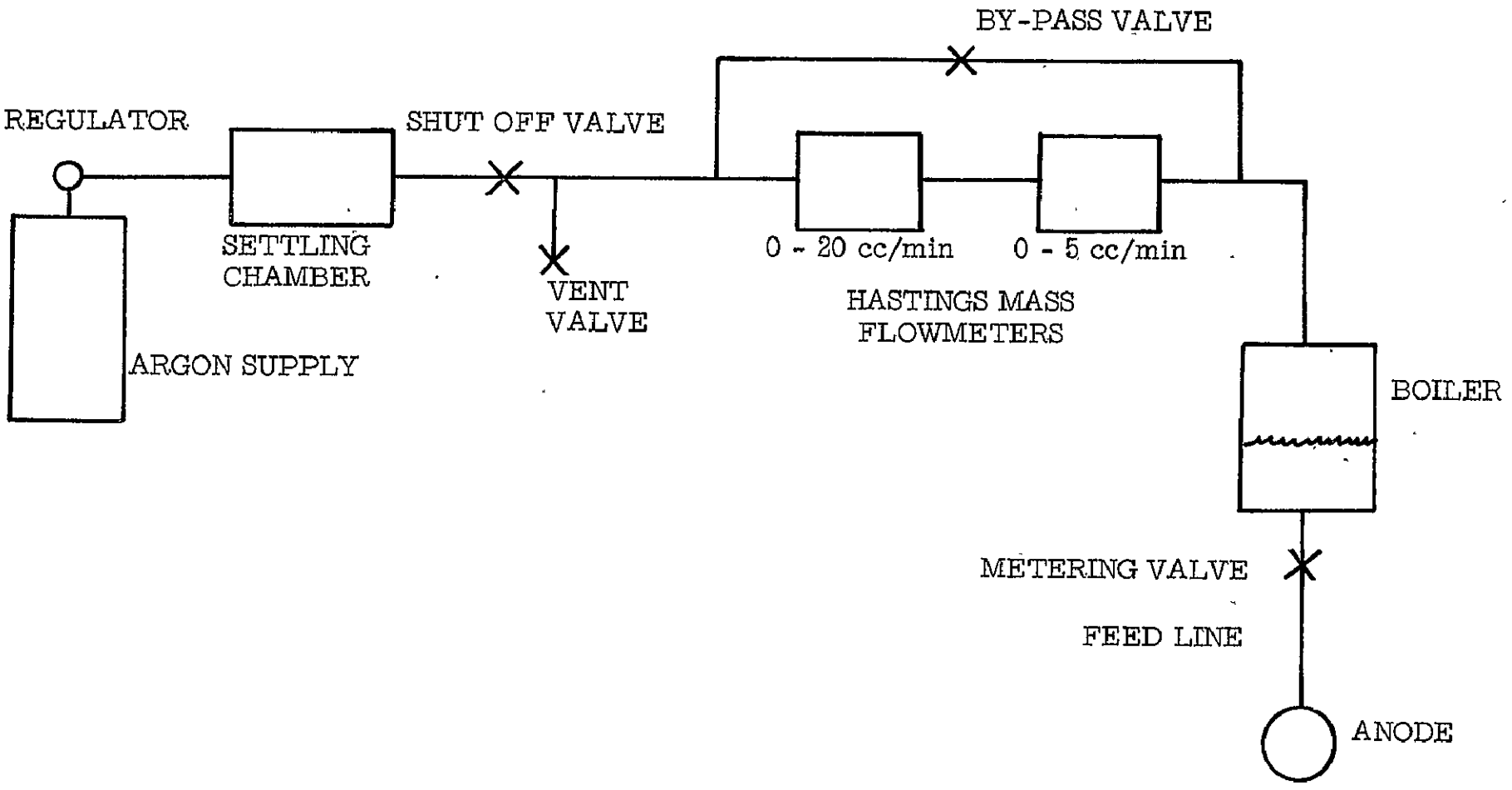

RESISTIVE INSTABILITIES FOR PLASMAS IN CROSSED ELECTRIC AND MAGNETIC FIELDS

Ram K. Varma[+]
NASA Langley Research Center
Hampton, Virginia

Instabilities of a partially ionized plasma in crossed electric and magnetic fields are investigated both in the low β (β = kinetic pressure/magnetic pressure = $4\pi nkT/B^2$) and high β limit with a view to understand the nature of the instability observed in the Linear Hall Accelerator. In the low β limit an instability has been proposed by Simon and Hoh,[1] who find that the system is unstable if there exists a density gradient in the direction of the external electric field. Morse[2] has attempted to solve the problem exactly, determining the complex eigenvalues and eigenfunctions and has arrived at the conclusion that an instability is also possible for the density gradient against the direction of the electric field.

It is noted that in all the treatments of this instability the inertial term has been ignored and quasi-neutrality has been used instead. This does not seem to affect the conclusions of Simon and Hoh within the framework of their approximate procedure. This, however, leads to incorrect eigenvalue equations in Morse's treatment, so that the conclusions of the latter are unreliable, in particular that an instability is possible for the density gradient against the direction of the electric field.

Two observations are significant in connection with the observed instability: (1) the instability is found to exist all along the length of the accelerator; (2) the instability appears even at as low a magnetic field as 10 G, and kinetic pressure ~2 - 30μ. Item (2) implies conditions of $\beta \geq 1$, and opens a possibility for a high β instability. Item (1) points to the fact that one probably should not depend too heavily on the density gradient for the instability. In view of these observations, an investigation for high β instabilities is made of a homogeneous resistive plasma in crossed electric and magnetic fields. We find an instability of the magnetic compression wave traveling normal to electric and magnetic field. This is found to be coupled to an electrostatic wave if the propagation is not entirely normal to the electric field. The instability does not depend on any density gradients

---

[+]NAS-NRC Regular Post-Doctoral Resident Research Associate.

and is resistive in that the growth rate vanishes for zero resistivity. For lower magnetic fields such as are consistent with high β, this instability is found to have the characteristics of the observed instability in the Linear Hall Accelerator. A further study of instabilities for high magnetic fields (low β) is in progress.

---

[1] A. Simon, Phys. Fluids 6, 382 (1963); F. C. Hoh, Phys. Fluids 6, 1184 (1963).

[2] D. L. Morse, Phys. Fluids 8, 1339 (1965).

LANGMUIR PROBE TECHNIQUES FOR THE MEASUREMENT OF ELECTRON TEMPERATURE DISTRIBUTIONS IN HIGH ENERGY LOW DENSITY PLASMA STREAMS

D. R. Brooks and J. M. Hoell, Jr.

NASA, Langley Research Center
Hampton, Virginia

The objective of present Langmuir probe studies is to measure spatial distributions of ion flow velocities and plasma potential for a large range of operating conditions. Since both of these measurements depend critically on electron temperature distributions, suitable techniques have been developed for measurement of electron temperature in an environment which can be summarized as follows: (1) electron density of 10^{11} - $10^{13}/cm^3$, (2) magnetic fields on the order of 10^3 gauss, (3) supersonic flow velocities several times larger than the ionic sound velocity based on electron temperature. Preliminary results of potential measurements and the application of the detailed electron temperature surveys described here to potential measurements in a hollow cathode Hall current plasma accelerator are discussed in a companion abstract.[1]

Because of the high heat load on the probes, and the necessity for good spatial resolution, an accurate driving mechanism has been developed that is capable of moving probe assemblies with three degrees of freedom at speeds greater than 1 inch/sec. This device not only provides a simple way of obtaining large quantities of position-correlated data, but also keeps to a minimum the time spent by the probe in the discharge region.

The circuit of figure 1 has been used at a frequency of 60 cps for obtaining probe curves at the rate of about 100 per inch in the radial direction. Data are recorded at several axial positions for each operating condition. Net probe current is circuit-limited to about 100 mA in the case of the hollow cathode accelerator. For the small wire probes used, this value is large enough to achieve ion current saturation but keeps excessive electron current from heating the probes to emission temperature. It is generally recognized that in the presence of a strong magnetic field, the portion of the Langmuir probe curve due to low energy electrons cannot be used for temperature measurement. For this reason, restricting the net probe current (thereby losing the low energy end of the electron curve) causes no loss of information. However, in this case the ion current must be subtracted from the net current, since the determination of the electron temperature involves only the electron current. This procedure is not so important in cases where no magnetic field is present, since in that case a portion of the probe curve can be used in which the ion current is negligible with respect to the electron current. The standard method of extrapolating the saturation ion current into the region of the probe curve where the electron current becomes large and subtracting this extrapolated value from the net current has been put on a relatively sound theoretical basis. The summarizing article of Chen[2] and the recent work of Laframboise[3] have shown how the ion saturation current can be predicted under various conditions. Laframboise has shown that as long as

the probe voltage is much less than the plasma potential, the variation of ion current with voltage is small. This variation has been obtained from the ion saturation part of the curve.

Figure 2 shows a flow diagram for computer analysis of recorded probe data. Digitization of the tape yields a resolution of more than 100 points per curve, which is sufficient for averaging out high frequency noise in the accelerator. The original data are plotted along with a computer-generated straight line fit to the ion saturation current. The extrapolation of this line is the ion current which is subtracted from the net current to yield electron current. The log of the electron current versus voltage and the best straight line fit to this log curve is plotted. This slope gives the electron temperature for Maxwellian distributions. Of course, visual inspection of both of these curves is necessary. In the case of the ion saturation current fit, a distortion of the slope can result from noisy data or using too many or too few points for the fit. In the case of the electron current, it is mandatory to assure that the log of the electron current versus the voltage is, in fact, a straight line because the computing scheme forces upon the data an analysis based on Maxwellian distributions which is not valid for other distribution functions. Excellent straight line plots of log I_e versus voltage have been obtained so far.

The manner of data recording and reduction described here has been developed for the purpose of handling large quantities of data in an objective fashion. The ideas utilized have been combined in a system which is capable of providing the detailed surveys which are required in the analysis of the high energy plasma streams under study. The computer program is flexible enough to include refinements to theory as needed. Future plans call for a more exact application of the ion current theory of Laframboise. This will include effects due to the ratios of ion to electron energy and probe radius to Debye length although these effects require modification in the presence of a magnetic field. It should be emphasized that inclusion of such refinements is impractical in a project of this magnitude unless tape recording and computing techniques are used for the accumulation and analysis of data. Future work will also include an examination of time fluctuations in the quantities being measured, as these can be helpful in understanding how to average the results of probe measurements which are made on the assumption that average variations correspond to spatial nonuniformities and not to changes with time in arc conditions.

References:

1 Hoell, Jr., J. M., Brooks, D. R. and Weinstein, R. H.: Effect of Mass Injection on Voltage Distribution in Hollow Cathode Accelerator. To be presented at the Fifth Intercenter and Contractor Conference on Plasma Physics, Washington, D. C., May 24-26, 1966.

2. Chen, F. F.: Numerical Computations for Ion Probe Characteristics in a Collisionless Plasma. Plas. Phys. (J. of Nuclear Energy, Part C) 1965, vol. 7, pp. 47-67, Pergamon Press, Ltd.

3. Laframboise, J.: Theory of Cylindrical and Spherical Langmuir Probes in a Collisionless Plasma at Rest. Rarefied Gas Dynamics, J. H. DeLeeuw, ed., Academic Press, N. Y., 1965.

PROBE CIRCUIT FOR ELECTRON TEMPERATURE MEASUREMENTS

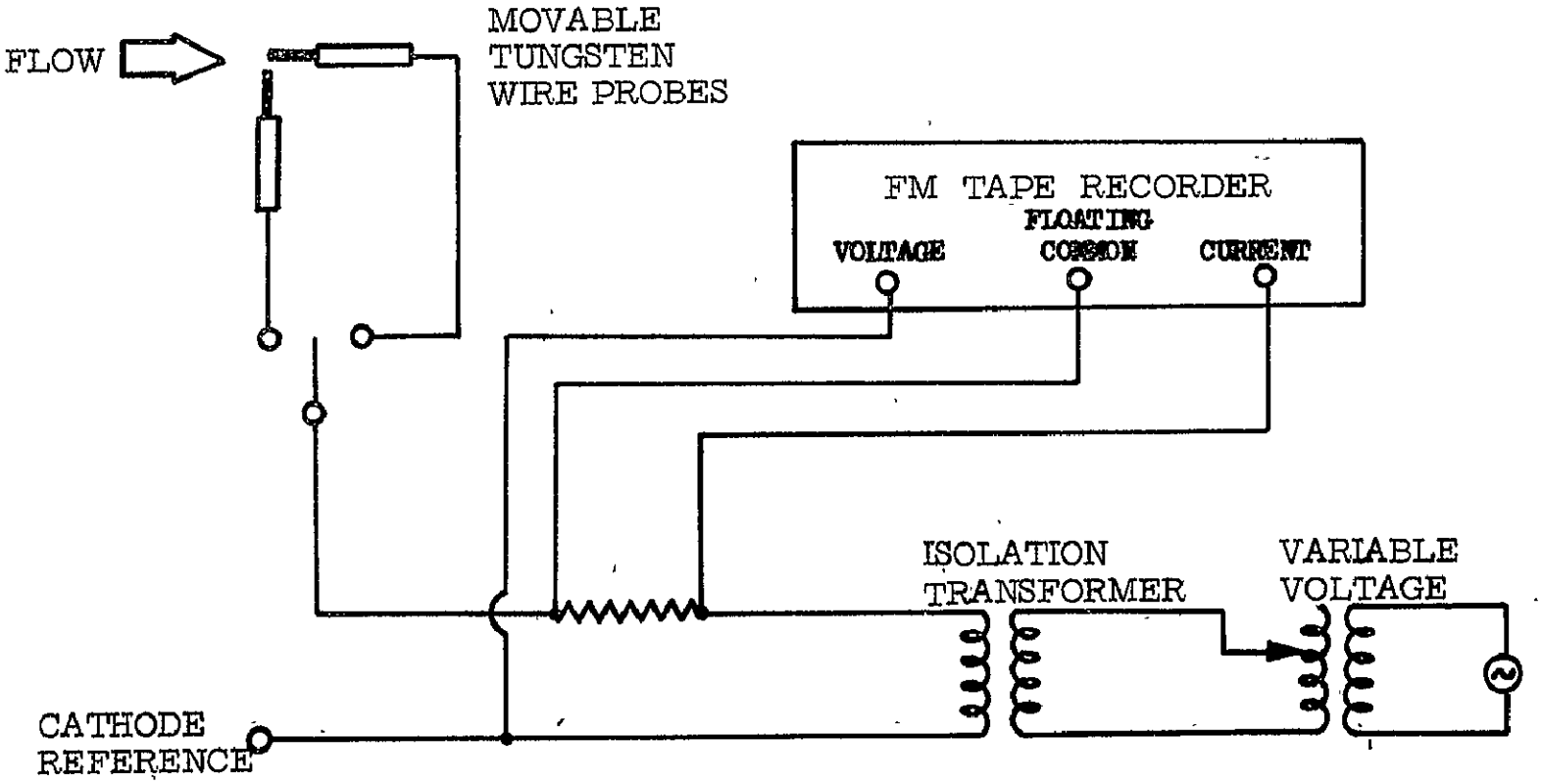

Brooks-1

REDUCTION OF PROBE DATA FOR CALCULATION OF ELECTRON TEMPERATURE

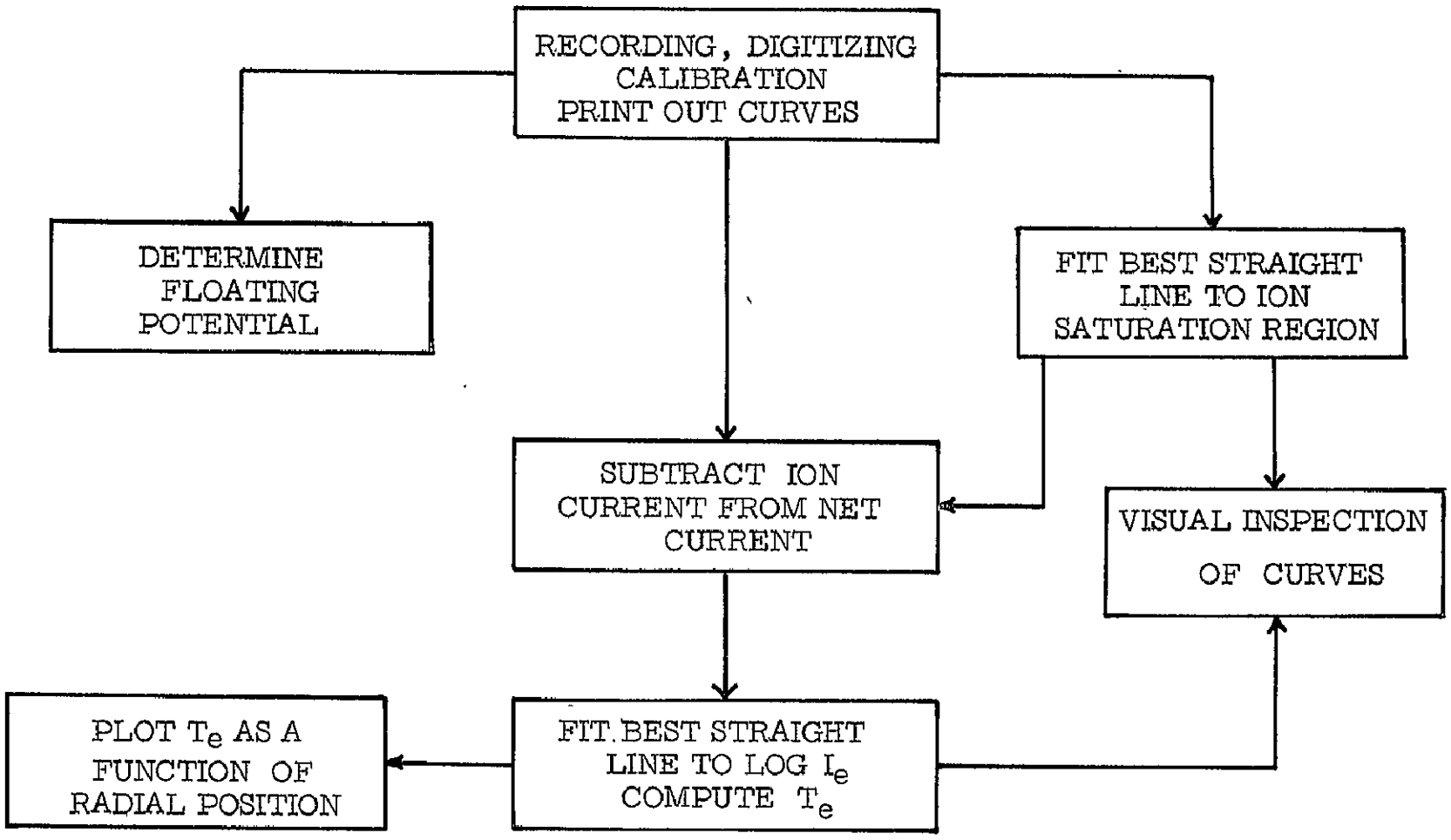

OPTICAL MEASUREMENTS OF TEMPERATURE AND VELOCITY IN LOW DENSITY PLASMA STREAMS

By F. W. Bowen, Jr., G. Oertel, R. V. Hess, N. Jalufka and J. Burlock
NASA Langley Research Center
Hampton, Virginia

Optical methods of measurement are being employed in the co-axial Hall current plasma accelerator. These include spectroscopic measurements of degree of ionization, electron temperature, and ion velocity by the Doppler shift method. Techniques using laser radiation are being developed for time of flight and Doppler shift velocity measurements. The accelerator is operated with an argon mass flow rate of 0.01 gram per second and a vacuum chamber pressure about 2×10^{-2} Torr. The arc current is kept constant at 300 amperes, the arc voltage at 40 volts; and the magnetic field at 3000 gauss.

Degree of Ionization.- Spectroscopic observations for determining the degree of ionization of the plasma have been made both end-on and side-on with respect to the plasma stream (fig. 1). From the resulting spectrograms, spectral lines of singly ionized argon (AII) and doubly ionized argon (AIII) have been identified. Contamination lines exist in the end-on views and in side-on views close to the anode, but the lines disappear at distances 5 centimeters or greater downstream from the anode. The AIII lines appear to exist with approximately the same intensity as the AII lines. Identification of spectral lines from side-on views 25 centimeters downstream from the front face of the anode shows that the AIII lines remain strong. Absence of AI lines from spectrograms obtained by both end and side observations indicates that the plasma may be fully ionized.

Electron Temperature Measurements.- Electron temperature determinations are made on the basis that the appearance of a characteristic spectral line in a steady-state plasma provides an indication of the corresponding electron temperature. However, calculations have shown that the plasma is not in equilibrium, since the time required for ionization is greater than the residence time of the plasma in the accelerator. Hence, if the electron temperature is increasing in the anode region, then the temperature obtained by the spectral line identification method is a lower limit to the equilibrium temperature, that is, the equilibrium temperature has not been reached and excitation has not stabliized. Since thermal non-uniformities exist both axially at some distance downstream and radially, the measured temperature will instead be a range of temperatures corresponding to a hot inner region in addition to cooler outer layers. The decaying end of the plasma stream as well as the accelerator region is observed in the end-on view, while the expanding outer plasma as well as the inner core is seen in the side-on view. These thermal non-uniformities prevent the line intensity ratio method of temperature measurement from being made axially, while a lower limit temperature may be obtained radially by the ratio method with the aid of an Abel inversion.

Calculations of spectral line intensities of excited states of AI, AII, AIII, and AIV give the relation of the line intensities to the electron temperatures and allows interpretation of the data over the temperature range of interest. The attenuation of the spectral line intensity by optical components in the system is such, that if the emitted line intensity is a factor 1/100 less than the maximum value it can attain as a function of temperature, then it will in all probability not be seen on the spectrographic plate. Conversely, line intensities greater than 1/100 of their maximum intensities may be seen. Therefore, in interpreting the data using figure 2, the low end of the temperature range is obtained by using the increasing part of the AII intensity curve at 1/100 of the maximum intensity, or 1.5 eV (17,000 ^{o}K). The upper end of the range is the temperature corresponding to the increasing part of the AIV curve which is 1/100 of the maximum intensity, or 3.4 eV (40,000 ^{o}K). It is important to note, however, that intense AIII lines indicate that AIV levels are becoming populated, and hence a temperature higher than 3.4 eV is suggested. Higher estimates may not be made, though, until positive identification of the AIV lines is made. Since the AIV lines accessible with the optical path in the atmosphere exist in regions where contamination lines interfere, vacuum spectroscopy is required to find lines farther down into the ultraviolet region.

Ion Velocity by Doppler Shift Method.- Axial ion velocities are being determined from the Doppler shifts of the emitted spectral lines. A low pressure argon lamp is used to produce AI reference lines for measuring the shift of AII lines in the plasma. Since the end-on observation penetrates the entire plasma, velocity measurements determined from these Doppler shifts are not spatially resolved. The velocities thus measured then are at best average velocities. Only the Doppler shifts of AII lines near the AI reference lines have been measured. The measurements so far yield velocities on the order of 10,000 meters per second. Some experiments for measuring the Doppler shifts of AIII lines were made with the use of an iron arc as a reference source. AIII lines originate in the accelerator region, so it was believed that measurements of AIII line shifts would provide a reasonable degree of spatial resolution for the velocities. As mentioned previously, however, side-on observations of the plasma revealed AIII lines 25 centimeters downstream from the front face of the anode. Hence, velocity measurements from AIII lines would not provide spatially resolved velocities much better than those from AII lines.

Use of Lasers for Velocity Measurements.- Lasers will be used to excite ions with frequencies near the laser frequency for local spectroscopic velocity measurements. Velocities have been measured at higher pressures by ionizing a gas with a pulsed laser and measuring the velocity of the ionized region using photographic techniques and probes.[1] The laser ionizing process is not effective at low pressures. However, excitation of particles with the same frequency as that of the laser photons is possible. Spectroscopic techniques may then be used to isolate the excited line so that it may be used to detect motion. The experimental arrangement is shown in figure 1. A giant (125 MW) Q-switched ruby laser with a frequency multiplier is used to obtain a laser out-put wavelength of 3472 Å. The laser beam is focused to a point inside the plasma stream to excite ions emitting the

3472 Å AII line. A monochromator fixed on 3472 Å will observe the laser pulse, and with the aid of a half-silvered mirror, will observe the radiating ion as it passes a given point downstream. The time between the phototube observations of the spectral line at the two positions will be recorded on an oscilloscope and the velocity determined directly. Doppler shift measurements of the excited particles will also be made.

---

[1]Chen, Che Jen, "Experimental Study of Breakdown Phenomena in Argon Gas by a Laser Beam at Low Pressure." Paper presented at AIAA Plasmadynamics Conference, Monterey, California, March 2-4, 1966. AIAA Paper No. 66-176.

ACCELERATOR AND OPTICAL APPARATUS

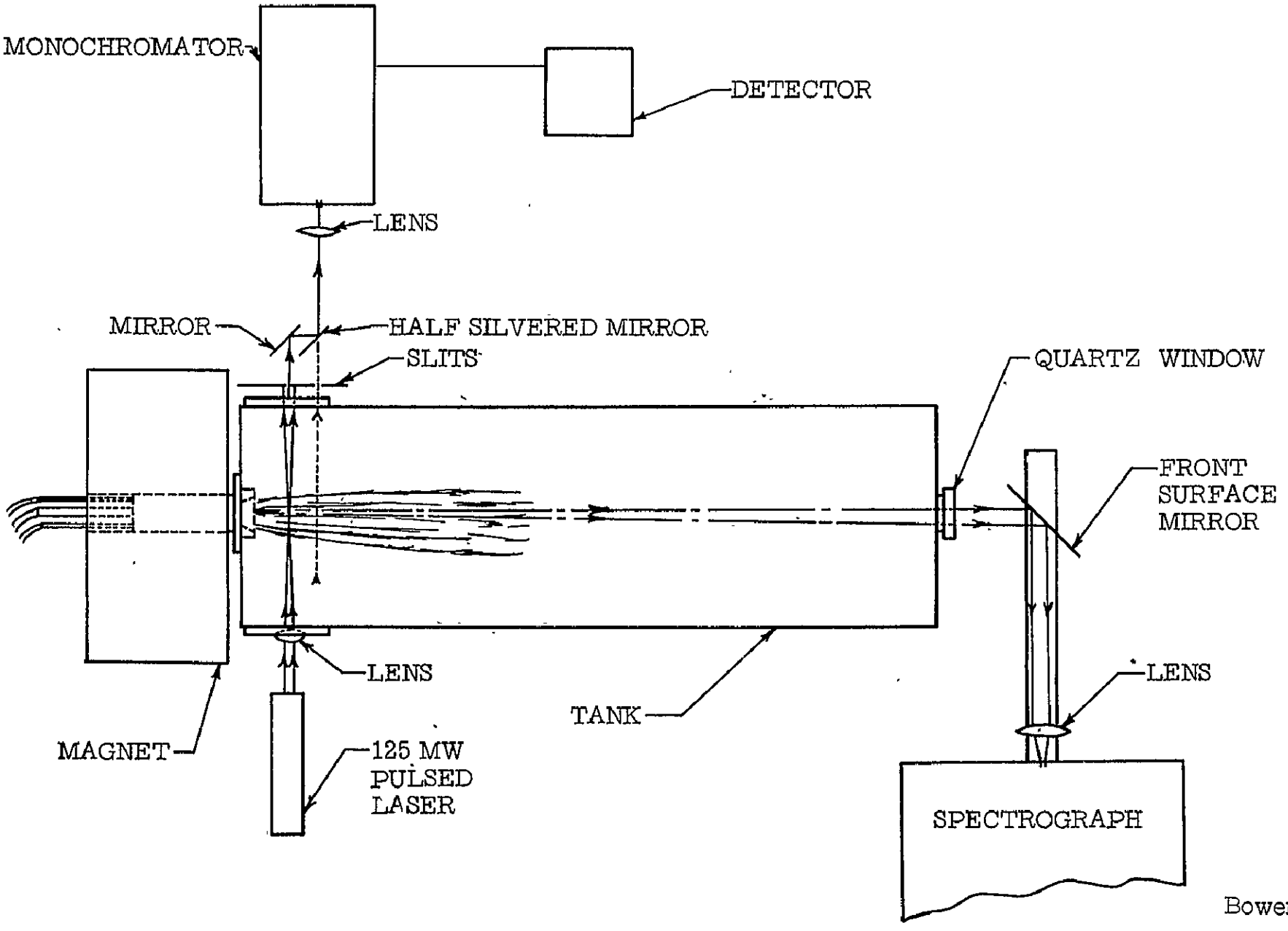

INTENSITIES AS FUNCTIONS OF TEMPERATURE FOR LINES OF AI, AII, AIII AND AIV

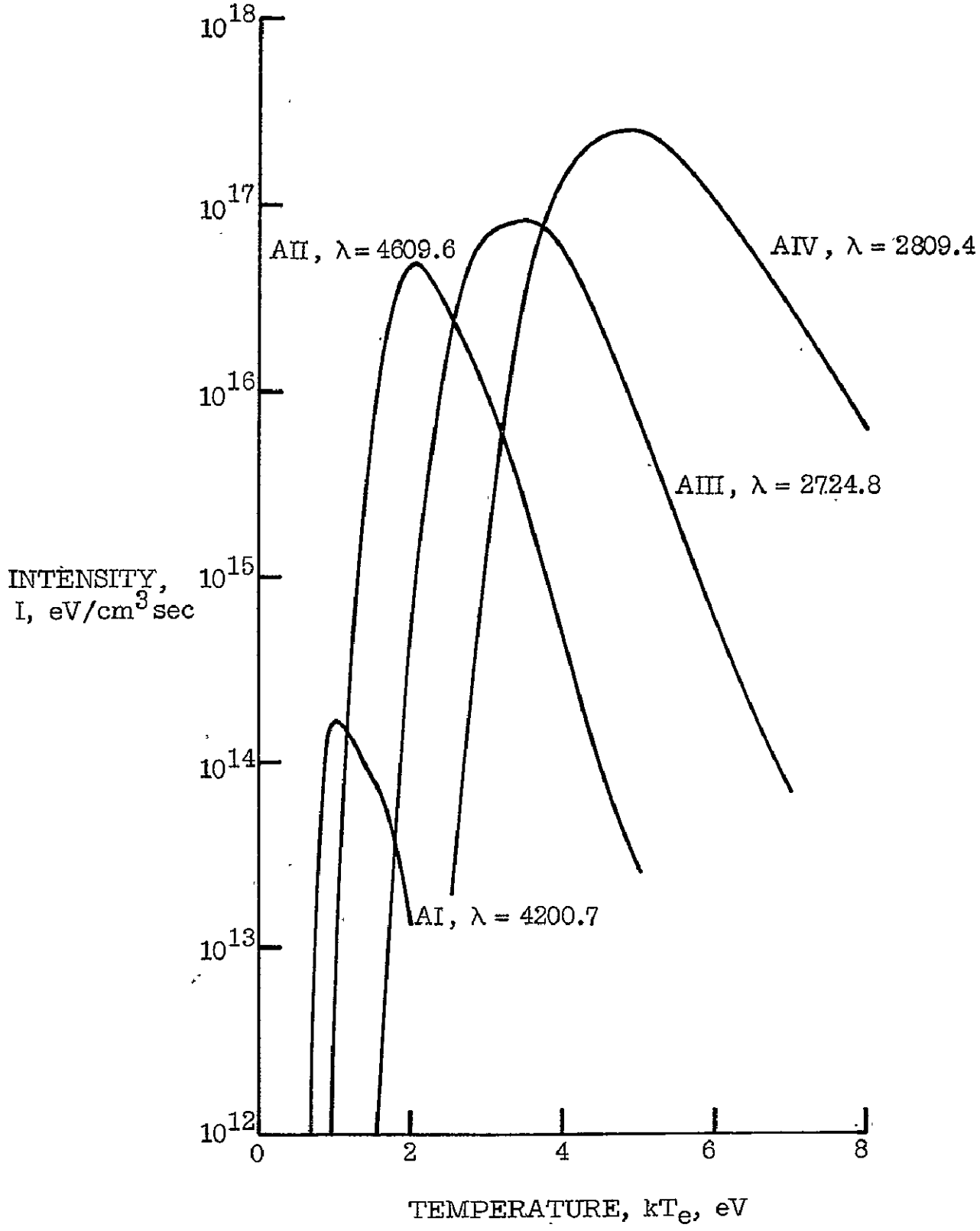

Bowen-2

MICROWAVE MEASUREMENTS OF PLASMA DENSITY FLUCTUATIONS

J. Burlock and T. M. Collier

NASA, Langley Research Center
Hampton, Virginia

The linear Hall accelerator, because of its uniform geometry and field distribution, is being used for study of processes that affect the efficiency of the closely related coaxial accelerator now under development at the Langley Research Center. The processes of most interest are the anomalous conductivity, associated with plasma fluctuations. Previous work at Langley (ref. 1) and other laboratories (ref. 2, 3) has shown the presence of both coherent and random potential and density fluctuations, and a probable mechanism for the coherent part has been discussed (ref. 4). Anomalous conduction, referred to on occasion as "electron back-streaming" or "electron back-flow" limits the efficiency of plasma devices that depend on current controlled by magnetic fields. The effectiveness of the magnetic field in controlling current is measureable in these experiments by the ratio of transverse to Hall current, neglecting ion slip

$$\frac{J_\perp}{J_H} = \omega_e \tau_e = \mu_e B$$

where ω_e is electron cyclotron frequency, τ_e is collision time for momentum transfer, μ_e is electron mobility and B is magnetic field. The fact that the ratio is not necessarily as predicted has been related to instabilities that produce correlated density and velocity fluctuations (ref. 5). Measurements of these quantities has generally been done with electrostatic probes and Langmuir probes operating in the ion saturation region. However, saturation ion flux to the probe is controlled by both the plasma density, and a velocity depending on probe sheath conditions. For the present experiments these result in a probe current

$$J_i = cne\left(\frac{kT_e}{m_i}\right)^{1/2}$$

where T_e is electron temperature, k is Boltzmann's constant, m_i is ion mass, and the value of c depends on the sheath condition. The large fluctuating potentials present in the plasma, produce associated electric field that could increase the ion velocity and add to the ion saturation current. A plasma density measuring technique sensitive to plasma density only, would allow separation of the density and velocity components of ion flux.

A microwave system using a short antenna and coaxial construction similar to reference 6 has been developed for obtaining both average and fluctuating components of plasma density (fig. 1). Simultaneous measurements of

flux, using the same probe, allow determination of ion velocity. To avoid complications resulting from resonance at electron plasma frequency, and the effect of magnetic field on the plasma conductivity, a frequency higher than the maximum electron plasma resonance frequency and much higher than the maximum electron cyclotron frequency have been chosen. The microwave detector system is arranged as a reflectometer. Plasma density changes produce impedance variations at the antenna, (fig. 2) changing the amount of reflected wave power. The antenna is in the form of a short stub, 1/16 wavelength long. This presents a capacitive impedance (ref. 7) to the system

$$C = \frac{\pi \varepsilon h}{\ln \frac{h}{a} - 1}$$

where h and a are probe length and radius, respectively, and ε is the plasma dielectric constant:

$$\varepsilon_p = \varepsilon_o \left(1 - \frac{\omega_p^2}{\omega^2}\right).$$

The small size of the antenna produces an electric field configuration which makes the system sensitive only in the immediate vicinity of the exposed stub. Exploratory sweeps, with perturbing conductors of different shapes, indicate a sensitive region of about the diameter of the outer conductor of the coaxial structure of the probe, one-eighth inch. To minimize power loss, a problem because of the small coaxial cross section, small support beads, are used rather than a dielectric filling. The microwave antenna also serves simultaneously either as a biased Langmuir probe, or potential probe, for obtaining correlated measurements of density, ion flux, and potential. Electrostatic coupling to the microwave system was reduced by introducing a thin insulating plate between waveguide sections. In addition to fluctuation amplitudes, average values of the ion saturation current from the Langmuir probe and microwave system are recorded for information on depth of modulation. A sensor coil surrounds the accelerator for determining the value of Hall current. This gives information on $\omega_e \tau_e$ of the plasma in the magnetic field and can be interpreted to give plasma density.

A limited number of runs covering a restricted range of parameters has been made with the complete system, so far. The frequency response has been limited to 100 kilocycles, to allow visual estimate of phase correlation. The runs have been taken in sets with constant current of 3 amperes and variable magnetic field, 100 - 700 gauss, and also constant magnetic field of about 100 gauss and variable current of 3 to 22 amperes, at 0.1 and 0.03 Torr.

The following preliminary observations may be made on the basis of this data: In the range of parameters used, the value of Hall current tends to remain constant with increase in magnetic field. This is accompanied by an

increase of both coherent and random noise. The random noise covers the whole frequency spectrum to the 100 kc limit of the filtering which has been introduced. At constant magnetic field and variable current, the ratio of Hall current to axial current remains fairly constant. The coherent oscillation amplitude increases, but the random noise is quite small. The comparative effects on the conduction of coherent low pressures oscillations and high frequency noise must be evaluated. On the result will also depend the applicability of the approach in reference 5 which emphasizes the influence of the higher frequency noise on the conduction process. The parameter range covered has not as yet been extended to higher currents, over a variation of magnetic field strengths which give the full range of effects on $\omega_e \tau_e$ (ref. 8).

References:

1. Hess, R. V., Burlock, J., Sidney, B., Brockman, P., Brooks, D.: Study of Instabilities and Transition to Turbulent Conduction in the Presence of Hall Currents. Int. Symp. on Diffusion of Plasma Across a Magnetic Field. Feldafing, Germany, June 1964.

2. Janes, G. S. and Lowder, R. S.: Anomolous Electron Diffusion and Ion Acceleration in a Low Density Plasma. RR-224 7/65 AVCO-Everett Research Laboratory, Everett, Mass.

3. Pinsley, E. A., Brown, C. O. and Barnes, C. M.: A Hall Current Accelerator Utilizing Surface Contact Ionization. Preprint No. 64-23, Aerospace Science Meeting, Jan. 1964.

4. Burlock, J. and Brooks, D. B.: Correlations of Coherent Oscillations and Hall Currents in the Linear Hall Accelerator. Applied Physics Letters, Aug. 1, 1965.

5. Yoshikawa, S. and Rose, D. J.: Anomalous Diffusion of a Plasma Across a Magnetic Field. Phys. Fl. v. 5, no. 1, March 1962.

6. Guthart, H., Weissman, D. E. and Morita, T.: Measurement of the Spectrum of Ionized and Neutral Density Fluctuations in a Thermally Produced Turbulent Plasma. Tech. Report 25, 1965. Stanford Research Institute, Menlo Park, Cal.

7. King, R., Harrison, Jr., C. W. and Denton, Jr., D. H.: The Electrically Short Antenna as a Probe for Measuring Free Electron Densities and Collision Frequencies in an Ionized Region. J. of Res., NBS, v. 65, no. 4, 1961.

8. Brockman, P., Hess, R. V. and Weinstein, R.: Measurements and Theoretical Interpretation of Hall Currents for Steady Axial Discharges in Radial Magnetic Fields. Fifth Biennial Gas Dynamics Symposium, Evanston, Ill., August 1963.

LANGMUIR AND MICROWAVE PROBE SYSTEM

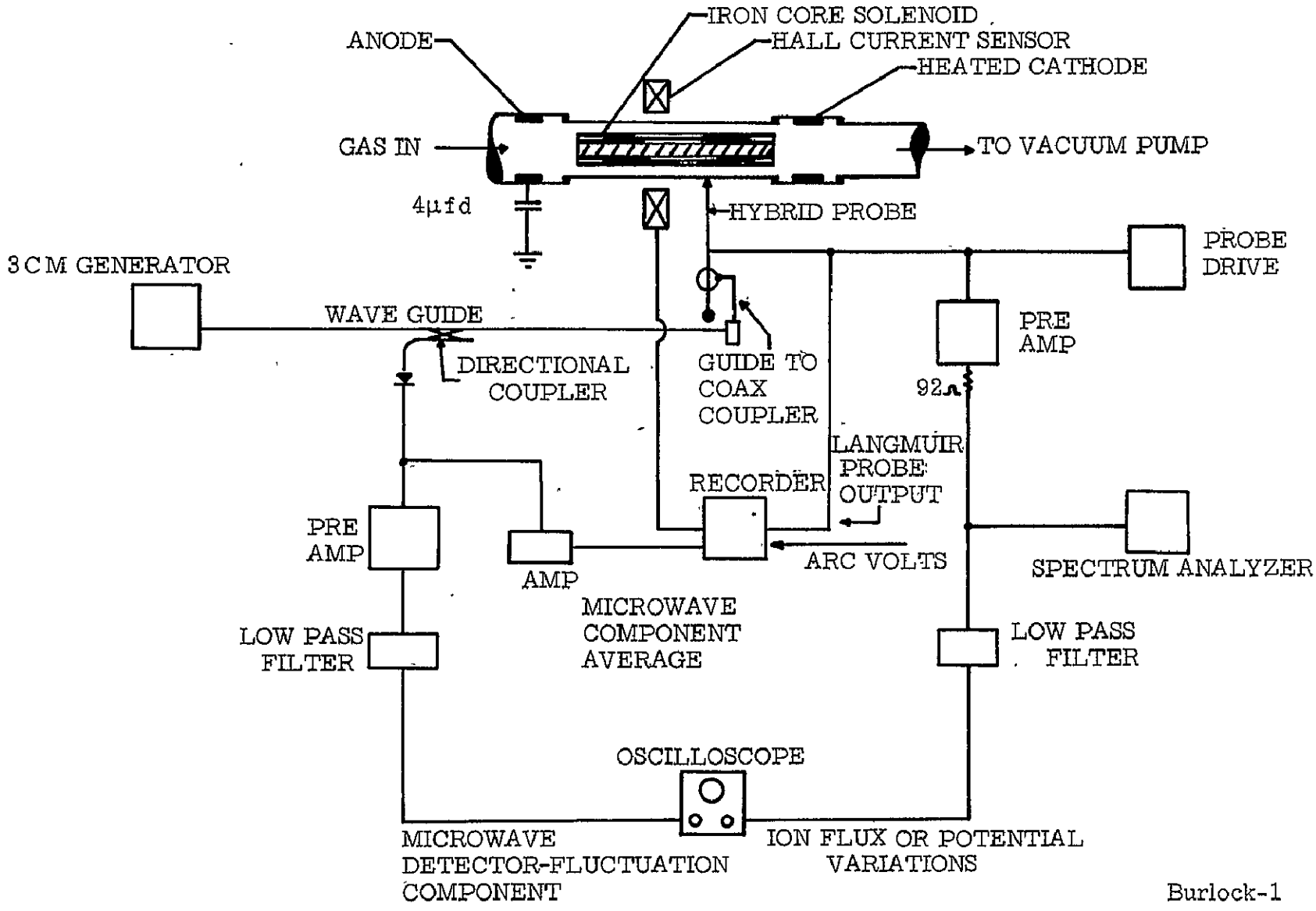

Burlock-1

PROBE FOR ION FLUX AND μ WAVE DENSITY MEASUREMENT

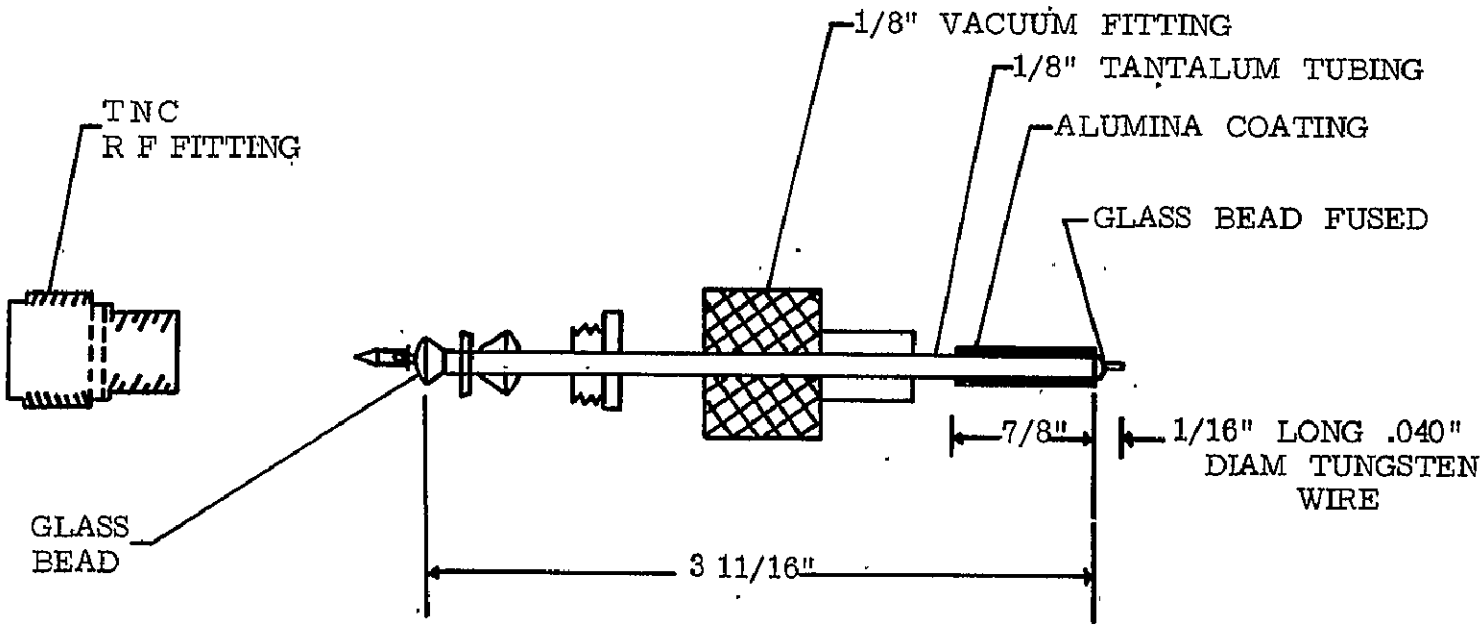

Burlock-2

FORCED OSCILLATIONS IN COLLISIONAL PLASMAS AND RAREFIED GASES

By Gary A. Massel and M. R. Feix[+]
NASA Langley Research Center
Hampton, Virginia

Forced oscillations in a plasma,[1] in contradistinction to free oscillations, better illustrate the kinetic nature of the plasma. In addition to the collective nature of the plasma described by the Debye pole for $\omega < \omega_p$, the "streaming nature" of the Vlasov operator manifests itself in a branch-line integral where the branch-line lies along the continuum of eigenvalues in the k-plane. Thus the solution of the problem cannot be represented entirely as the sum of poles as in the initial value problem.

To investigate this problem in detail, the B-G-K[2] equation for an absolute equilibrium was assumed. This describes the collision effects of the electrons with the background of massive ions and neutrals. The ions are assumed to remain fixed, i.e. $\omega >> \omega_{pi}$. Thus the linearized system is described by

$$\frac{\partial f(x,v,t)}{\partial t} + v\,\frac{\partial f(x,v,t)}{\partial x} + \frac{e}{m}\,E(x,t)\,\frac{\partial F(v)}{\partial v} = -\,\nu\left[f(x,v,t) - n(x,t)\,F(v)\right] \tag{1}$$

$$\frac{\partial E(x,t)}{\partial x} = 4\pi e\left[\int f(x,v,t)\,dv - n_o\right] \tag{2}$$

where $F(v)$ is a Maxwellian distribution.

Considering the case of a pair of closely-spaced grids immersed in the plasma and solving for the electrostatic field, one finds for $x > 0$,

$$E(x) = \frac{E_o \Delta}{2\pi}\left\{-2\pi i \sum_j \left[\frac{\partial\,\varepsilon(\theta, i\omega)}{\partial\theta}\right]^{-1}_{\theta=\theta_j} \exp\left\{-\frac{i\omega+\nu}{\sqrt{2}v_T}\,\frac{x}{\theta_j}\right\}\right\}$$

$$+\int_0^\infty \theta^{-2}\left[\frac{1}{\varepsilon\left(\theta_r+i0_+, i\omega, \nu\right)} - \frac{1}{\varepsilon\left(\theta_r+i0_-, \omega, \nu\right)}\right]\exp\left\{-\frac{i\omega+\nu}{\sqrt{2}\,v_T}\,\frac{x}{\theta}\right\}d\theta \tag{3}$$

[+]NAS-NRC Senior Post-Doctoral Resident Research Associate.

where

$$\varepsilon(\theta, i\omega, \nu) = \frac{1 - \frac{2\omega_p^2}{(s+\nu)^2}\theta^2 \int \frac{\frac{dF}{d\xi}}{\sqrt{2}\,\theta - \xi}\,d\xi - \frac{\nu}{s+\nu}\sqrt{2}\,\theta \int \frac{F(\xi)}{\sqrt{2}\,\theta - \xi}\,d\xi}{1 - \frac{\nu}{s+\nu}\sqrt{2}\,\theta \int \frac{F(\xi)}{\sqrt{2}\,\theta - \xi}\,d\xi} \tag{4}$$

and

$$\varepsilon(\theta_j, i\omega, \nu) = 0 \qquad \text{for} \qquad \mathrm{Im}\,\theta_j < 0 \tag{5}$$

The only pole admitted by equation (5) is the Debye pole for ω less often some critical frequency, ω_c, which is a function of ν. For $\omega > \omega_c$, there exists no solution to equation (5). This pole dominates at distances near the grids for $\nu \leq \omega_p$. For $\nu > \omega_p$ and $\nu > \omega$ (i.e. hydrodynamic limit) it dominates at all but very extreme distances. The Debye pole is illustrated in figure 1.

The branch-line integral yields an asymptotic field varying as

$$E(x) \sim \left[\left(\frac{\omega^2}{\nu^2} + 1\right)^{1/2} \frac{x}{\lambda}\right]^{1/3} \exp - \left\{\left(\frac{\omega^2}{\nu^2} + 1\right)^{1/2} \frac{x}{\lambda}\right\}^{2/3} \tag{6}$$

which dominates at large $\frac{x}{\lambda}$ for $\nu < \omega_p$. Figure 2 illustrates the two field contributions and figure 3 illustrates the enhanced excitation (for $\nu \leq \omega$) due to collisions.

For forced oscillations in a rarified gas, it is necessary to assume a local equilibrium and the set of equations which must be solved is

$$\frac{\partial \phi(x,\xi,\tau)}{\partial \tau} + \xi_1 \frac{\partial \phi}{\partial x} + \phi = \hat{\rho} + \xi_1 \hat{u} + \hat{T}\,\frac{1}{2}(\xi^2 - 3)$$

$$\hat{\rho}(x,\tau) = \int F(\xi)\phi(x,\xi,\tau)\,d\xi$$

$$\hat{u}(x,\tau) = \int \xi_1 F(\xi)\phi(x,\xi,\tau)\,d\xi$$

$$\hat{T}(x,\tau) = \int \left(\frac{1}{3}\,\xi^2 - 1\right) F(\xi)\phi(x,\xi,\tau)\,d\xi \tag{7}$$

Again the solution for any of the state functions is expressed in two parts. One contribution due to poles and another due to a branch-line integral which dominates at distances less than a mean-free path from

the oscillating surface. In the limit as $\nu \to 0$, this gives the collisionless result obtained by Maidanik, Fox, and Heckl.[3] The significance of the branch-line contribution at large distances has not yet been fully determined.

---

[1] G. A. Massel, M. R. Feix, submitted for publication.

[2] P. L. Bhatnagar, E. P. Gross, M. Krook, Phys. Rev. 94 (1954) 511.

[3] G. Maidanik, H. L. Fox, M. Heckl, Phys. Fluids 8 (1965) 259.

DEBYE POLE AND PRANCH LINE FOR $\nu/\omega_p = 0.1$

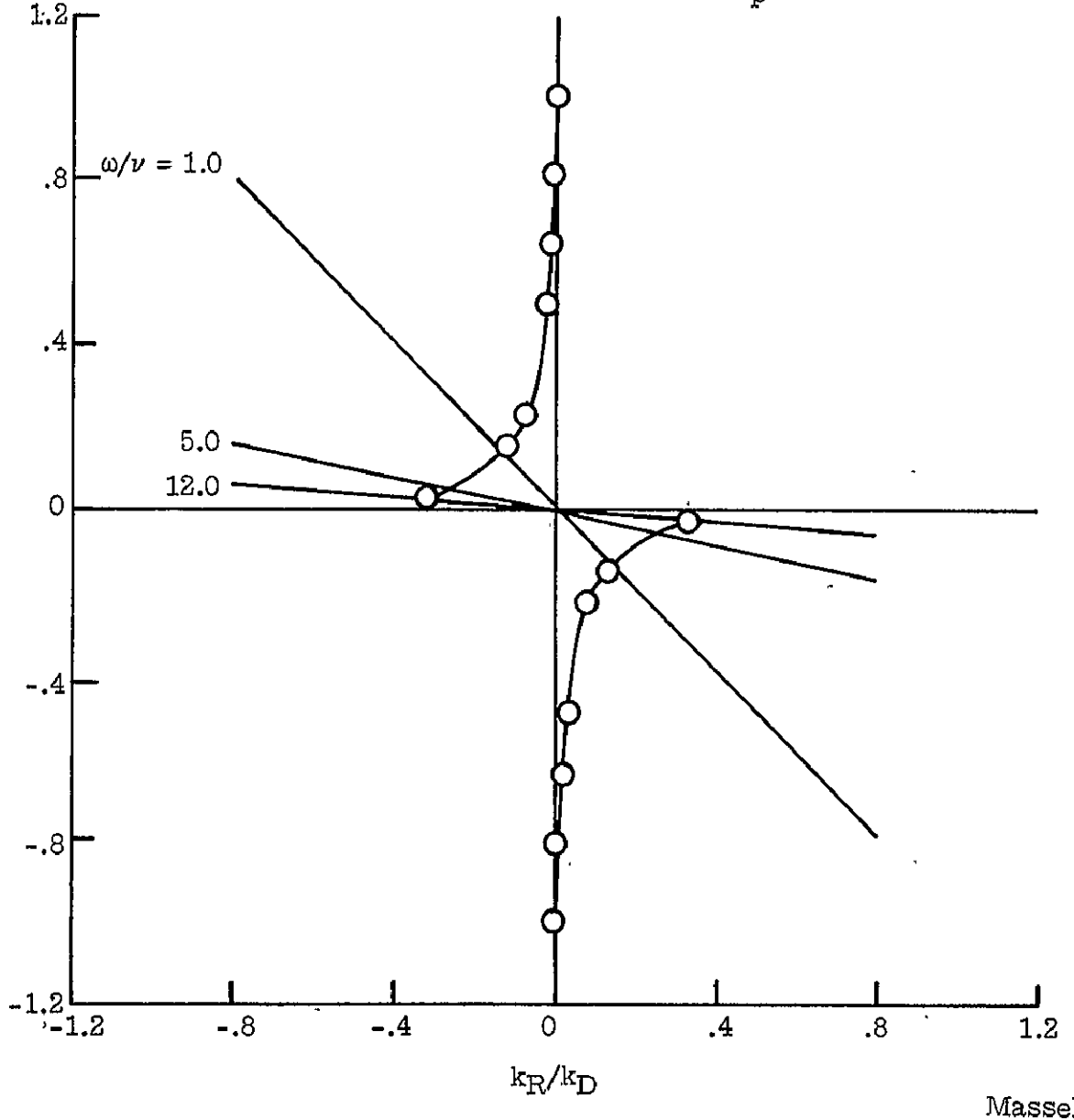

Massel et al-1

DEBYE POLE AND BRANCH LINE CONTRIBUTIONS TO THE ELECTRIC FIELD

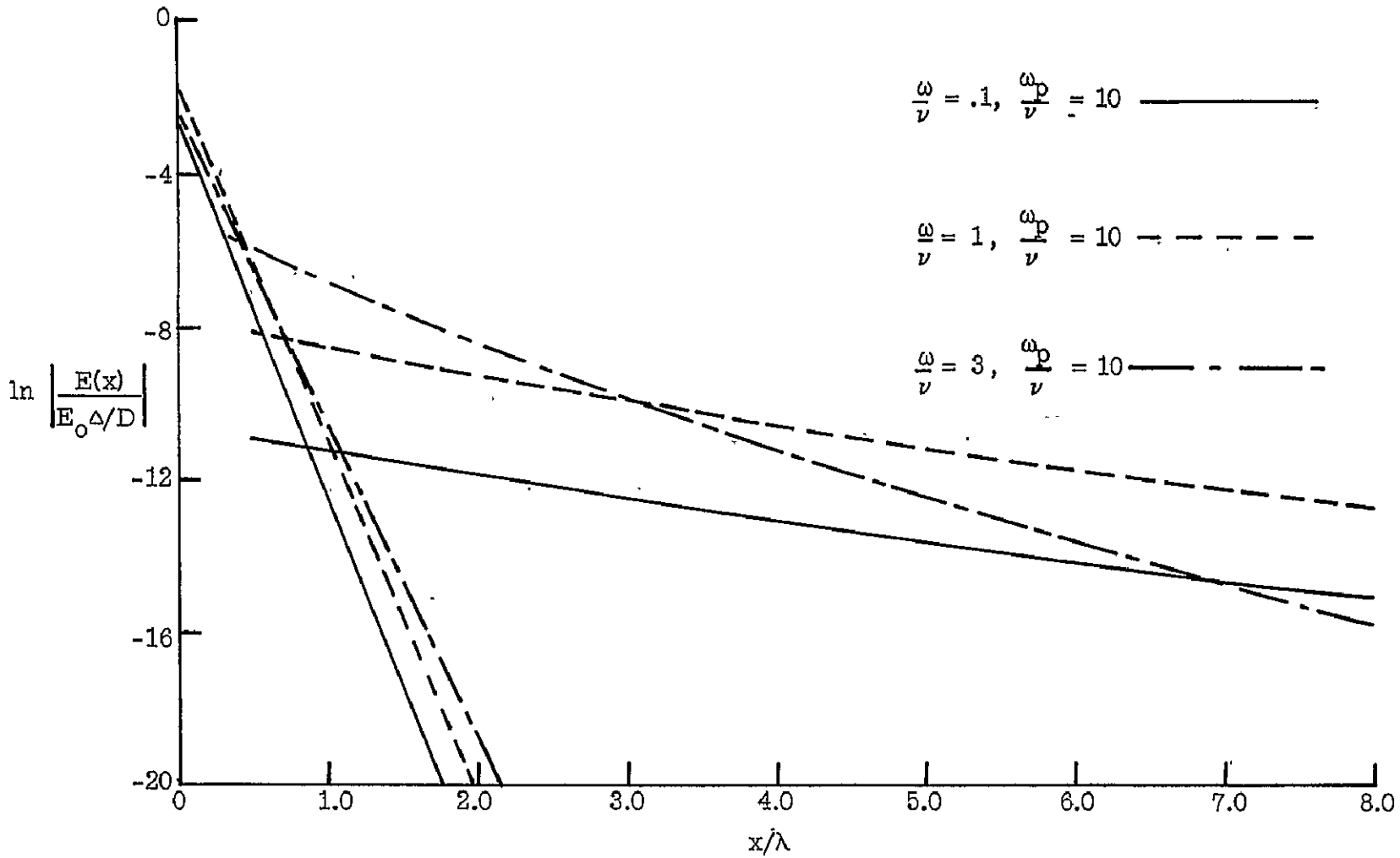

Massel et al-2

EXCITATION OF BRANCH LINE CONTRIBUTION

Excitation

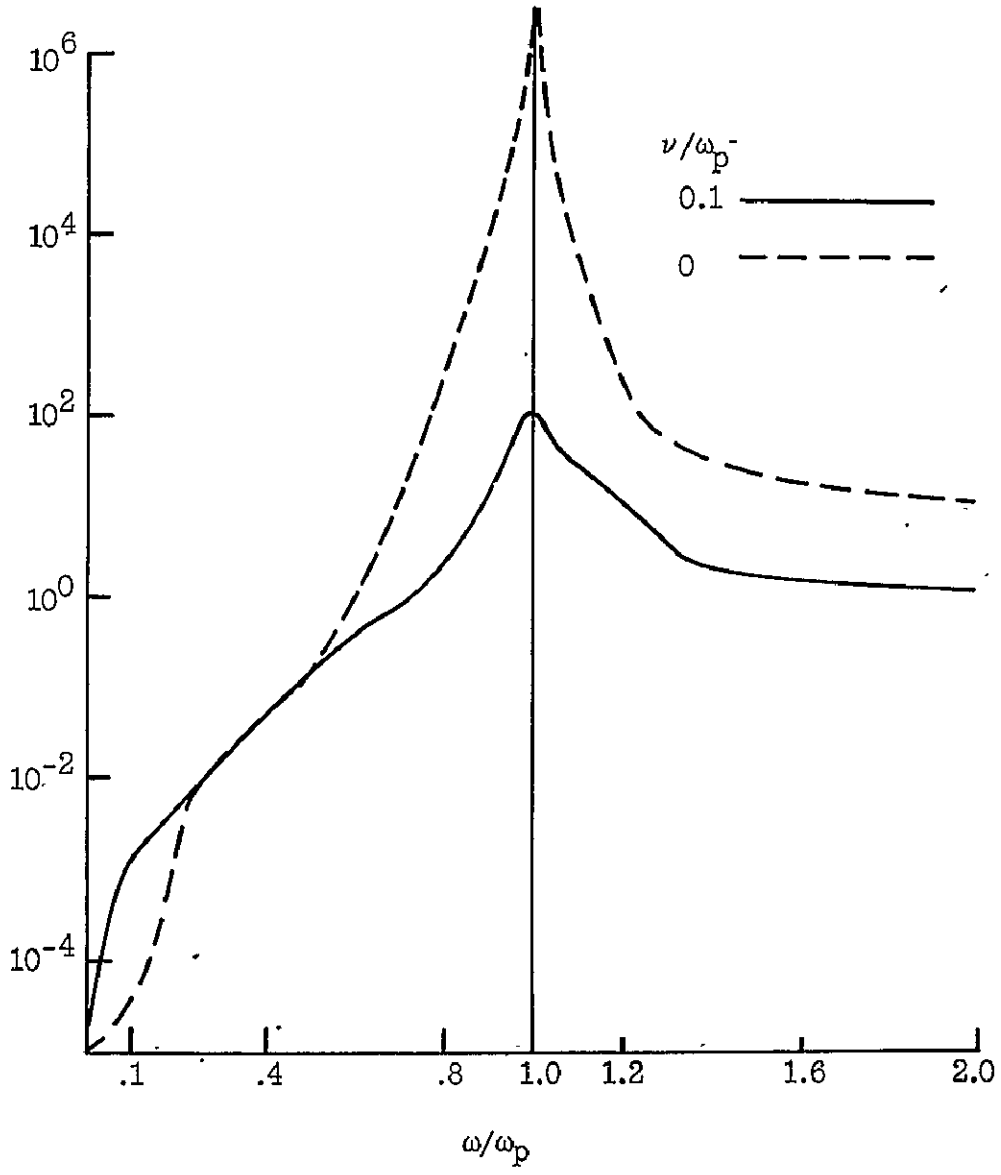

Massel et al-3

COMPUTER SIMULATION OF COLLISIONLESS ONE-DIMENSIONAL PLASMAS

R. H. Weinstein and M. R. Feix*

NASA, Langley Research Center
Hampton, Virginia

Using the NASA Langley IBM directly-coupled 7094-7040 computer system, calculations describing the incremental, self-consistent motions of up to 3000 parallel charged sheets have been used to simulate a collisionless, one-dimensional plasma. These calculations are viewed as an "experiment" against which the predictions of theory can be checked; both equilibrium fluctuations and nonequilibrium relaxation effects are studied. Times are scaled to the plasma frequency and velocities are scaled to $\langle v^2 \rangle$. The present method is approximate and differs from a previous study of the same problem[1] in that a fixed incremental time step Δt in the equations of motion permits an average of several crossings per particle per cycle. In this way it was hoped to speed up the calculations for plasmas with large nD (number of particles per Debye distance).

Since the electric field E seen by a particle depends on the excess charge it sees around it, particle crossings change the field during the motion and make it inexact. The total energy is, therefore, not precisly conserved and the deviation shows up as an increase in the kinetic energy. If, however, the equations of motion are completed to second order in Δt by adding an $\dot{E}$ term to the velocity equation, the total energy growth is drastically reduced and is typically $0.036\%/\omega_p^{-1}$ for $nD=20$ and $\Delta T = \Delta t\, \omega_p^{-1} = 0.1$. The improvement due to the inclusion of $\dot{E}$ is shown for a variety of conditions in Fig. 1.

Taking the Fourier transform of the particle density, i.e., $\rho(k,t) = \int_{-\infty}^{\infty} n(x,t) e^{ikx} dx$, the auto-correlation function $\langle |\rho(k)|^2 \rangle_t = \int_{t_1}^{t_2} \rho^*(k,t)\, \rho(k,t) dt$ can be used to calculate E_k^2, the Fourier modes of the potential energy. Poisson's Law and an assumed exponential dependence on k for all quantities gives $E_k^2 \propto \frac{\langle |\rho(k)|^2 \rangle}{k^2}$. Experimentally the density spectrum is discrete (a sum of δ functions) but its Fourier transform is smooth, i.e.,

$$\rho(k,t) = \int n(x,t) e^{ikx} dx = \frac{1}{L} \int_0^L \sum_{j=1}^{N} \sigma_j \delta(x - x_j) e^{ikx_j(t)} dx$$

$$= \frac{1}{L} \sum_{j=1}^{N} \sigma_j [\cos k\, x_j(t) + i \sin k x_j(t)]$$

* NAS-NRC Senior Post-Doctoral Resident Research Associate

Using the Fourier-Laplace transform of the density one can derive[2] the spectrum dependance on the distribution function $f(v)$, i.e.,

$$|\rho(k,\omega)|^2 = \frac{n}{k} \frac{f(\omega/k)}{|\varepsilon|^2} .$$

Substitution of specific distribution functions and contour integration over the complex ω half plane gives $|\rho(k)|^2$ and, therfore, E_k^2.

We have studied distributions of the form $f(v) = Ae^{-\alpha v^n}$ where $n = 2$ yields the Maxwellian distribution, $n = 4$ the Druvesteyn distribution and $n = \infty$ the square distribution. Figure 2 shows the theoretical curves of E_k^2 for $n = 2, 4, \infty$ and the first twenty experimental modes for an equilibrium plasma (n=2). In spite of the large fluctuations, the convergence of terms is good and the sum deviates from the theory by only 3.4% for the modes shown. As a further check, we have calculated the spatial correlations of the electric field, i.e., $C(\lambda) = [E(x)E(x+\lambda)]_{x,t}$. In addition to demonstrating the collective nature of the plasma through the Debye screening, the additional averaging over both time and space should reduce the fluctuations. Figure 3 shows $C(\lambda)$ for a 1000 particle Maxwellian plasma, where the experimental data is compared with an exponential normalized to the value at $\lambda/D = 0$; both the fit and smoothness are good. The small positive value at large λ/D indicates incomplete shielding, probably due to the inexact nature of the particle motions.

Unfortunately, the experimental potential energy spectra of the non-equilibrium distributions do not go to zero at long wavelengths (small kD); these over-excited and under-damped modes dominate the sum and yield an incorrect ratio of potential to kinetic energy. The approximate form of the distribution function is maintained in meta-equilibrium, as predicted by the one-dimensional Balescu-Lenard equation[1] and in agreement with the experiments of Dawson.[3] The potential energy behavior, however, points to a breakdown of the theory at small kD for $g = 1/nD \neq 0$. If collisional damping dominates Landau damping, then it may be impractical to make $g = 1/nD$ small enough to fit the theory in a range of kD where the distributions can be separated. In the experiment the finite number of particles aggravates the difficulty because there are no particles with velocities high enough to damp the long wavelength disturbances. Calculations are being made to follow the behavior of a group of test particles in an effort to determine in detail how well the meta-equilibrium is maintained.

References: 1. Eldridge, O. C. and Feix, M. R.: Numerical Experiments with a Plasma Model, Phy. of Fluids 6, 398, 1963.
2. Feix, M. R. and Von Hagenow, K.: Connection Between Correlations and Fluctuations in a Plasma. Phys. of Fluids 8, 1565, 1965.
3. Dawson, J.: One-Dimensional Plasma Model. Phys. of Fluids 5, 445, 1962.

FRACTIONAL ENERGY GAIN PER ω_p^{-1}

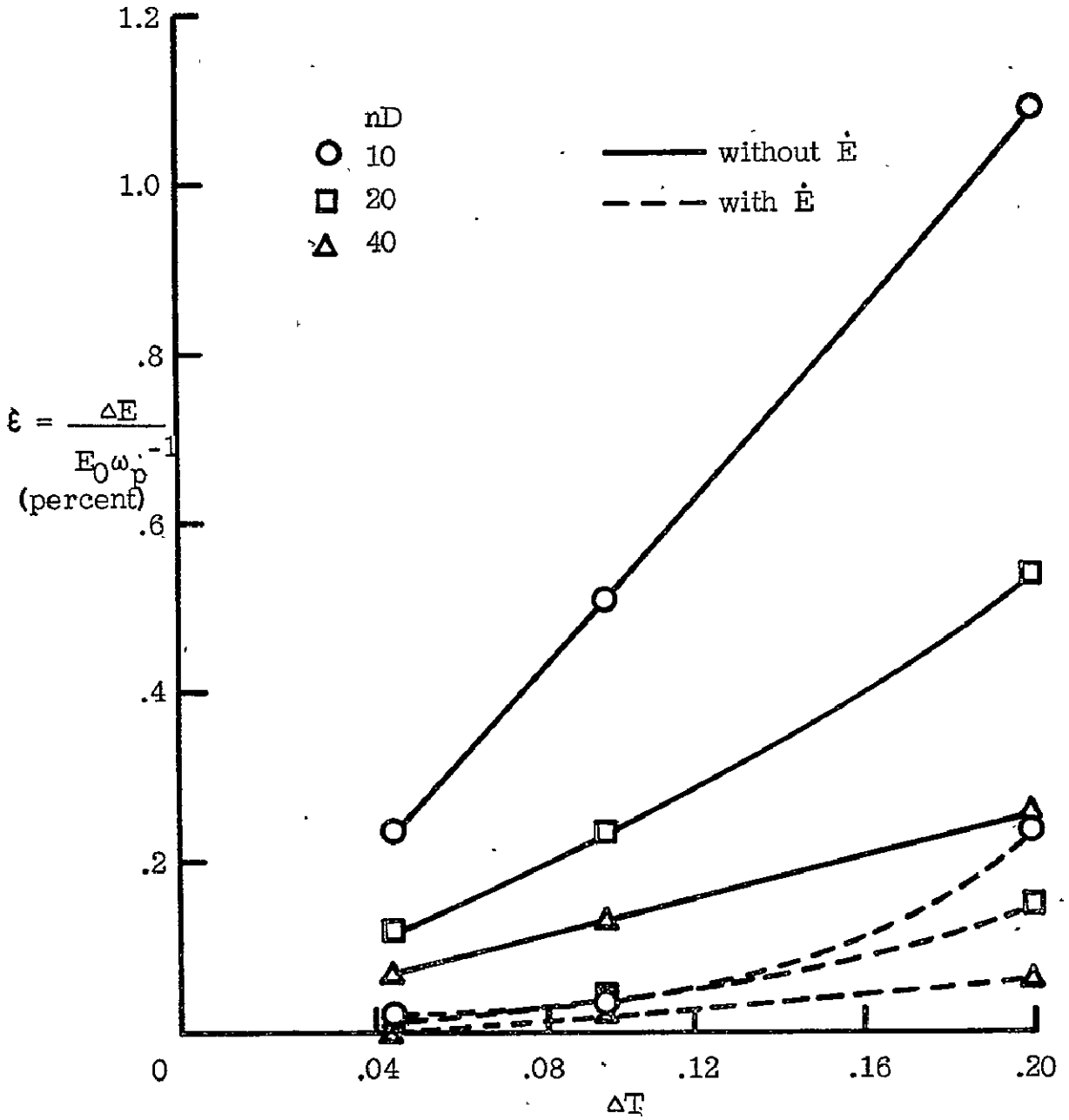

POTENTIAL ENERGY SPECTRUM

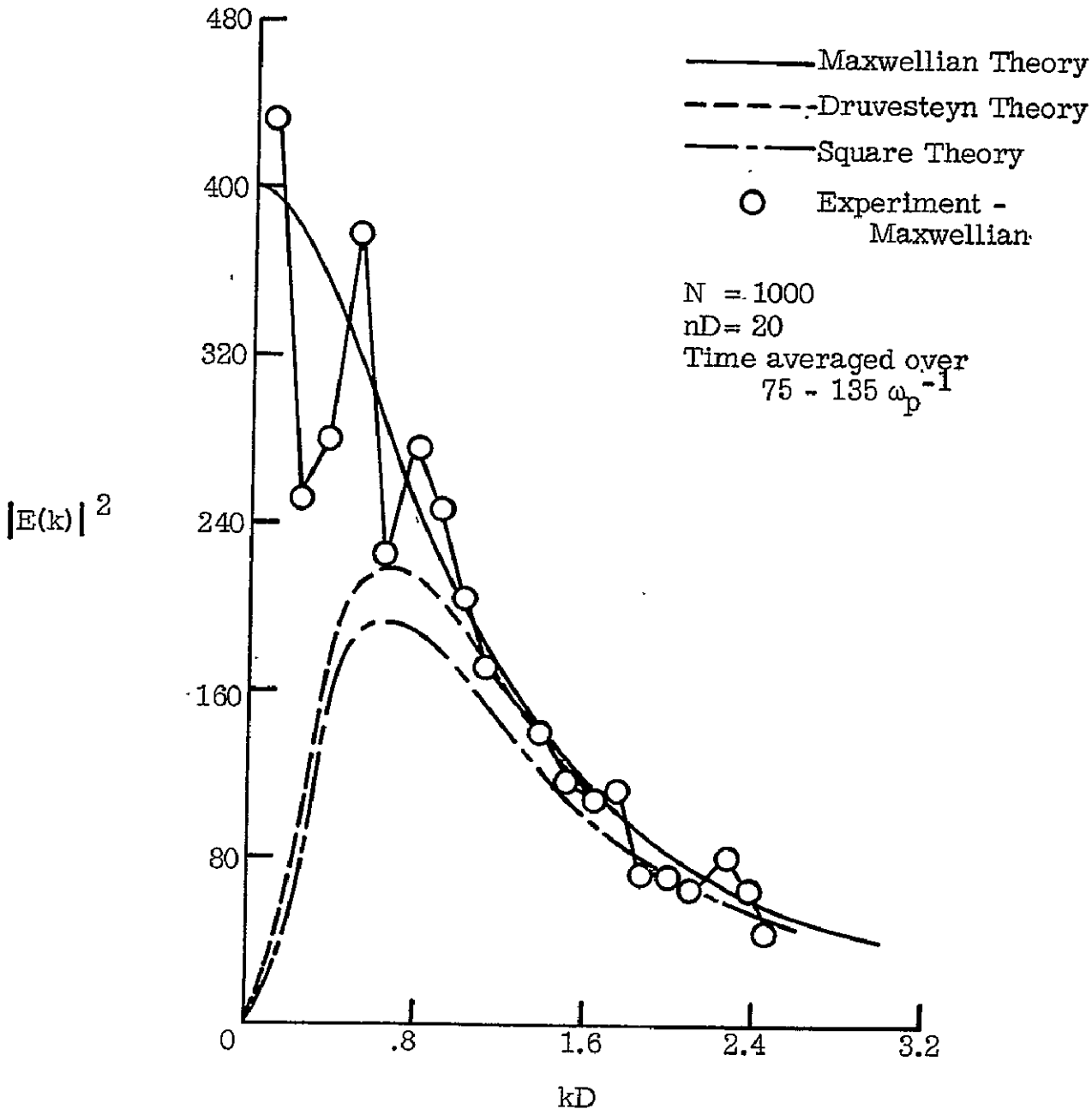

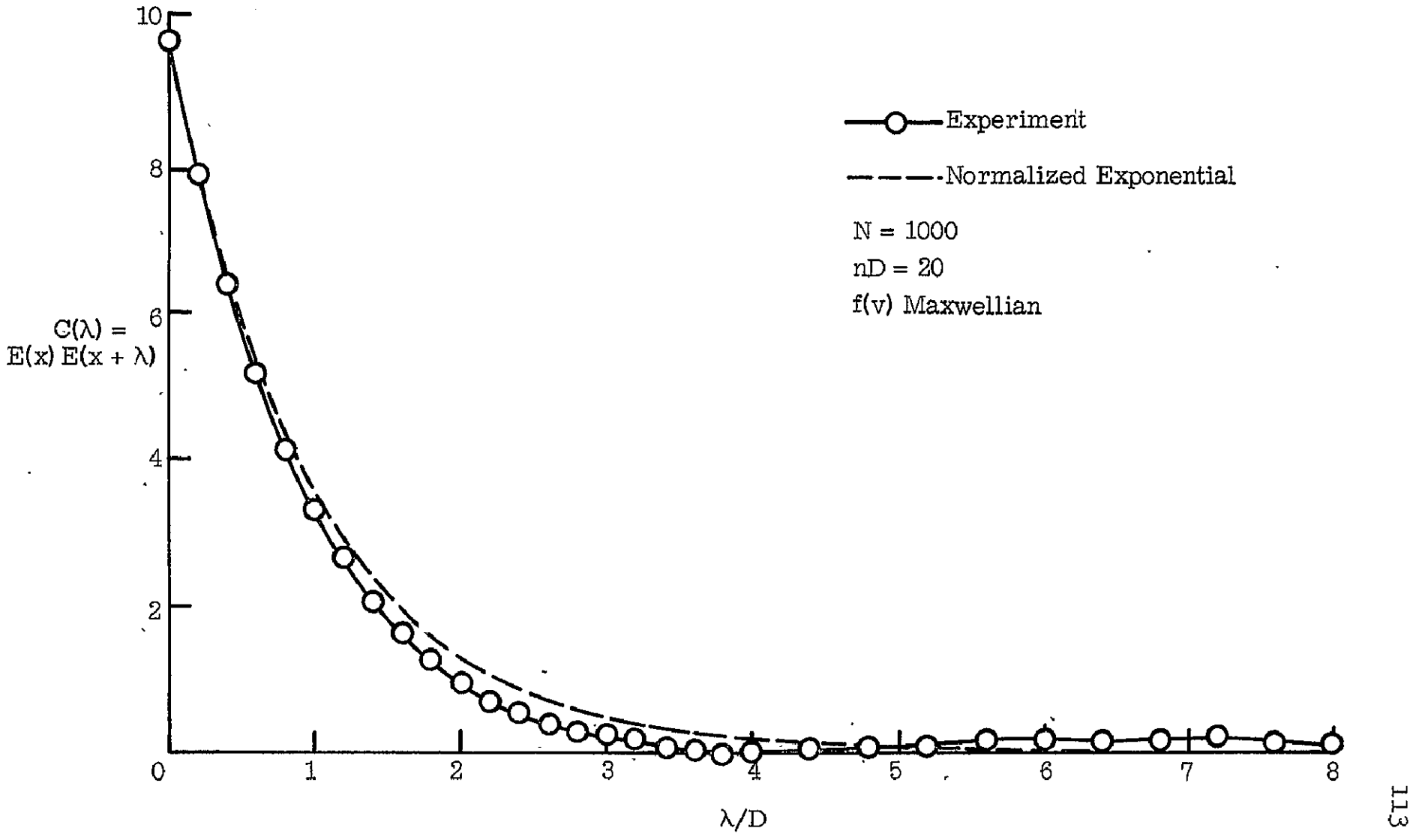
E(x) E(x + λ) VERSUS λ/D
10
8
6
4
2
0
1
2
3
4
5
6
7
8
C(λ) =
E(x) E(x + λ)
λ/D
Experiment
Normalized Exponential
N = 1000
nD = 20
f(v) Maxwellian

LINEAR AND NONLINEAR TREATMENT OF THE VLASOV EQUATION BY MEANS OF A FOURIER-HERMITE TRANSFORMATION

F. C. Grant and M. R. Feix*

NASA, Langley Research Center
Hampton, Virginia

Introduction

Various transformations of the Vlasov equations have been used. Among these are the Fourier-Laplace transform of the coordinate-time space; Hermite transform of the velocity space alone; and Fourier-Fourier transform of the coordinate-velocity space. All of the transformations avoid a difficulty of the coordinate-velocity space, namely, an oscillatory and secular growth of the solutions in the velocity space. However, new difficulties arise in the transformed spaces which are associated with cutoff of the representation in the transformed space.

The Fourier-Hermite transformation of the coordinate-velocity space has an advantage in that it leads to ordinary differential equations, but again there are difficulties associated with the necessity to limit the transformed space. A limitation on the time of good representation arises which is a function of the size of the subspace used after transformation and on the amplitude of the disturbance of the plasma which is considered. There is a limitation of the wave length which favors the longer waves. In the linearized limit of the F-H transform just the wave length limitation and the cutoff of the transformed velocity space are operative. The analysis has been limited to the one-dimensional nonlinear Vlasov equation for the motion of electrons against a uniform positive neutralizing background.

Fourier-Hermite Transformation

The F-H transformation of the Vlasov equations corresponds to a double series expansion of the distribution function followed by substitution into the Vlasov equation which yields a doubly infinite set of ordinary first-order differential equations in the time for the histories of the expansion coefficients. These coefficients may be regarded as the elements of a matrix and truncation of the matrix to a finite size corresponds to keeping a finite number of Fourier components, or wavelengths, as well as a finite number of Hermite functions, or velocity moments. Since macroscopic quantities of interest depend on moments of low order in velocity space the expectation was that truncation at low order in the Hermite space would be unimportant for reasonable time intervals.

Linearized Limit

The ordinary linearized theory of the Vlasov equation corresponds, in the F-H transformation, to retention of two rows of the matrix: one corresponding to the uniform base velocity distribution which does not change; the

* NAS-NRC Senior Post-Doctoral Resident Research Associate

other corresponding to an inhomogeneous perturbation of the plasma. The general dispersion relation of the linearized F-H analysis may be written down in terms of a certain set of polynomials. Two interesting special cases have been analyzed in some detail: Maxwell's distribution, and a double streaming distribution. For Maxwell's distribution it turns out that all the eigenfrequencies are real which makes contact with the work of Van Kampen. The set of eigenfrequencies is finite, however, which raises the question: How is Landau's damping to be recovered? Calculations for the case of one hundred eigenvalues have shown the tendency of the analysis to converge toward the result obtained in VanKampen's limit of a continuum of eigenvalues. For the double streaming case, imaginary eigenfrequencies appear. Comparison with the results in an unlimited velocity space show convergence toward the limiting growth rate curve except in the region of the short wave length cutoff where anomalous behavior appears. The correct wavelength of evanescence of the instability is always provided even at low levels of approximation, but the slopes of the approximate and limiting curves always differ at the wave length of evanescence.

Nonlinear Case

In the linearized cases studied it was found that the longer wave lengths received better treatment, and that time limits existed for a given wave length beyond which the representation became inaccurate. In the nonlinear case it has been found that, in addition, relatively weak disturbances must be used or the representation rapidly deteriorates. By means of numerical calculations the boundaries of the parameter regions in which the truncated-nonlinear F-H analysis is accurate are being explored. In particular, the times of good representation corresponding to retention of different orders of Hermite function are being calculated.

NONHOMOGENEOUS PLASMA KINETIC THEORY

By Leo D. Staton and Marc R. Feix[+]
NASA Langley Research Center
Hampton, Virginia

The problem of oscillations in nonhomogeneous, collisionless, one-dimensional plasmas is being studied by means of a linear integral equation derived from the Vlasov-Maxwell equations. The integral equation is the counterpart for nonhomogeneous plasmas of the usual dispersion equation for homogeneous plasmas, but because of its greater complexity significant progress can be made only by treating specific cases.

A specific case of much theoretical interest is that stationary solution of the Vlasov-Maxwell equations whose distribution function is constant for energies less than some prescribed value and zero elsewhere. The integral equation for oscillations in such a plasma, just as for a cold plasma, is rigorously reducible to a differential equation analogous to that obtained in fluid theory discriptions of plasmas.

Usual linearized theory treatments of perturbations about stationary plasma states are not concerned with the initial accessibility of the stationary state from more general nonstationary states. Interesting results in this regard have been obtained for the specific case at hand. The distribution function in x-v space for such a case is constant (for a finite system) within some closed curve in the x-v plane and zero elsewhere. The time dependent Vlasov equation requires, for a constant total number of particles, that the area of this curve be constant even though its boundary changes shape in the nonstationary situation. By means of a variational principle it has been shown that the stationary state bounding curve corresponds to a minimum total energy for the given number of particles. Since energy must be conserved, this suggests that, in the absence of the formation of highly singular spikes in the distribution function, such a stationary state is inaccessible, in general, from a given initial state. Results from computer experiments at Langley seem to lend support to this conclusion. Work is currently underway to find what conclusion can be drawn about the accessibility of a stationary state for more general distribution functions.

The linearized theory of perturbations about the stationary bounding curves has been developed and by a suitable transformation of variables an overly stringent requirement on the allowed perturbations, which has been enforced by previous authors (e.g. ref. 1), has been removed. Detailed results are not available at this time, but the expected result is that no decay of initial perturbations toward the stationary state will be found.

[+]NAS-NRC Senior Post-Doctoral Resident Research Associate.

All of the above work is based upon collisionless kinetic theory. It is well known that to first order in the reciprocal of the number of particles in a Debye length collisions have no effect upon the distribution function of a one-dimensional plasma. Work is now underway to ascertain the effect of collisions in higher order, taking into account some of the aspects of three body correlations in the plasma.

---

[1] D. C. de Packh, J. of Elec. and Control 13, 417 (1962).

A ONE-DIMENSIONAL MODEL FOR A SELF-GRAVITATING STAR SYSTEM

by Frank Hohl

NASA, Langley Research Center
Hampton, Virginia

and

Marc R. Feix*

NASA, Langley Research Center
and

College of William and Mary

We have used a one-dimensional sheet model to investigate the time behavior of a gas of stars. The characteristic time in the consideration of collective effects in stellar systems is $\tau_c = (4\pi G\rho)^{-1/2}$ where ρ is the mass density and G is the gravitational constant. Irregular forces due to stellar encounters are negligible for times of the order of τ_c. However, through collective effects the system will attempt to reach a metaequilibrium state in this time interval.

The stars are represented by identical mass sheets constrained to move along the x-axis. We use an electronic computer to follow the motion of large numbers of sheets. If the graininess structure of our sheets is small enough, our model will in fact solve the one-dimensional self-consistent Vlasov equation for a gas of stars. Also the collective behavior of the bulk of matter in the one-dimensional system should then be equivalent to the three-dimensional case. The fact that the graininess plays no role has been checked by doubling the number of sheets of a system while keeping its total mass constant. This does not change the behavior of the system. Similarly, whether or not the particles have equal masses plays no role since the Vlasov equation describes a set of particles with different masses as well as with equal masses.

The collective effects of stellar systems are described by the Vlasov equation

$$\frac{\partial f}{\partial t} + v\,\frac{\partial f}{\partial x} - \frac{\partial \phi}{\partial x}\,\frac{\partial f}{\partial v} = 0, \tag{1}$$

where ϕ is obtained from the Poisson equation

$$\frac{\partial^2 \phi}{\partial x^2} = 4\pi G m \int f\, dv. \tag{2}$$

* NAS-NRC Senior Post-Doctoral Resident Research Associate

From eq. (1) we obtain the result that the metaequilibrium state of the system will be described by a distribution function $f(x,v,t \to \infty) = F(U)$ where $U = (1/2)mv^2 + m\phi$ is the total energy of a star. The form of $F(U)$ depends on the initial distribution function and must in general be obtained by following the time development of the nonlinear Vlasov equation. However, there is one type of initial distribution where $F(U)$ is known without actually solving the time dependent Vlasov equation. For this distribution the initial f is constant over a certain region of phase space and is zero outside this region. According to the Liouville theorem f will remain constant over a region of phase space so that the region can only change its shape with time while keeping its area constant. The above initial distribution is of interest primarily because it allows us to calculate exactly the equilibrium configuration of the one-dimensional star gas for comparison with the computer results. The results presented here are all for such an initial distribution; however, other initial distributions give results which are very similar to those presented here.

Taking the initial shape of the area in phase space to be a rectangle defined by $\pm x_o$ and $\pm v_o$, the steady-state solution is easily obtained. $F(U)$ has a constant value for $0 \leq U \leq m\varepsilon$ and is zero for $U > \varepsilon m$. Eq. (2) then becomes

$$\frac{d^2\phi}{dx^2} = [2\sqrt{2}\pi GNm/(x_o v_o)] \ (\varepsilon - \phi)^{1/2}, \tag{3}$$

where $\varepsilon = [3\pi GNm x_o v_o/(2\sqrt{2})]^{2/3}$, N is the number of sheets, and m is the mass per sheet. Integration of eq. (3) gives the result

$$\pm x = \frac{3x_o v_o}{8\sqrt{2}\pi GNm} \int_0^{\phi} [\varepsilon^{3/2} - (\varepsilon - \xi)^{3/2}]^{-1/2} \, d\xi. \tag{4}$$

If we apply the virial theorem to the one-dimensional star gas we can show that in equilibrium the total kinetic energy is one-half the potential energy of the system. To obtain eq. (4) we have only made use of conservation of entropy or area in phase space. If this state is to be reached then the energy of the initial and final state must also be equal. By using a variational method we found that the stationary state described by eq. (4) is a minimum energy state. Thus, starting from any initial state other than the equilibrium state the system can never completely reach the equilibrium state. Nevertheless, the system does its best to approach the stationary state whenever the initial energy is not too far from the energy of the stationary state given by eq. (4).

Fig. 1 shows how a system of 2000 "stars" with a ratio of initial to equilibrium energy of 1.9 approaches its equilibrium configuration in phase space. While approaching equilibrium the system rotates in phase space with a frequency near $1/\tau_c$. After only a few periods, orbital (or phase) mixing has brought the system very near the equilibrium value indicated by the oval in figure 1(d). Also the ratio of kinetic to potential energy is very nearly equal to 0.5 as required by the virial theorem. The behavior indicated in fig. 1 is characteristic of the time behavior of systems where the initial energy is near the equilibrium value. If the initial energy is much larger than the equilibrium value, the system will break up into individual clusters. Fig. 2 shows the time development of a system of 1000 "stars" with a ratio of initial to equilibrium energy near 6. We see that the system breaks up into three clusters, each one individually tending to approach an equilibrium configuration.

For the particular class of initial distribution discussed, the stationary state described by the time independent Vlasov equation can never be completely reached. Since the results of our computer calculations for other initial distributions are very similar to those presented in this paper, it appears likely that the minimum energy principle applies also to other distributions.

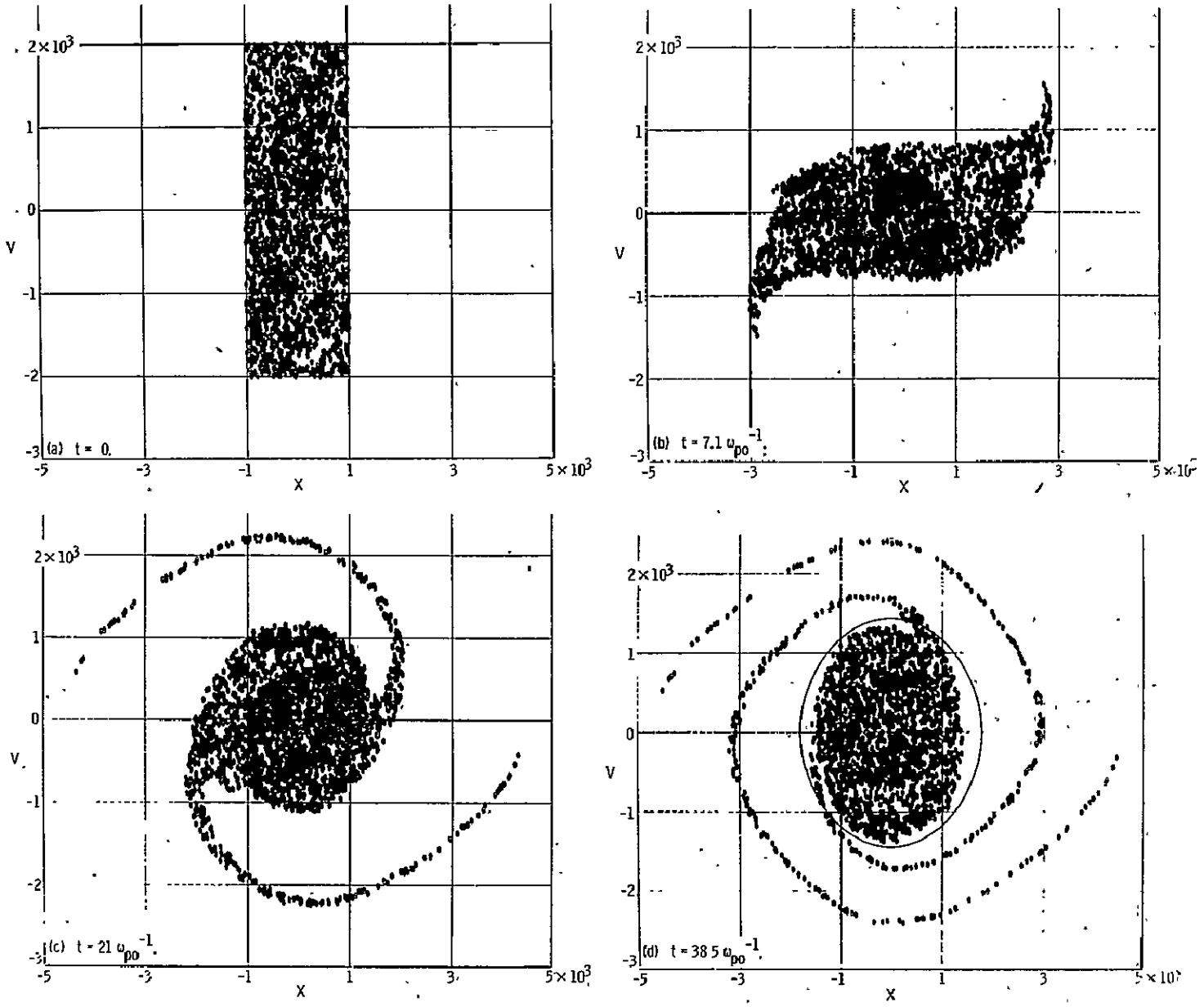

Figure 1. - Approach to equilibrium for a system of 2000 "stars" with a ratio of initial to equilibrium energy equal to 1.9. The system has been normalized such that

$$4\pi G = 1, \; m = .1, \; \tau_c \, (t=0) \; = \omega_{po}^{-1} = 1.$$

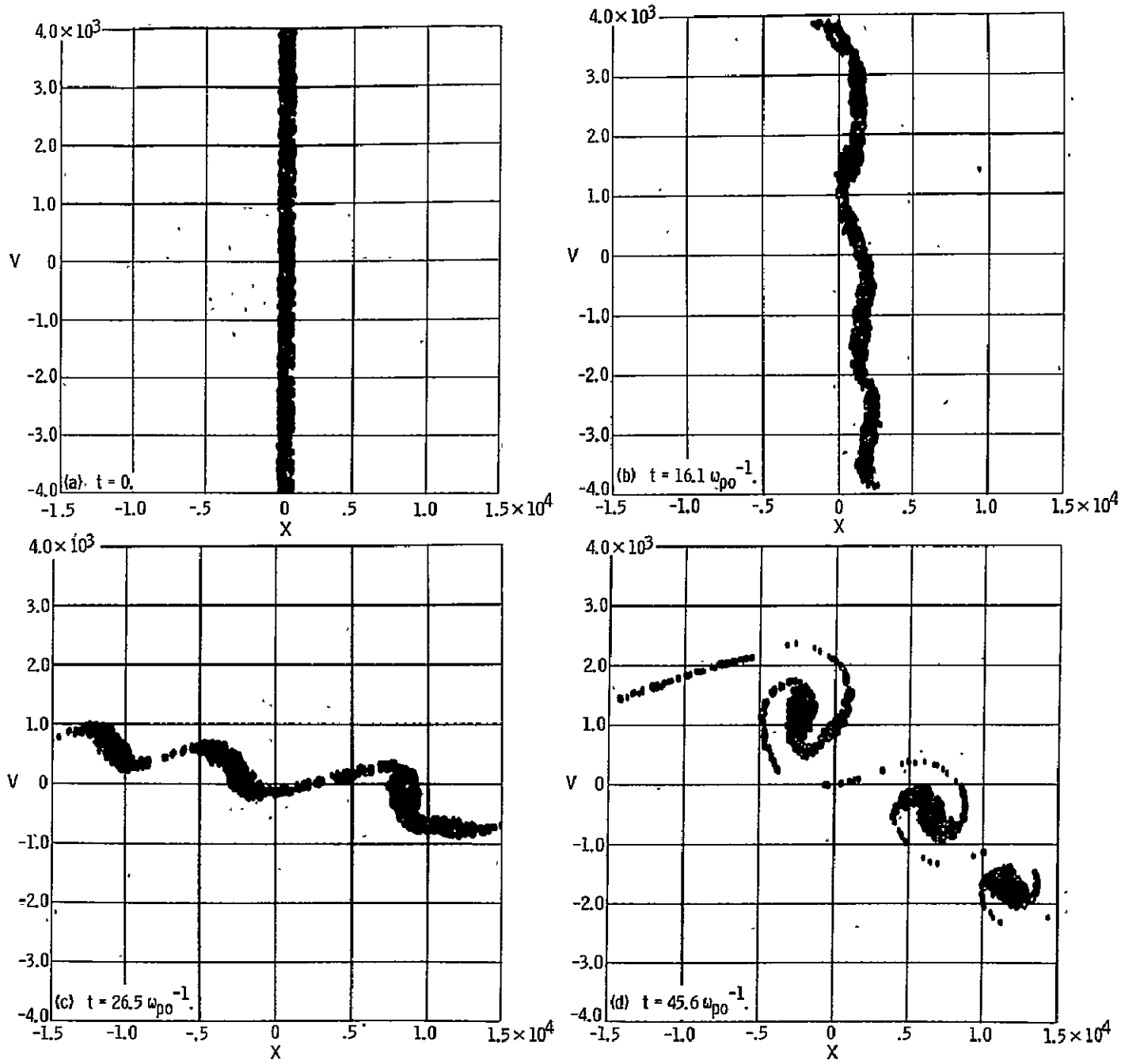

Figure 2. - Time development for an unstable system of 1000 "stars" with a ratio of initial to equilibrium energy equal to 6. The normalization is identical to that used for figure 1.

DETERMINATION OF REENTRY PLASMA PROPERTIES FROM INTERPRETATION OF MANNED SPACECRAFT FLIGHT DATA

P. W. Huber

NASA, Langley Research Center
Hampton, Virginia

Efforts to understand and alleviate the loss of RF tracking and communications which occurs with reentering space vehicles, due to the reentry flow field plasmas, are directed in two principal areas of research. These are, (1) determination of the flow field plasma properties in terms of the vehicle shape, attitude, and reentry flight conditions, and (2) effects of these flow field plasmas on the antenna RF properties and the em wave propagation in or near the plasmas. Since reentry communications typically involves low RF power levels in the plasma, the two parts of the problem are uncoupled and hence observations of signal loss under conditions where one of the two parts can be considered reasonably well understood can lead to a "diagnosis" of the other part. Such data have been obtained from the manned orbital reentries of the Mercury and Gemini spacecraft and, when evaluated in the light of existing theoretical knowledge supplemented also by experimental data from ground facilities, lead to a greatly improved understanding of the reentry flow field plasmas.

Three types of reentry plasma are pertinent to this blunt body problem, depending on the location of antenna on the spacecraft. These are (1) the inviscid plasma between the bow shock and viscous layers near the vehicle, (2) the boundary-layer plasma generated at the body surface, and (3) the near wake plasmas, including the free shear layer and separated zone. The inviscid plasma problem for earth reentry is one dominated by air chemical kinetics. At very high altitudes the species production kinetics are dominant in the problem, while at medium and low altitudes the species recombination kinetics are dominant when considering the usual aft antenna locations. Figure 1 illustrates the importance of recombination kinetics for a hypothetical Apollo reentry in which deceleration occurs at medium altitude. These results were computed using best available rate knowledge for each of 46 reactions in the flow. The curves labelled "frozen" and "equilibrium" are those idealized models generally used to illustrate conceptual limits to the influence of chemical kinetics. However, it is seen that such simplified approaches are grossly inadequate from a numerical standpoint. The undershoot of complete equilibrium at velocities below 30 k ft/sec is due to the relatively fast ionic recombinations which occur in the expanded flow which is relatively cold due to frozen neutral chemistry. It would furthermore be seen to be a serious misinterpretation to deem the plasma in equilibrium at the points where the finite rate results cross those for equilibrium. The very striking drop in electron concentration which occurs at velocities around 31 k ft/sec at this altitude is due to the two-body ionic recombinations which can occur at these and lower

velocities. Such can occur due to the trace of undissociated molecules and diatomic ions left over from the nose region production processes which, considering also the relatively fast charge transfer, allow for two-body recombination paths for electrons and ions. These recombinations are very fast at levels of electron concentration of the order or greater than 10^{12} cm^{-3}. When the concentrations are lower than this value the rate slows considerably and becomes "frozen" at values of the order 10^{11} cm^{-3}.

The second type (boundary layer) plasma is one in which chemical kinetics is also an important factor, but the problem is much more complex due to a chemistry "contaminated" by ablation products - in addition to the effects of viscosity, diffusion, etc. Fortunately, the boundary-layer problem only becomes first order for blunt body reentries at high altitudes where the thickness is large enough to engulf the nose region flow. It is, however, the dominant plasma in slender body problems at all altitudes, since the inviscid layer is not so intensly shock-heated.

The shear layer and separated zone plasmas can be shown, on the basis of flight results, to be plasmas of prime importance for blunt bodies during certain portions of reentry, depending on Reynolds number, look angle, and the amount of inviscid two-body recombination. Consider first the "observations" of electron concentration shown in figure 2 for Mercury and Gemini reentries. These values are deduced from signal data at times in the flights at which attenuation was first detectable and at which "blackout" occurred for both signal frequencies shown, as well as for the corresponding signal recovery points. The values are derived using an idealized em wave propagation model which is believed appropriate for these configurations and signal conditions. The position along the propagation path (the plasma layer responsible for the degradation of signal) is not determined from this data. To help establish the pertinent plasmas in the problem, consider next the theoretical curves shown. The solid lines represent the peak N_e's in the inviscid flow at the appropriate antenna locations using finite-rate flow field calculations for these bodies. The dashed lines represent the N_e's in the separated zone, which is assumed to be homogeneous pure air in equilibrium, due to the low velocity and long dwell time of the recirculating flow. The enthalpy and pressure appropriate to the fluid is taken from hypersonic tunnel data for these bodies at flight Reynolds numbers. It is seen that neither the inviscid air nor the separated air theoretical models will account for the observations in the c-band attenuation region by a large N_e factor, although in the VHF region the agreement with inviscid air theory appears good. Now consider the remaining theoretical curve which represents a separated flow model similar to the pure air model, but with an easily ionized species impurity level appropriate to the attached nose flow boundary layer. The species N_a and K were assumed present in the boundary layer to an extent determined from the heat shield ablation loss rate, the alkali impurity level in the heat shield, and the estimated boundary-layer mass flow. It can be seen that the agreement with the c-band data is very good using this model, but that in the high altitude and low velocity portions

of reentry the model is not consistent with the VHF data by a large N_e factor. However, in this model there is no allowance made for mixing and diffusion of impurities in the attached boundary layer flow which might occur in the detached shear layer and separated flow region. Such viscous spreading effects would be expected to be a minimum at high laminar Reynolds numbers, and be more pronounced at both very low laminar or very high turbulent Reynolds numbers. In figure 3, a spreading factor, $\sigma = \frac{x_{alk,BL}}{x_{alk,obs}}$, is introduced which is, in reality, a correlation factor to account for spreading of the boundary layer ablation impurities to levels in the separated zone which will give agreement with the observed data throughout the reentry. It is seen that this factor does indeed exhibit a strong Reynolds number dependency which is, furthermore, similar to that of other viscous parameters in which transition occurs. As noted on the figure, values of σ in the VHF portions of reentry may be higher than shown, but cannot be lower, since such a condition would be incompatible with the observed signal data. It is interesting to note that these indicated transition altitudes are in good agreement with thermocouple data obtained for these reentries by the Manned Spacecraft Center, for sensors located near the point of boundary layer separation on the leeward flow body side, which is the side appropriate to the signal propagation path for the attenuation data.

APOLLO, TYPICAL STREAMLINE

ALTITUDE = 175 kft

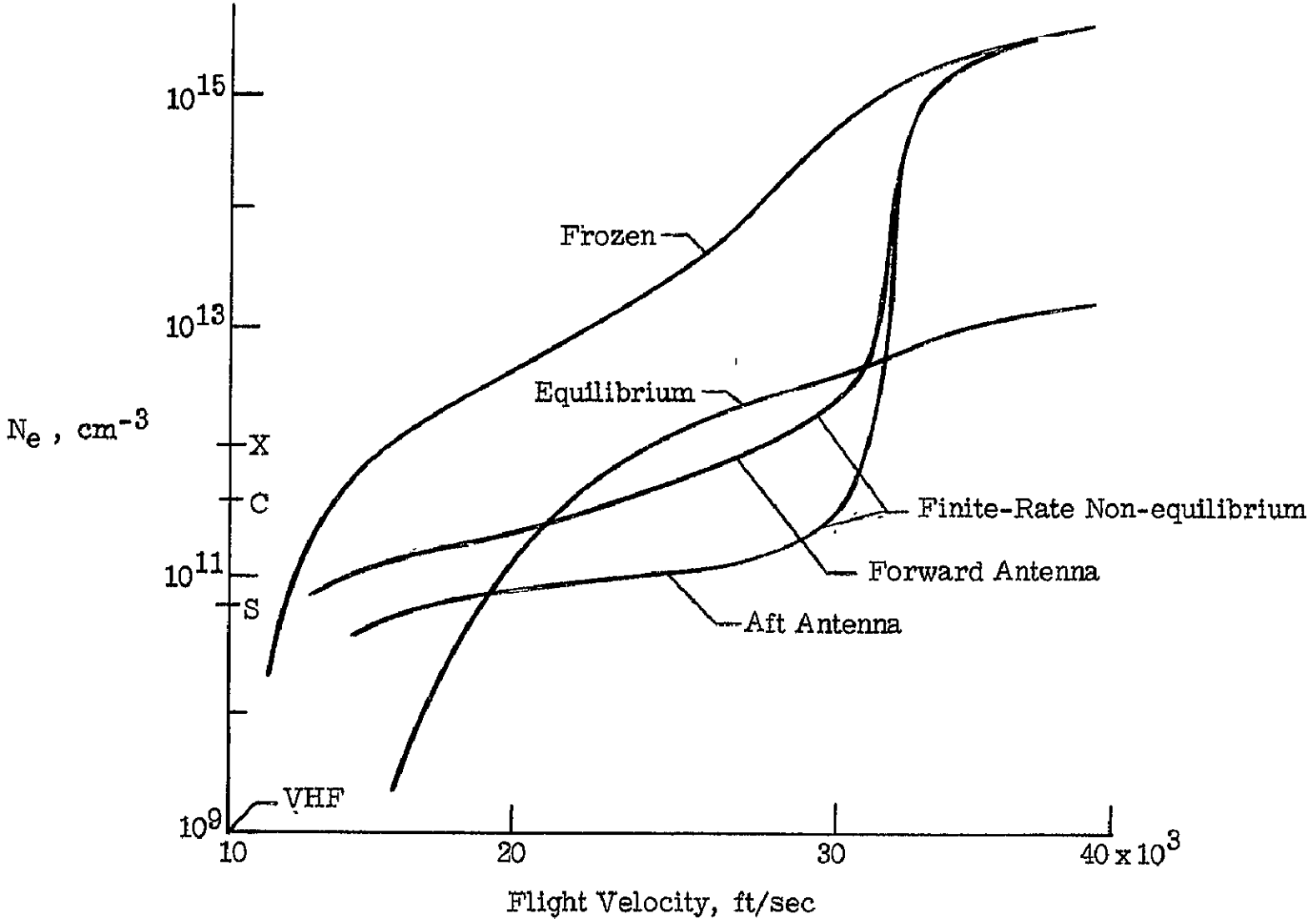

G-T, M-A REENTRY PLASMAS

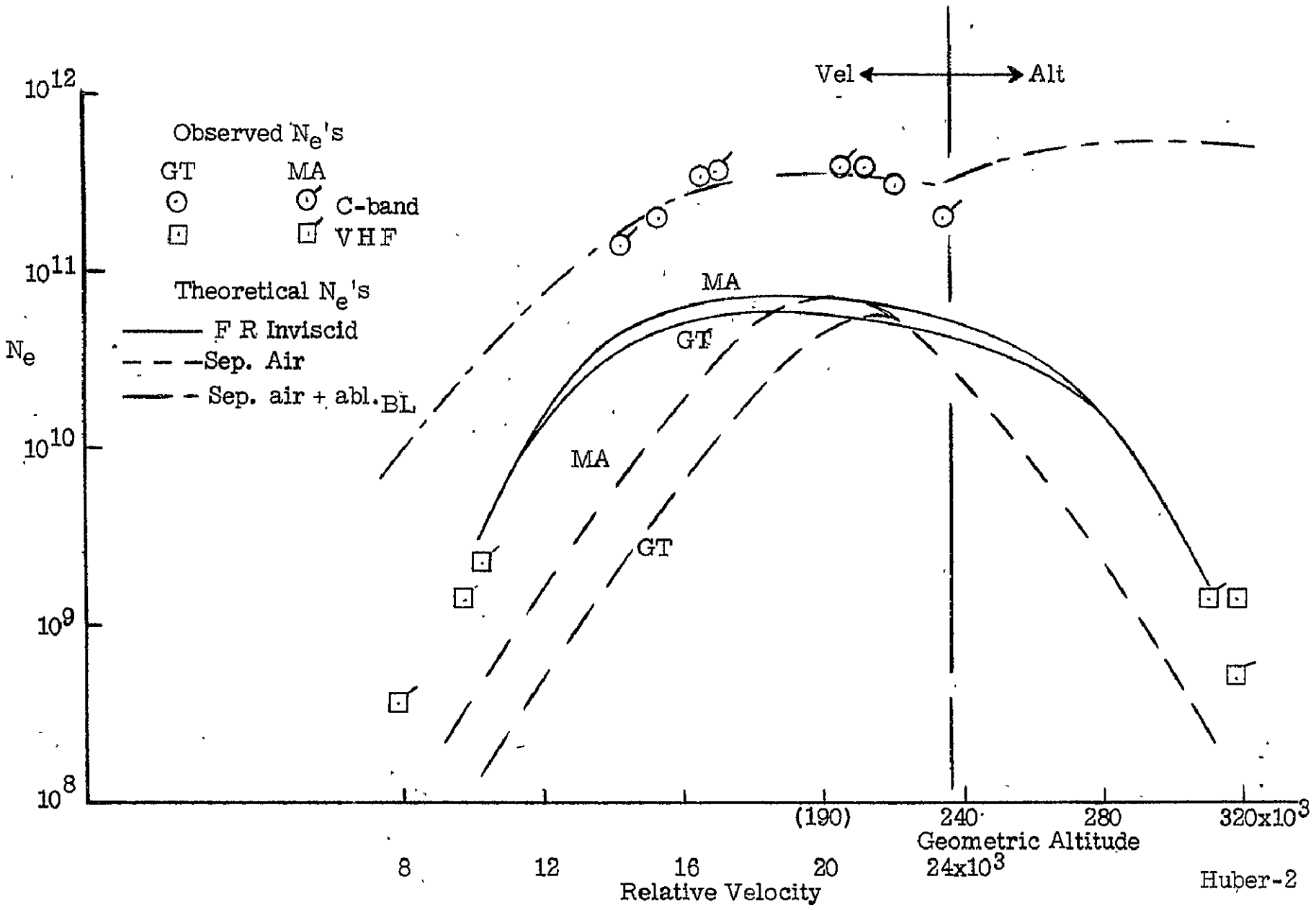

G - T, M - A SPREADING FACTORS

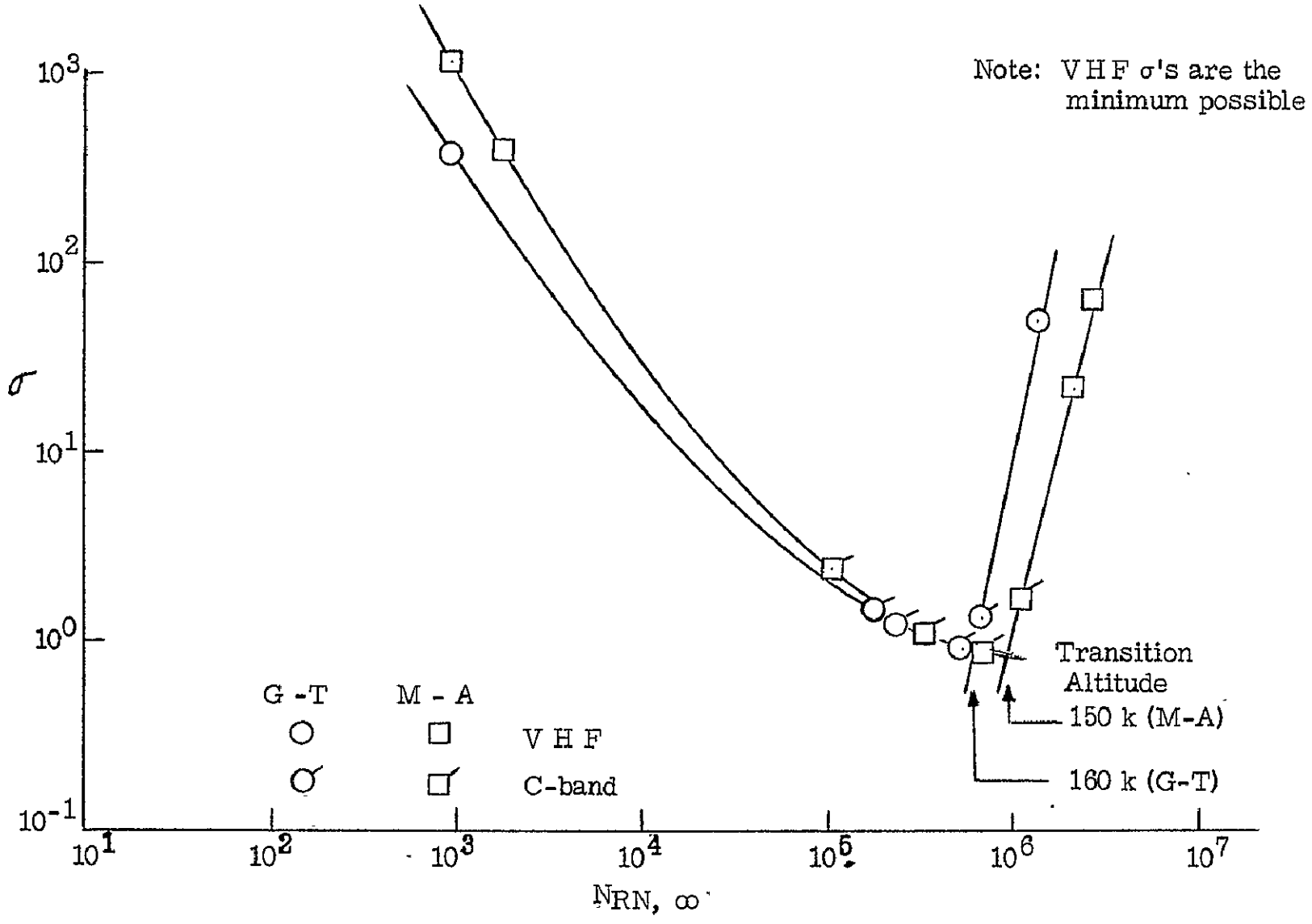

Huber-3

PRECEDING PAGE BLANK NOT FILMED

EVALUATION OF REENTRY AIR CHEMICAL KINETICS USING INSTRUMENTED FLIGHT PROBES

By J. S. Evans and C. J. Schexnayder, Jr.
NASA Langley Research Center
Hampton, Virginia

Microwave reflectometer probes developed for the RAM project were successfully used on the RAM B-3 flight to measure shock layer electron concentrations over a wide range of reentry velocities and altitudes. The availability of this data offers a unique opportunity to verify the results of flow field calculations involving non-equilibrium chemical kinetics and also to determine values for some of the reaction rates to closer limits than heretofore available.

The wide range of flight conditions from 140,000 feet to 245,000 feet in altitude and from 11,600 ft/sec to 18,150 ft/sec in velocity and the great differences in the nature of chemical kinetic processes as they occur in the hot and relatively dense gas covering the blunt nose of the vehicle as compared with the much cooler, expanded gas over the afterbody made it possible to analyze the combined theoretical and experimental data in considerable depth and, as a result of this, the production and recombination of electrons in the RAM B-3 reentry flow field can be discussed in general terms. For example, electrons are always produced in the nose cap region and usually approach local ionic equilibrium values (chemical equilibrium was not reached at any points in the flow fields in any of the calculations made). For the lower velocities or for the higher altitudes, even local ionic equilibrium was not approached, and this phenomenon (see fig. 1), which results in greatly lowered electron concentration values, is referred to as "production droop." Two versions of the high altitude "production droop" are shown in figure 1. Values of ambient air density from standard atmosphere tables were used for the solid lines. For the dotted lines the standard densities were revised to somewhat lower values to obtain better agreement with experimental data. Electron production in the "production droop" region is evidently sensitive to the ambient air density.

Another effect which was always present (see fig. 1)(and which, incidentally, can be present only when diatomic species are not completely removed by dissociation) is the "self-limiting" effect which causes electron concentration levels in the expanded afterbody region to decrease very rapidly from any initial value greater than a certain roughly-defined lower limit until they approach the lower limit and after that the decrease in degree of ionization is slow and usually negligible. (Decrease in gas density will cause electron concentration to decrease further, however.)

An important aspect of the theoretical analysis was the fact that it was often possible to determine that, under given conditions, only a few reactions (sometimes only one) were principally responsible for the changes in air composition taking place (see fig. 1). This ability to isolate the effects of certain reactions proved, in some cases, to be a sensitive means for determining values for the reaction rates involved. (The rates were varied to obtain agreement between calculated and measured values of electron concentration.)

It should be emphasized that occasional good numerical agreement between calculated and measured electron concentration during the flight could not be considered to be verification of the calculated results by experiment. Indeed, such occasional good agreement can be, and has been in the past, obtained by comparing equilibrium or frozen flow field calculations with experimental measurements. Instead, it is necessary to reproduce observed trends in the measured electron concentration over a wide range of conditions, and it is just the fact that the RAM B-3 flight obtained the necessary measurements over a wide range of conditions that makes it uniquely valuable for testing the correctness of the chemical kinetic model.

A comparison between the experimentally measured values of electron concentration and the theoretical values will be given in a technical memorandum now being prepared. (The experimental data has already been published in NASA TMX-1035.) Since the comparison is satisfactory in the sense described in the preceding paragraph, the flow field calculation computer program developed at Langley is considered to be useful for predicting electron concentrations and other flow field properties needed in designing radio communication systems for reentry vehicles.

CALCULATED ELECTRON CONCENTRATION FOR RAM B-3 FLIGHT ; k_f REFERS TO $N + O \underset{k_r}{\overset{k_f}{\rightleftharpoons}} NO^+ + e^-$

(Calculations for symbols were done with standard ambient air density)

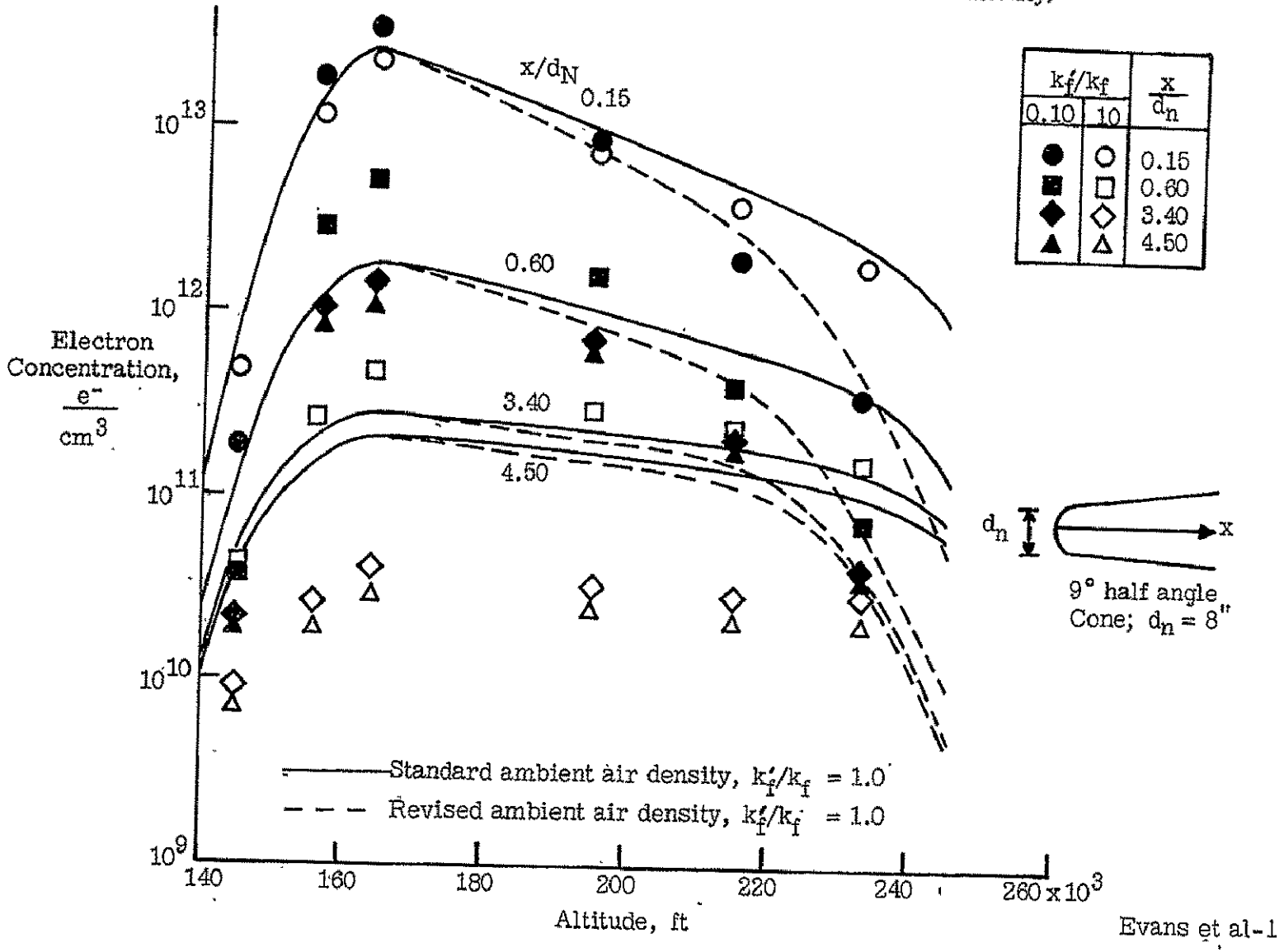

Evans et al-1

IMPEDANCE AND RF PROPAGATION FROM DIELECTRIC AND PLASMA COVERED APERTURES

C. T. Swift

NASA, Langley Research Center
Hampton, Virginia

When an aperture antenna, such as the one shown in figure 1, is coated with a dielectric slab or a plasma, significant changes may occur in the input admittance. This will lead to a change in the absolute signal level of the radiated power, and will also alter the amount of power reflected back into the antenna. In addition, a certain percentage of energy will be coupled into the dielectric coating and remain trapped as a surface wave.

The input admittance is related to the reflection coefficient, Γ, in the following way:

$$\frac{1-\Gamma}{1+\Gamma} = y = (g_r + g_s) - jb$$

where g is the conductance, and b the susceptance. The radiation conductance, g_r and the surface wave conductance, g_s are independently computed. Physically, g_r is the amount of power supplied to the antenna, which radiates into free space, and g_s is that which remains trapped as a surface wave within the dielectric.

The input admittance properties of the antenna, shown in figure 1, are currently being investigated. It consists of a large coaxial transmission line, opening onto an infinite conducting ground plane, coated with a plasma, or other dielectric material.

For computational purposes, the dielectric constant of the slab was taken to be 2.57 (polystyrene); the ratio of the radius of the outer to inner conductor was fixed at 2.00, and the line was assumed to be filled with material of dielectric constant equal to 2.00 (teflon). The admittance was then computed as a function of the slab thickness in wavelengths, and the circumference-to-wavelength ratio of the inner conductor.

The radiation conductance is shown in figure 2. Generally, the conductance increases with increasing circumference-to-wavelength ratio, and a maximum or a minimum in the conductance occurs approximately at every quarter wavelength as the thickness in wavelengths increases.

The surface wave conductance is plotted in figures 3 and 4. In general, g_s rises sharply for the initial values of thickness and then oscillates, much in the same manner as the radiation conductance.

It is of interest to note that, in some cases, nearly all the energy is dumped into surface waves. It is also interesting that some combinations of parameters give practically no energy appearing as surface waves.

The susceptance has been computed; however, more work is needed to improve the accuracy of the computations.

The sensitivity of the input admittance to changes in the thickness of dielectric cover suggests that measurements of the admittance may be used to infer ablation rates during reentry. It is also expected that the admittance should be equally sensitive to changes in the electron density of a reentry plasma. Therefore, the input admittance method may possibly be a powerful method for plasma diagnostics. These applications are currently being investigated experimentally.

TRANSMISSION LINE ANTENNA

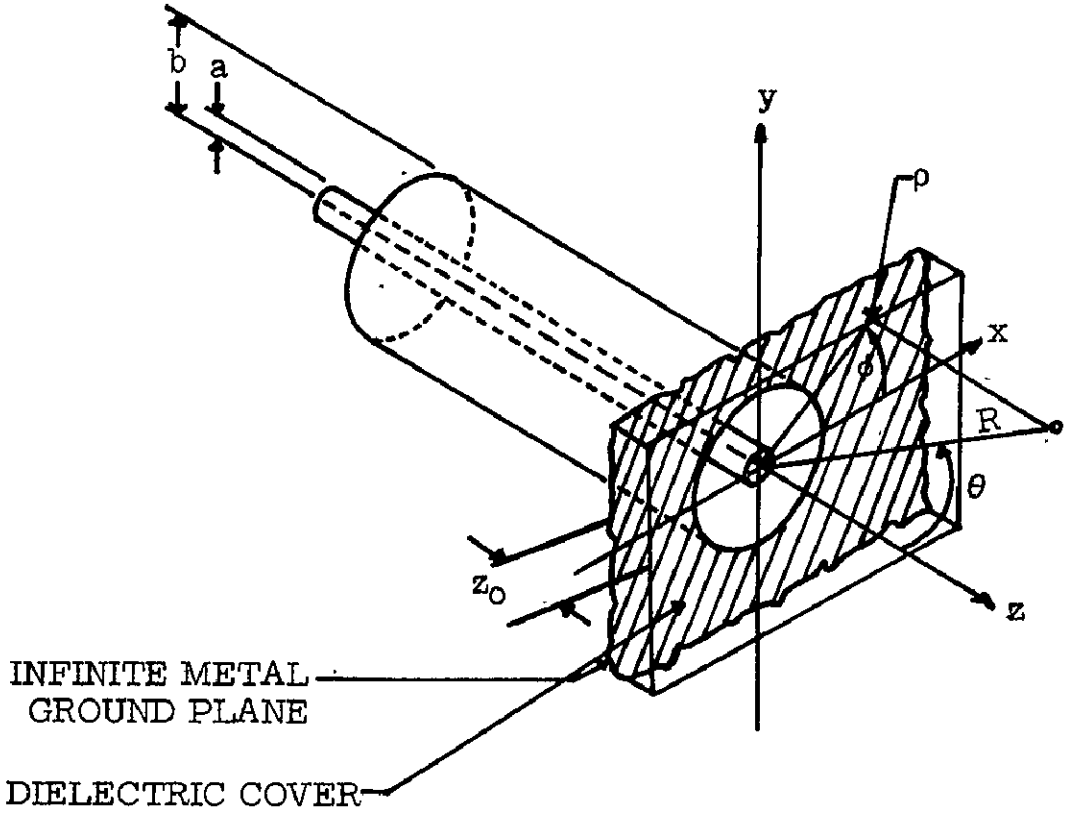

RADIATION CONDUCTANCE

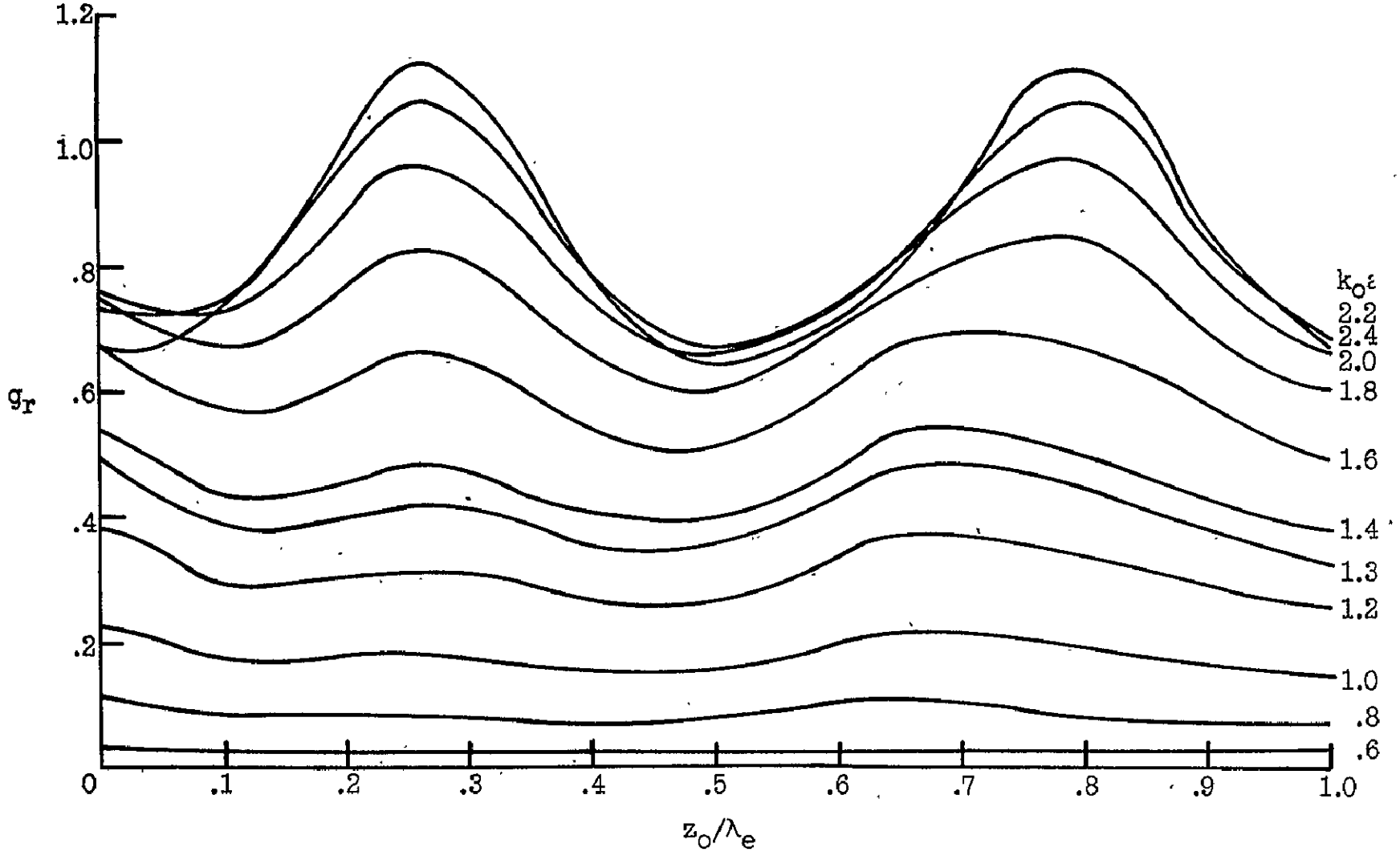

Swift-2

SURFACE WAVE CONDUCTANCE

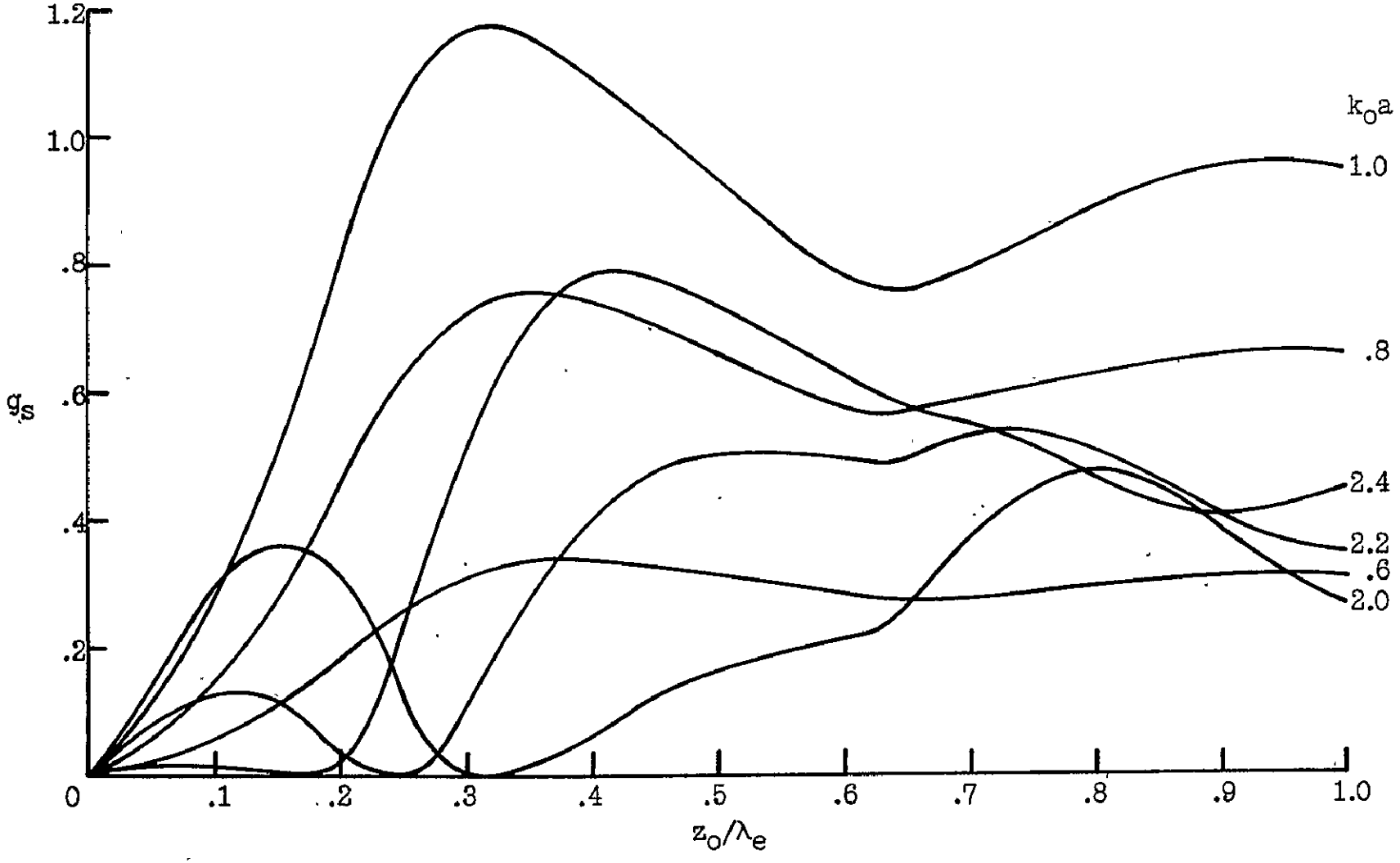

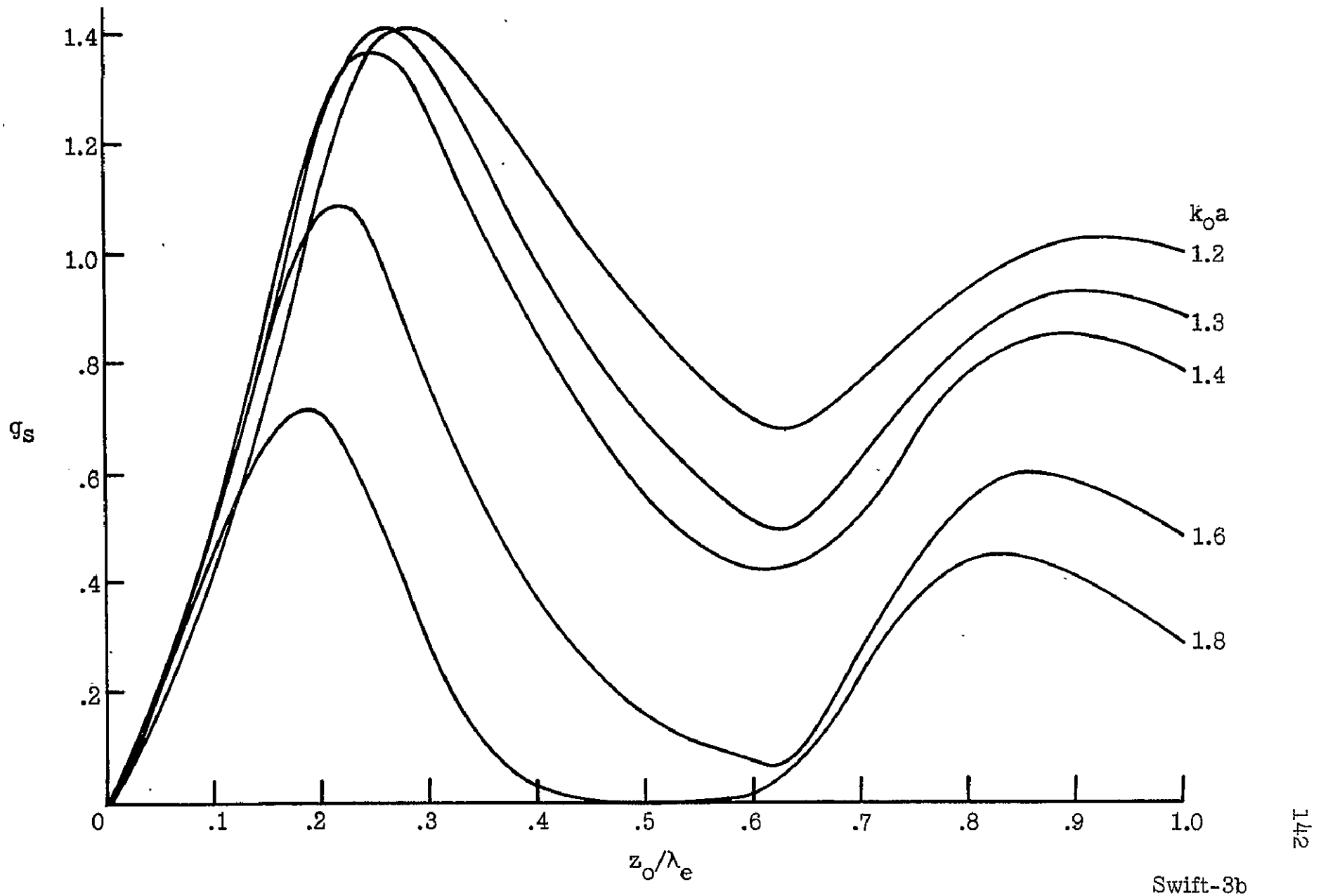
SURFACE WAVE CONDUCTANCE
1.4
1.2
1.0
.8
.6
.4
.2
g_s
$k_o a$
1.2
1.3
1.4
1.6
1.8
0
.1
.2
.3
.4
.5
.6
.7
.8
.9
1.0
z_o/λ_e
Swift-3b

BARIUM RELEASE EXPERIMENT

David Adamson

NASA, Langley Research Center
Hampton, Virginia

The space physics group has a continuing interest in the earth's magnetic field and convective motions and transient fluctuations within it. Much useful data has been obtained using satellites and space probes and the picture depicted in figure 1 has emerged. There is a continuous outpouring of plasma from the sun, the so-called solar wind. This plasma, by virtue of its high conductivity cannot penetrate the earth's magnetic field but flows around it forming the so-called magnetospheric cavity. There are many questions pertaining to this cavity which remain unresolved, i.e., is the cavity open or closed; what is the nature of the convective motions that are taking place within it; and, what are the nature of the changes that take place within it during geomagnetic storms? Magnetometer data is subject to certain inherent limitations, thus one cannot distinguish between spatial inhomogeneities and time-wise fluctuations. Moreover, it is a matter of considerable difficulty to monitor the electric field strengths and hence we have no direct observational data pertaining to the $\frac{E \times B}{B^2}$ drift motions (which we somewhat loosely refer to as motions of magnetic field lines). Also, when one bears in mind that extensiveness of the magnetospheric cavity it is clearly an overwhelming task to chart in detail such an extensive field by point measurements.

Use of an ionized cloud, on the otherhand, provides a ready means of discerning on a large scale the topology of the earth's field and motions within it. The principle is simple. If a charged particle is projected into a magnetic field it spirals along a field line until it is dislodged from same by colliding with another particle. If one pictures then a cloud of such charged particles, sufficiently dispersed to ensure virtual absence of collisions, the cloud will be frozen to the field lines to the extent that motion perpendicular to the field lines is entirely inhibited. Of course, the cloud will diffuse along the field lines and as it does so will serve to define their shape. Furthermore, motion of the field lines will be imparted to the cloud.

Assuming the cloud is released as a neutral cloud, two requirements must be imposed. In the first place it must be readily ionized by the sun's ultra violet and secondly, it must have strong resonance lines in the visible portion of the spectrum in order that the ionized cloud can be seen against the night sky background. One of the substances most adequately filling these requirements is barium and in the calculations that have been made to date, bearing on the feasibility of the techniques in achieving the objectives outlined above we have limited consideration up to the present to barium.

In the calculations made to date, it has been assumed that the cloud is released in the magnetic equatorial plane and viewed from a vantage point lying directly beneath the point of release. Plots have been made of the number of particles per unit area along line of sight (which is proportional to cloud luminosity) as a function of angular coordinates defined in inset of figure 2. One such plot is found in figure 2. It refers to a release of 1 mole of neutral barium at a height of one earth radius. The photoionization probability used in these calculations of 2.5×10^{-4} sec^{-1} was based on a laboratory determination of ionization cross section. It appears from rocket observations made by the Max Planck group that this may be an underestimate by at least an order of magnitude.

CONFINEMENT OF EARTH MAGNETIC FIELD BY SOLAR WIND

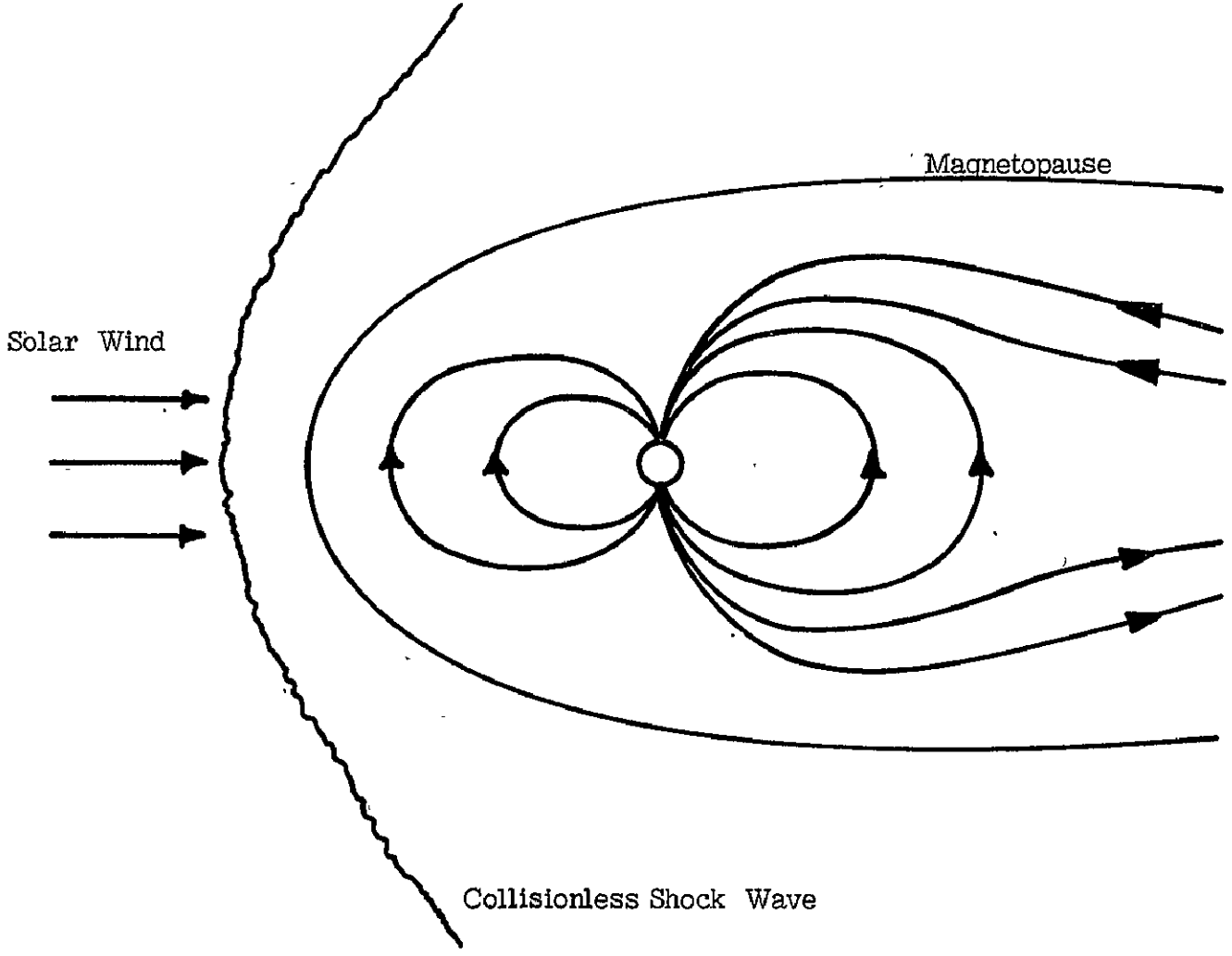

Adamson -1

INTENSITY CONTOURS CORRESPONDING TO RELEASE AT 1 EARTH RADIUS FROM EARTH SURFACE

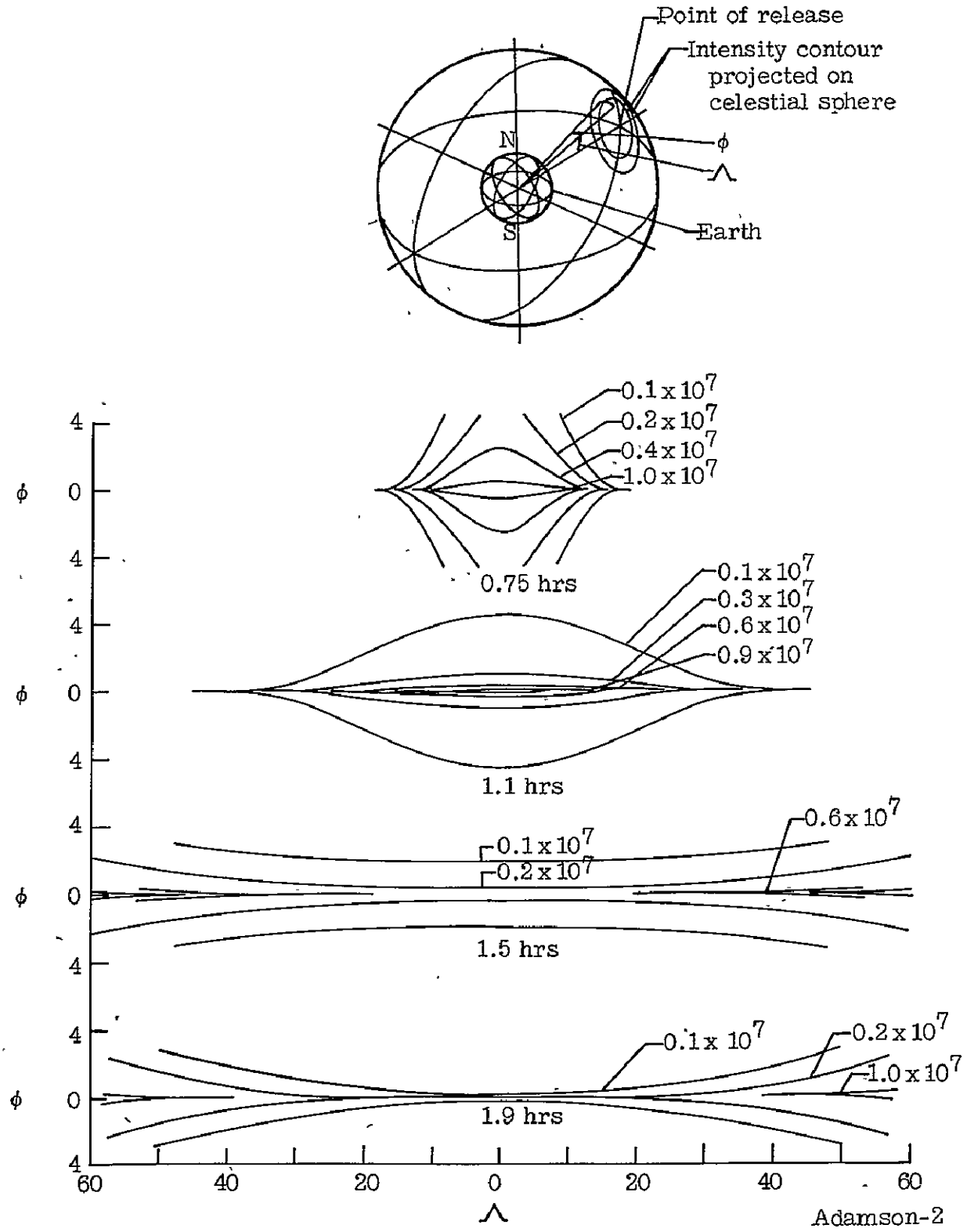

NONEQUILIBRIUM PROPERTIES OF PLASMAS

by W. E. Meador

NASA, Langley Research Center
Hampton, Va.

Unlike thermodynamic properties, the behavior of a partially ionized gas slightly displaced from equilibrium is not well understood. Such nonequilibrium aspects as electrical and thermal conductivities, viscosity, and diffusion are essential to the solution of many practical problems, e.g., heat transfer to reentering space vehicles, drag, radar attenuation, thermonuclear machines, and areas of astrophysics. Two phases of this general domain have been considered: kinetic theory and statistical mechanics, molecular quantum theory.

The first prerequisite of any treatment of transport processes is the adoption of a reasonable kinetic equation for the time evolution of the one-particle distribution function; accordingly, the Boltzmann equation was chosen as the one most completely analyzed in the literature. Although such a theory was not designed originally for plasmas, there are several arguments to indicate that it suffices for these purposes. Not the least of the arguments, although the solutions were accomplished in a fashion so as to essentially force the conclusions, is the quantitative agreement between Boltzmann theory and Spitzer's Fokker-Planck results at full ionization. Grad also has contributed to the general understanding.

Chapman and Enskog's first-order perturbation solution to the Boltzmann equation was applied (reference 1) to a ternary mixture of electrons, ions, and neutrals, and general formulae for the electrical and thermal conductivities and other transport coefficients were derived. When the effects of induced electric fields (ambipolar diffusion) were included, it was found that the field-reduced thermal conductivity was the sum of four terms: translational, internal, reactive, and thermal diffusion, the last of which is always less than 6% of the total. There were two surprising features: the field reduced reaction conductivity, by reason of extensive cancellations, is nearly identical with that of Butler and Brokaw; secondly, thermal diffusion is not important except in its role as the justification behind Muckenfuss and Curtiss' translational contribution. Several discrepancies in the literature were explained in terms of the proper choices of generalized fluxes and forces in irreversible thermodynamics.

An additional paper (submitted for publication) concerns the electrical resistivity and thermal diffusion tensors defined according to the generalized Ohm's Law, i.e., with specific reference to Joule heating. Onsager's reciprocal relations were used in conjunction with complete first-order Chapman-Enskog theory to establish a firm kinetic basis for Spitzer's assumptions for a fully ionized gas. These results were extended to ternary mixtures in order to illustrate the full impact of first-order simplifications

to the formulation of Schlüter and others, i.e., to show the scalar characteristics even in the presence of a magnetic field. All of this was accomplished through the introduction of tensors (neighborhood versus point analyses) for the customary scalar drag coefficients, thereby providing a broader framework for the treatment of first-order limitations (aged systems).

Formulae for transport coefficients only provide the statistical structure; it is necessary also to have estimates of the collision cross sections before numerical work can be accomplished. New treatments, both theoretical and semi-empirical and differing from those in the literature by an increased use of correlation analyses, have been applied (submitted for publication) to several atmospheric species. Only the results for oxygen show a significant departure from the work of Mason, Venderslice, et al, whereas no success has yet been obtained by this method for heteronuclear molecules. Nitrogen is well established, for example (cf, reference 2).

As a final problem, C. Fricke of the Space Physics Group is calculating thermal conductivity from the Balescu kinetic equation. This equation also features binary encounters, but with the partners changing at an infinite rate; accordingly, the Debye shielding (with cloud distortions) is automatically included. Previous calculations (Sundaresen and Wu, et al) of similar nature have, indeed, supported the Boltzmann and Fokker-Planck applications, but convergence of the series solutions was in no way evident. Results of this research are not presently available.

References

1. W. E. Meador and L. D. Staton, Phys. Fluids 8, 1694 (1965).

2. W. E. Meador, NASA Technical Report R-68 (1960).

$$\lambda' = \lambda_\infty + \lambda_{int} + \lambda_r + \lambda_d .$$

$$\lambda_r = \frac{n\, n_e\, n_a\, kT^2\, D_{ai}}{(n_e+n_a)^2}\left(\frac{\partial \ln K_p}{\partial T}\right)^2 .$$

$$\lambda_\infty = \lambda_o - \frac{(n_e+n_e)k\,(D_e^T)^2}{n\, n_e\, m_e^2\, D_{ei}} .$$

$$\lambda_d = \frac{n_a\, kT\, D_{ei}\, D_e^T}{(n_e+n_a)m_e\, D_{ei}}\,\frac{\partial \ln K_p}{\partial T} .$$

Scalar Drag Coefficients:

$$\underset{\sim}{\eta} = [e^2 n_1{}^2(\rho_1+\rho_2)]^{-1}\{[(\rho_1+\rho_2)A_{12}+\rho_1 A_{23}]\,\underset{\sim}{U} + (\rho_2 A_{13}-\rho_1 A_{23})\underset{\sim}{g}\}.$$

$$\vec{u_3} - \vec{u_1} = \underset{\sim}{g}\cdot(\vec{u_2} - \vec{u_1}),$$

Tensor Drag Coefficients:

$$\eta_x = \frac{\rho\rho_3(f_x\rho_1+\rho_2)kT}{e^2 n(\rho_1+\rho_2)\{\rho_2[\rho_3+(1-f_x)\rho_1]D_{12}+\rho_1[f_x\rho_3-(1-f_x)\rho_2]D_{21}\}}$$

$$\approx \frac{\rho kT}{e^2 n\rho_2 D_{12}}. \qquad \text{(Similar for } \tau_x\text{)}$$

$$f_x = \frac{(\rho_2-\rho_1-\rho_3)\nabla_x p_1+\rho_2\nabla_x p_3+en_1\rho(\vec{E}+\vec{u}_1\times\vec{B})_x + (\rho_1+\rho_3)(\vec{j}\times\vec{B})_x}{(\rho_2-\rho_1+\rho_3)\nabla_x p_1-\rho_1\nabla_x p_3+en_1\rho(\vec{E}+\vec{u}_1\times\vec{B})_x + \rho_1(\vec{j}\times\vec{B})_x}.$$

$$\eta_x' = \frac{E_x}{j_x} = \eta_x\left\{\frac{f_x\rho_1+\rho_2}{\rho_1+\rho_2}\left[1 + \frac{(\vec{u_1}\times\vec{B})_x}{E_x} + \frac{\rho_1(\vec{j}\times\vec{B})_x}{en_1\rho\,E_x} + \frac{(\rho_2-\rho_1+\rho_3)\nabla_x p_1}{en_1\rho E_x} - \frac{\rho_1\nabla_x p_3}{en_1\rho E_x}\right]\right.$$
$$\left. + \frac{en_1\eta_x(\rho_2 D_1{}^T-\rho_1 D_2{}^T)\,\nabla_x \ln T}{\rho_1\rho_2\,E_x}\right\}^{-1}$$

$$\underline{\eta}\cdot\vec{j} = \vec{E} + \vec{u}_{12} \times \vec{B} + \frac{m_2-m_1}{en_1(m_2+m_1)} (\nabla p_1 - \vec{j}\times\vec{B}) + \underline{\tau}\cdot\nabla \ln T.$$

$$(\rho_1 + \rho_2)\ \vec{u_{12}} = \rho_1\ \vec{u}_1 + \rho_2\ \vec{u}_2.$$

$$\underline{\eta}\cdot\vec{j} - \underline{\tau}\cdot\nabla \ln T = \frac{\rho_2\vec{D_1}-\rho_1\vec{D_2}}{en_1(\rho_1+\rho_2)}$$

$$\vec{D_i} = \sum_j \underline{A_{ij}}\cdot[\vec{u_j}-\vec{u_i} + (\rho_i\rho_j)^{-1}\ (\rho_i D_j^T - \rho_j D_i^T)\ \nabla \ln T].$$

K I N E T I C T H E O R Y

$$\rho p \vec{d}_i = \rho \vec{D}_i$$

$$= \rho \nabla p_i - \rho_i \nabla p - e_i n_i \rho (\vec{E} + \vec{u}_i \times \vec{B}) + \rho_i \vec{j} \times \vec{B},$$

$$\rho_i (\vec{u}_i - \vec{u}_o) = \sum_j H_{ij} \vec{D}_j - D_i^T \nabla \ln T.$$

$$H_{ij} = (\rho k T)^{-1} n m_i m_j D_{ij}.$$

$$\rho_i \vec{a}_i = \rho_i \vec{F}_i - \nabla p_i + \vec{D}_i. \qquad \text{(Eq. of Motion)}$$

$$\sum_i (H_{ij} - H_{ik}) = 0.$$

$$\sum_{i,j>i} (-1)^{i+j} \rho_i \rho_j (H_{ij} - H_{ji}) = 0. \qquad \text{(Onsager Relations)}$$